Experimental Constraints on the Rheological Behavior of Olivine at Upper Mantle Conditions

by

Nathaniel Adams Dixon

B.A., Carleton College (2007)

Submitted to the Department of Earth, Atmospheric and Planetary Sciences
in partial fulfillment of the requirements for the Degree of

Doctor of Philosophy in Geophysics

at the

MASSACHUSETTS INSTITUTE OF TECHNOLOGY

June 2014

Signature redacted

Author..... .....
Department of Earth, Atmospheric and Planetary Sciences
May 28, 2014

Signature redacted

Certified by..... .....
William B. Durham, MIT
Senior Research Scientist
Thesis Supervisor

Signature redacted

Accepted by..... .....
Robert D. van der Hilst
Schlumberger Professor of Earth and Planetary Sciences
Head, Department of Earth, Atmospheric and Planetary Sciences

Experimental Constraints on the Rheological Behavior of Olivine at Upper Mantle Conditions

by

Nathaniel Adams Dixon

Submitted to the Department of Earth, Atmospheric and Planetary Sciences on May 8, 2014 in partial fulfillment of the requirements for the Degree of Doctor of Philosophy in Geophysics

ABSTRACT

Since the discovery of plate tectonics, geophysicists have sought to understand the dynamic system driving the evolution of the earth, both at the surface and in the deep interior. While the deep earth contains far fewer phases than the crust, the inaccessibility of the mantle and core present a different challenge: unraveling the physical behavior of materials at conditions beyond our intuitive, observational, and experimental grasp.

Among the most persistent of problems has been determining the influence of pressure on the mechanical behavior of deep rocks. Deformation experiments have typically been limited by equipment capabilities to only a tiny fraction of the pressure of the deep mantle, and thus our understanding pressure effect on rock strength has remained insufficient to precisely model the convection of the mantle at large scales in time and space.

In the last decade, a promising new campaign in mantle rheology has been waged with two powerful emerging technologies: synchrotron x-ray diffraction, and complementary multi-anvil deformation machines. These advancements have allowed precisely controlled deformation experiments at conditions representative of the deep upper mantle, with unprecedented measurement precision.

Here I present a detailed experimental study of the behavior of olivine at upper mantle conditions. Among the results is evidence of a significant pressure effect on the strength of olivine (an activation volume of 14 ± 3 cm^3/mol), as well as pioneering in situ measurements of fabric development, slip system transitions, and stress heterogeneity.

Thesis Supervisor: William B. Durham
Title: Senior Research Scientist, Department of Earth, Atmospheric, and Planetary Sciences

Acknowledgments

At the conclusion of this thesis, I have spent a quarter of my life as a graduate student at MIT. Over these years, a few people have made my time as an apprentice scientist in Cambridge particularly memorable and surprisingly joyful.

Nearly all research is collaborative, and this project has been no exception. I owe the completion of my degree to the talent, insight, and hard work of a number of colleagues. No person has been more instrumental to this process than my advisor and mentor, Bill Durham. From my first days at MIT, Bill has shaped my approach to science in nearly every sense, based upon his exacting care and meticulousness in making experimental measurements. He has been a constant and vigilant advocate for my advancement in our field of mineral and rock physics, and I have also been uniquely fortunate to have an advisor who never once objected to my habit of sneaking out of lab on sunny days to ride my bicycle.

I owe a debt of gratitude to many other faculty members at MIT and beyond. In particular, David Kohlstedt, Dan Shim, and Brian Evans come to mind. David has welcomed me into his lab in Minneapolis on many occasions, while Dan and Brian served as crucial teachers and advisors from my early years at MIT through the completion of my thesis.

I had the very good fortunate upon arrival in Cambridge to be taken in by a group of grad students, who, to my surprise, endeavored to leave Building 54 on occasion to go have fun. Over beers at the Muddy Charles or trivia at Atwood's, Scott Burdick, Mike Krawczynski, Christy Till, Krystle Catalli, Noah McLean, Lindsay Hays, Kyle Bradley, and Jay Barr were responsible for making my time at MIT more enjoyable than I ever anticipated. Scott, as a roommate of three years and a cycling teammate, has been an especially prolific source of adventure and sharp wit.

I've had a series of tolerant and helpful officemates as well, none longer than Alejandra Quintanilla, who has worked one desk away for the past five years. Much more brief was the stay of Sudhish Bakku, whose desk I usurped after he abandoned rock physics for seismology. Nonetheless, he has remained a loyal friend and a perpetual source of good humor in the darkest hours of Ph.D. candidacy.

That I remain in decent health and of sound mind is entirely thanks to the MIT Cycling Team, which has perennially provided the highlights of my time as a student. Whether in the high mountains of California and Colorado or enduring the frigid spring weekends of road racing in along the East Coast, the cycling team has been a second family.

A great benefit to studying here in New England has been the proximity of my first family. My mother and father, to whom I owe everything, have welcomed me (and ravenous hordes of cyclists) to their farm at a moment's notice, while my

aunt and uncle, Sally and Andy, have opened their home and refrigerator in Lexington whenever I roll into their driveway unannounced.

I'll always cherish the memory of my late grandfather, George H. Dixon, who repeatedly made the trek down from New Hampshire in the tenth decade of his life to treat me to lunch and offer encouragement. Lastly, I dedicate this thesis to my brother, Dr. A. William Dixon, and to my sister May Dixon, who will likely author a far superior dissertation in a few years' time.

Contents

List of Figures

Chapter 1

Introduction

ABSTRACT

For decades, rheologists have demonstrated the value of deformation experiments as a means to understand the behavior of the natural rocks and minerals that make up the Earth and other planets. Necessarily, data collected in a laboratory on a small scale in space and time require enormous extrapolation to be applied to processes in the Earth, which occur over thousands of kilometers and many millions of years. Our experimental approach, with the use of the Deformation-DIA (D-DIA) apparatus and synchrotron x-ray diffraction, was developed to greatly expand both the range of conditions simulated in experiments, as well as to significantly refine the precision of rheological measurements, vastly improving our ability to apply the our results to Earth systems.

In this thesis, I focus on the mineral olivine because of its important role as the majority component of the upper mantle. The first project addresses the most persistent problem in mantle rheology, determining the direct affect of pressure on the strength of the mantle. The second project examines the role of grain size and other sample parameters in determining the strength of a polycrystalline rock, and the mechanisms that are active during deformation at high pressures. The third project makes use of the wealth of information contained in diffraction patterns, deciphered to show the heterogeneity of stress conditions, in situ.

In total, this work is a small part of a substantial step forward in mantle rheology, providing new access to the conditions of the lithosphere and asthenosphere, the ability to extrapolate rheological behavior to much greater depths, and a clearer and more comprehensive understanding of the underlying deformation physics at a lattice and grain scale.

1.1 Grand rheological challenges

Over the course of the 20th century, mankind made several soaring leaps in our basic understanding of the Earth, and by association, our understanding of other planets. In the year 1900, the best estimates of Earth's age were orders of magnitude too young, Richard Dixon Oldham's seismological case for the core was still around the corner (Oldham 1906), and the wide acceptance of plate tectonics and mantle convection was a lifetime away.

The Earth's deep interior has been illuminated by seismology, which, in concert with experimental petrology and ultra-high-pressure mineral physics research, has provided a wealth of information on the structure and composition of the mantle and core (e.g. Shim et al. 2004; Murakami et al. 2004; Kellogg, Hager, and van der Hilst 1999). Our modern model of an ancient and dynamic Earth is now vastly more sophisticated and precise than one hundred years ago, but in some ways, it is still profoundly lacking. Because of the practically infinitesimal pace of geologic processes, even our most precise observations of the Earth's interior provide just a snapshot of ancient and ongoing evolution (e.g. Van der Hilst, Widiyantoro, and Engdahl 1997). A clear understanding of the dynamics of the mantle and core remains elusive. Models of deep-earth dynamics, despite the availability of powerful computation, require a detailed understanding of the mechanical properties

of rocks under extreme conditions, which defy intuition, and are challenging to determine empirically.

Deformation experiments on Earth materials have been established for decades as a valuable tool for carefully constraining the properties of minerals and rocks (e.g. David T. Griggs 1936; D. T. Griggs, Turner, and Heard 1960; Brace and Kohlstedt 1980). The applicability of this approach to the deep Earth has been limited by the simple difficulty of generating deep-earth conditions in the laboratory, especially non-hydrostatic stress states, which, by nature, often lead to failure of equipment. Even when extreme conditions can be generated, there is a separate problem of precisely controlling an experiment and measuring the response of a sample, an obvious requisite if the results are to be useful.

The recent availability of 3rd-generation synchrotron x-ray facilities has provided a powerful means to measure conditions in deforming samples, and prompted the development of a new generation of deformation machines to take advantage of this technology. In particular, the Deformation-DIA apparatus has shown promise as tool for investigating the properties of mantle materials (Wang et al. 2003; Durham et al. 2009; Raterron et al. 2009; Hilairet et al. 2012). The research for this dissertation is amongst the first wave of experimental studies conducted with the synchrotron/Deformation-DIA technique, which, despite its youth, has already seen substantial refinement as we have explored its capabilities (Weidner et al. 2010). Thus,

our research has paired the task of confronting great geophysical challenges, and the process of developing a powerful and fascinating new technology, which has unforeseen capabilities.

1.2 Strategy for deformation experiments

Although we employ a range new technology for the projects in this dissertation, the fundamental experimental approach has been tested for decades in lower-pressure rheological studies (e.g. Hirth and Kohlstedt 1996; Hirth and Kohlstedt 2003; Hansen, Zimmerman, and Kohlstedt 2011): describing the relationship between stress and strain rate with an empirical "flow law". The steady-state creep of single crystals and aggregates follow the same basic form, where the accumulation of permanent strain is a function of the differential stress (σ_1-σ_3) and a number of environmental and state variables (Evans 2005).

$$\dot{\varepsilon} = A(\sigma^n, P, d, H_2O...)]$$

The strategy for experiments thus involves either fixing strain rate of a deforming sample and measuring differential stress, or fixing the differential stress and measuring strain, in either case, holding most other conditions constant. All experiments for this dissertation feature fixed strain rates; the measurement of stress in our samples is not instantaneous, and therefore it is difficult to hold stress constant.

It is well known that plastically deforming rock samples typically demonstrate a period of "transient" behavior before settling into steady state creep (Carter and Kirby 1978). Because we are most interested in the properties of mantle rocks, which have been deformed continuously for billions of years, we focus on steady-state deformation. Thus, each sample must be deformed substantially (typically >10% strain) for each experimental step.

1.3 The Deformation-DIA apparatus

1.3.1 Design

The Deformation-DIA (D-DIA) is a modified version of the earlier DIA apparatus, a six-anvil hydrostatic device. The DIA design is similar in principle to other multi-anvil machines, which have been used in a multitude of forms since 1958, when the cubic-anvil apparatus was developed for the original purpose of synthesizing diamonds (Hall 1958; Liebermann 2011). The DIA and other multi-anvil devices feature very hard anvils that squeeze into a much softer "pressure medium" surrounding the sample material. In this way, a sample can be brought to pressure conditions far above what is achievable with machines that use pressurized gas.

Like the original DIA, the D-DIA uses six truncated anvils, which form a cubic volume (Figure 1-1). The D-DIA, however, is modified to produce well controlled non-hydrostatic stress conditions, as required by rheologists. This is achieved by independently controlling the top and bottom anvils with their

own dedicated hydraulic rams, advancing them upon the sample faster or slower than the four side anvils. For our purposes, the top and bottom anvils are driven inwards during deformation as the side anvils are withdrawn slowly, producing an axisymmetric stress state with the greatest principle stress vertical, and constant mean stress (pressure). The ability of the D-DIA to produce deviatoric (non-hydrostatic) stress while maintaining constant sample volume, and thus constant pressure, is a first for a multi-anvil apparatus. With the top and bottom anvils advancing, our cylindrical olivine samples become shorter and fatter during the course of deformation. The cubic sample cell and pure shear deformation geometry result in a relatively simple state of stress within our deforming olivine, a great convenience for calculating flow laws.

1.3.2 Pressure and temperature capabilities

The original specifications of the D-DIA were designed to achieve a maximum pressure capability of ~15 GPa, the pressure at the bottom of the upper mantle. However, the actual pressure that can be reached during a given deformation experiment depends on the strength and of the anvil materials, and on the truncation of the anvils (which effectively limits sample volume). The use of x-rays in our experiments requires at least one "transparent" anvil that allows diffracted x-rays to travel through (Figure 1-2, inset). These anvils are made of sintered diamond, which fails at lower

stress than standard anvils made of tungsten carbide. To a lesser degree, pressure capabilities also depend on the materials of the sample assembly and on the temperature and stress conditions targeted for the experiment. With our anvil configuration and sample assembly, and with temperatures over 1300 K, the maximum pressure is approximately 9 GPa. The graphite furnace included in the assembly is easily capable of producing temperatures well above the melting point of olivine at upper mantle pressures, as we have proven accidentally on occasion.

1.4 Synchrotron x-ray diffraction

The technology to required to produce a multi-anvil deformation apparatus like the D-DIA has been available for decades, but without the ability to accurately measure the stress conditions and state of strain within the sample, it would not have been useful for rheological tests. The penetrating power of synchrotron x-rays allows us to observe a sample buried deep within an assembly, and to determine the stress conditions directly from the elastic strain in the sample's crystal lattice (Wang et al. 2003; Singh 1993; Singh et al. 1998). With x-rays, we are also able to measure stresses anywhere in the sample and in much of the surrounding assembly. As detailed in Chapter 2 and Chapter 4, our x-ray diffraction data are rich in other information on the state and structure of deforming samples.

1.4.1 System design

The D-DIA installation at NSLS beam line X17B2 features an energy-dispersive x-ray diffraction system, in which a "white" beam, containing x-ray energies from ~20 to ~100 keV, passes through the sample (Figure 1-2). Downstream of the sample, there is a set of collimating slits, which collect photons that are diffracted only at a very precisely defined angle. By measuring the energy of these collected photons, the lattice spacing (d-spacing) of the sample material can be determined. The advantage of this setup, as opposed to the more common monochromatic beam diffraction, is that it allows the detectors to be "aimed" directly at the sample: the slits exclude photons that are diffracted from other materials surrounding the sample, allowing greater freedom in picking sample assembly materials.

1.4.2 Calibration and precision

Although x-ray diffraction has been used in crystallography for a century now (Bragg 1913), the determination of elastic strain in a crystal lattice requires extraordinarily precise and challenging measurements (Singh 1993). The unit cell of olivine is orthorhombic with the greatest unit cell dimension just over a nanometer. The components of the stiffness tensor for olivine are on the order of 100 GPa, meaning that for a typical experimental differential stress of 0.1 GPa, the total differential displacement of the olivine lattice is on the order of 0.001 nm (Kumazawa and Anderson 1969). Thus, to

obtain a suitably precise measurement of differential stress, we must be able to resolve these incredibly small changes in lattice spacing, often down to 10^{-14} m. This capability depends on careful calibration of the diffraction system, before and during experiments, with the aid of known diffraction standards. Powdered corundum (Al_2O_3) is typically used as a standard, because it has lattice planes ranging widely in their spacial frequency, each of which produces an excellent diffraction peak. The radioactive decay of Co57 at fixed energies, which does not depend on diffraction or the collimating slit assembly, is used as an independent calibration of the detectors.

The detectors, slit system, and calibration technique have been updated and refined several times during the course of this research, improving the precision of stress measurements tenfold, from ±100 MPa to ±10 MPa under optimum conditions (Weidner et al. 2010).

1.5 Major obstacles

1.5.1 Water

For the past two decades, the role of water in mantle materials has been a primary concern of rheologists. In solid rocks, where oxygen is ubiquitous in its role as an anion, water takes the form of H^+ ions as an interstitial in crystal lattices or at grain boundaries. It has a profound effect on many deformation mechanisms in olivine and other mantle minerals,

typically causing substantial weakening (Hirth and Kohlstedt 1996; Jung and Karato 2001). The role of water has been particularly challenging to study in deformation experiments. Small samples deforming at high temperatures tend to dehydrate rapidly, and the effects of the resulting transient water conditions can be convolved with other influences on strength. To sidestep this issue, we have focused on experiments on dry olivine. Dry olivine is not representative of the entire upper mantle, which is expected to contain a large amount of water (Kohlstedt, Keppler, and Rubie 1996; Keppler 2014), but the elimination of water in our samples allows us to more carefully constrain the effects of other parameters like strain rate, pressure, and temperature.

1.5.2 Temperature measurement

Temperature, above all else, controls the ductility of rocks (D. T. Griggs, Turner, and Heard 1960; Kohlstedt, Evans, and Mackwell 1995). While high pressures are difficult to generate in the laboratory, high temperatures are comparatively easy to access. Because rock strength is so sensitive to temperature, uncertainty in temperature measurement can overwhelm otherwise precise measurements of rheological behavior. The small size of the furnace in D-DIA sample assemblies leads to large thermal gradients (>100 K/mm) (Liebermann and Wang 1992; Rubie 1999). Direct measurement of temperature with thermocouples is difficult and unreliable,

given the scale of the sample and the tendency of thermocouple wires to shift within the cell during deformation. The inclusion of thermocouples also drastically worsens the precision of sample cell construction, and the shifting thermocouple tends to destabilize the other cell components. We avoid the problem by deleting the thermocouple completely. Thus, there is no direct measurement of temperature in our experiments. Instead we predict temperatures in separate calibration experiments that mimic the conditions of our olivine runs. In these calibration experiments, deformation steps are done on a sample assembly with no olivine and thermocouple in the dead center of the cell. We have shown that there is very good repeatability of the calibrated relationship between furnace power and temperature. Nonetheless, uncertainty in temperature remains the largest source of uncertainty in all of our measurements. Fortunately, even with generous estimations of temperature uncertainty, we are able to produce results with profound implications for mantle rheology, and for the role of high pressure in particular.

Bibliography

Brace, W. F., and D. L. Kohlstedt. 1980. "Limits on Lithospheric Stress Imposed by Laboratory Experiments." *Journal of Geophysical Research: Solid Earth (1978–2012)* 85 (B11): 6248–52.

Bragg, William Lawrence. 1913. "The Structure of Some Crystals as Indicated by Their Diffraction of X-Rays." *Proceedings of the Royal Society of London. Series A* 89 (610): 248–77.

Carter, Neville L., and Stephen H. Kirby. 1978. *Transient Creep and Semibrittle Behavior of Crystalline Rocks*. Springer. http://link.springer.com/chapter/10.1007/978-3-0348-7182-2_16.

Durham, W. B., S. Mei, D. L. Kohlstedt, L. Wang, and N. A. Dixon. 2009. "New Measurements of Activation Volume in Olivine under Anhydrous Conditions." *Physics of the Earth and Planetary Interiors* 172 (1-2): 67–73.

Evans, Brian. 2005. "Creep Constitutive Laws for Rocks with Evolving Structure." *Geological Society, London, Special Publications* 245 (1): 329–46.

Griggs, D. T., F. J. Turner, and H. C. Heard. 1960. "Deformation of Rocks at 500° to 800° C." *Geological Society of America Memoirs* 79: 39–104.

Griggs, David T. 1936. "Deformation of Rocks under High Confining Pressures: I. Experiments at Room Temperature." *The Journal of Geology*, 541–77.

Hall, H. Tracy. 1958. "Ultrahigh Pressure Research." *Science* 128: 445–49.

Hansen, LN, ME Zimmerman, and DL Kohlstedt. 2011. "Grain Boundary Sliding in San Carlos Olivine: Flow Law Parameters and Crystallographic-Preferred Orientation." *Journal of Geophysical Research* 116 (B8): B08201.

Hilairet, Nadège, Yanbin Wang, Takeshi Sanehira, Sébastien Merkel, and Shenghua Mei. 2012. "Deformation of Olivine under Mantle Conditions: An in Situ High-pressure, High-temperature Study Using Monochromatic Synchrotron Radiation." *Journal of Geophysical Research: Solid Earth (1978–2012)* 117 (B1).

Hirth, G., and D. Kohlstedt. 2003. "Rheology of the Upper Mantle and the Mantle Wedge: A View from the Experimentalists." *Geophysical Monograph* 138: 83–105.

Hirth, G., and D. L. Kohlstedt. 1996. "Water in the Oceanic Upper Mantle: Implications for Rheology, Melt Extraction and the Evolution of the Lithosphere." *Earth and Planetary Science Letters* 144 (1-2): 93–108.

Jung, H., and S. Karato. 2001. "Water-Induced Fabric Transitions in Olivine." *Science* 293 (5534): 1460–63.

Kellogg, Louise H., Bradford H. Hager, and Rob D. van der Hilst. 1999. "Compositional Stratification in the Deep Mantle." *Science* 283 (5409): 1881–84.

Keppler, Hans. 2014. "Geology: Earth's Deep Water Reservoir." *Nature* 507 (7491): 174–75. doi:10.1038/507174a.

Kohlstedt, D. L., Brian Evans, and S. J. Mackwell. 1995. "Strength of the Lithosphere: Constraints Imposed by Laboratory Experiments." *Journal of Geophysical Research: Solid Earth (1978–2012)* 100 (B9): 17587–602.

Kohlstedt, D. L., H. Keppler, and D. C. Rubie. 1996. "Solubility of Water in the A, B and Γ Phases of (Mg, Fe) 2SiO4." *Contributions to Mineralogy and Petrology* 123 (4): 345–57.

Kumazawa, M., and O. L. Anderson. 1969. "Elastic Moduli, Pressure Derivatives, and Temperature Derivatives of Single-Crystal Olivine and Single-Crystal Forsterite." *J. Geophys. Res* 74 (5): 5961–77.

Liebermann, Robert C. 2011. "Multi-Anvil, High Pressure Apparatus: A Half-Century of Development and Progress." *High Pressure Research* 31 (4): 493–532.

Liebermann, Robert C., and Yanbin Wang. 1992. "Characterization of Sample Environment in a Uniaxial Split-Sphere Apparatus." *Geophysical Monograph Series* 67: 19–31.

Murakami, Motohiko, Kei Hirose, Katsuyuki Kawamura, Nagayoshi Sata, and Yasuo Ohishi. 2004. "Post-Perovskite Phase Transition in MgSiO3." *Science* 304 (5672): 855–58.

Oldham, Richard Dixon. 1906. "The Constitution of the Interior of the Earth, as Revealed by Earthquakes." *Quarterly Journal of the Geological Society* 62 (1-4): 456–75.

Raterron, P., E. Amiguet, J. Chen, L. Li, and P. Cordier. 2009. "Experimental Deformation of Olivine Single Crystals at Mantle Pressures and Temperatures." *Physics of the Earth and Planetary Interiors* 172 (1-2): 74–83.

Rubie, D. C. 1999. "Characterising the Sample Environment in Multianvil High-Pressure Experiments." *Phase Transitions: A Multinational Journal* 68 (3): 431–51.

Shim, S.-H., T. S. Duffy, R. Jeanloz, and G. Shen. 2004. "Stability and Crystal Structure of MgSiO3 Perovskite to the Core-Mantle Boundary." *Geophysical Research Letters* 31 (10). http://onlinelibrary.wiley.com/doi/10.1029/2004GL019639/full.

Singh, A. K. 1993. "The Lattice Strains in a Specimen (cubic System) Compressed Nonhydrostatically in an Opposed Anvil Device." *Journal of Applied Physics* 73 (9): 4278.

Singh, A. K., C. Balasingh, H. Mao, R. J. Hemley, and J. Shu. 1998. "Analysis of Lattice Strains Measured under Nonhydrostatic Pressure." *Journal of Applied Physics* 83: 7567.

Van der Hilst, R. D., Sri Widiyantoro, and E. R. Engdahl. 1997. "Evidence for Deep Mantle Circulation from Global Tomography." *Nature* 386 (6625): 578–84.

Wang, Y., W. B. Durham, I. C. Getting, and D. J. Weidner. 2003. "The Deformation-DIA: A New Apparatus for High Temperature Triaxial Deformation to Pressures up to 15 GPa." *Review of Scientific Instruments* 74: 3002.

Weidner, D. J., M. T. Vaughan, L. Wang, H. Long, L. Li, N. A. Dixon, and W. B. Durham. 2010. "Precise Stress Measurements with White Synchrotron Xrays." *Review of Scientific Instruments.*

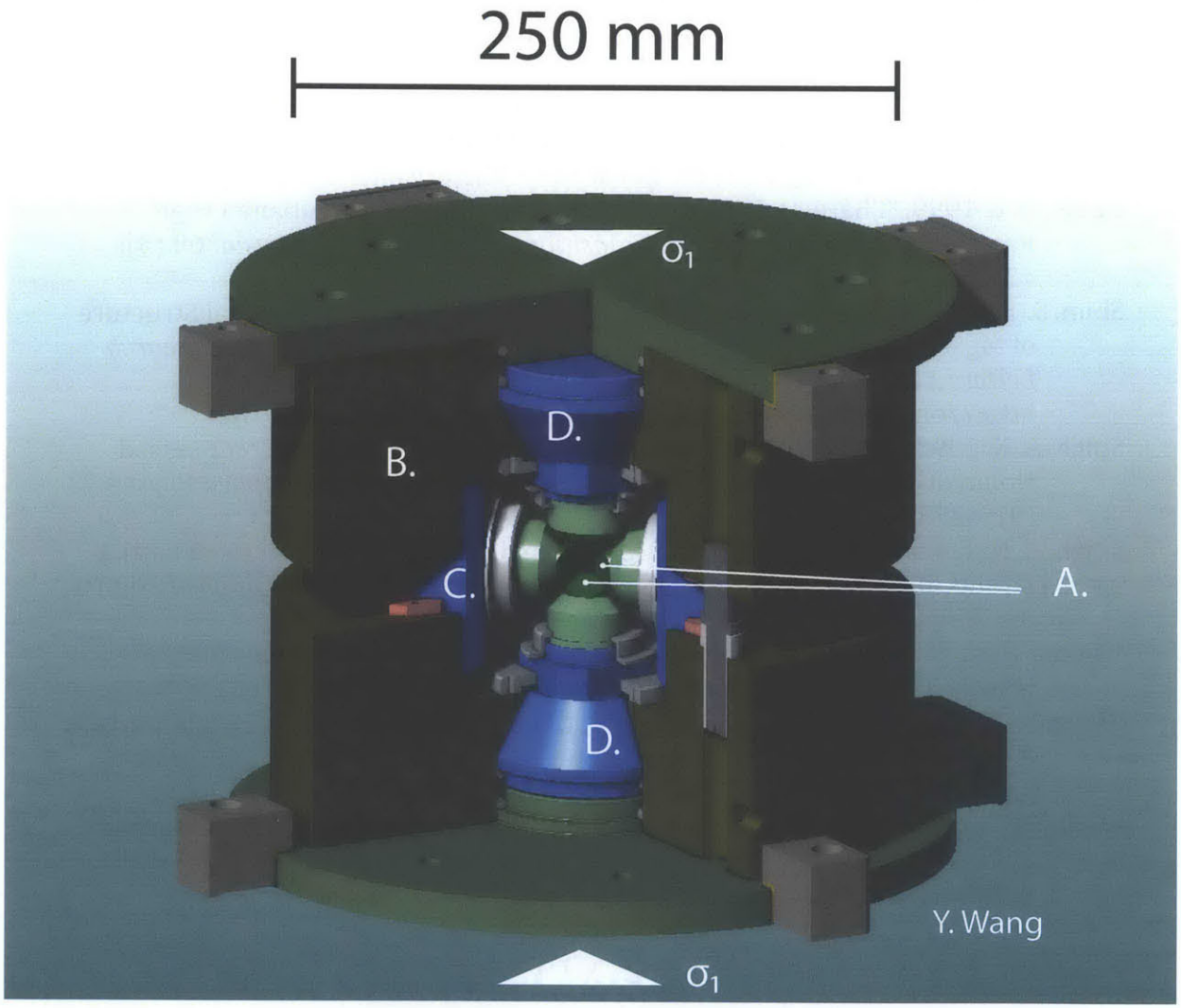

Figure 1-1. Cutaway view of the D-DIA. Independently controlled differential rams (D) are top and bottom, while the horizontal anvils are mounted on wedges (C) and pushed inward by the guideblocks (B) in which they sit. Anvils (A) are made of tungsten carbide (WC) or sintered diamond (SD). Image courtesy of Y. Wang.

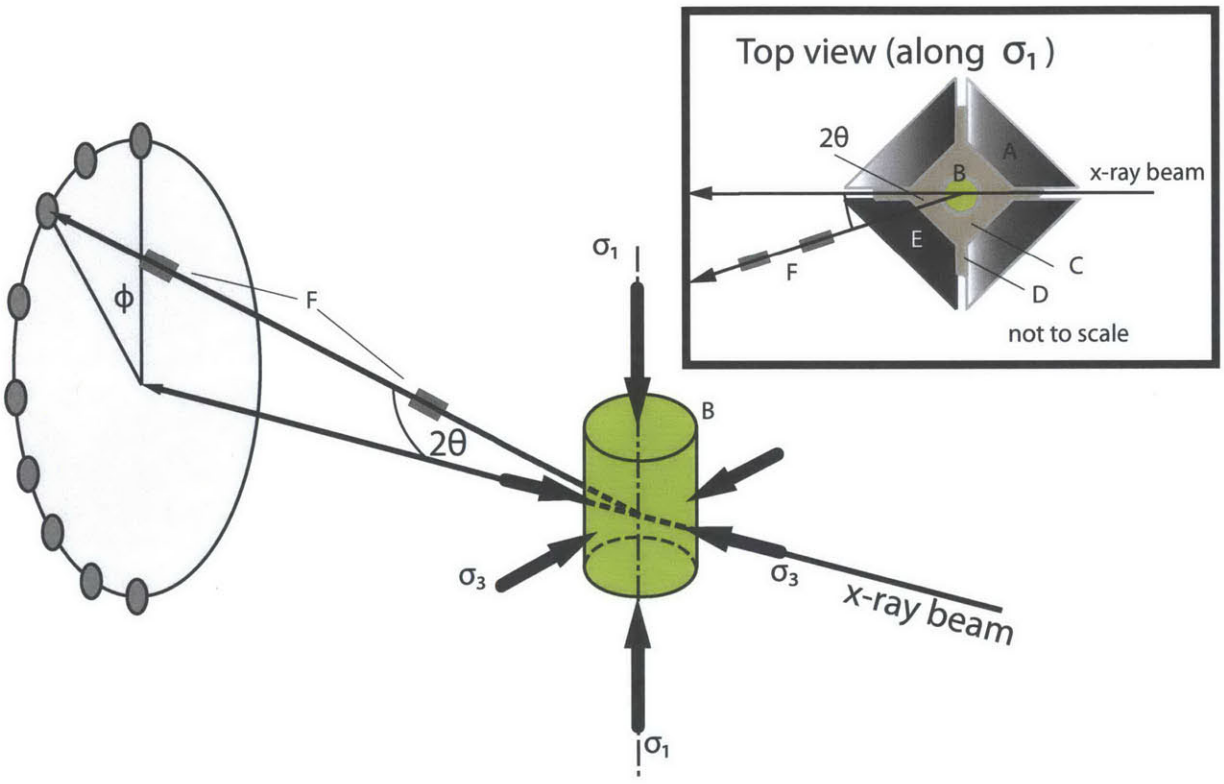

Figure 1-2. Diagram of beam path through sample to plane of detectors. The Bragg angle (θ) is fixed by collimating slits, while there are nine detectors spaced evenly from $\phi = 0°$ to $\phi = 180°$. *Inset:* Schematic top-view of sample assembly squeezed by horizontal anvils. The incident beam passes between the WC upstream anvils (A) and through the sample (B) and pressure medium (C) which squeezes between anvils to form gaskets (D). X-rays diffracted at an angle of 2θ pass through the transparent anvil (E), through the collimating slits (F) and to the detectors .

Chapter 2

Measurement of activation volume in olivine

ABSTRACT

Olivine is the most abundant and amongst the weakest phases in the upper mantle, and thus its rheological properties have a critical role in controlling convective flow in this region. A persistent obstacle to understanding the behavior of olivine in the mantle has been the difficulty of determining activation volume (V^*), the influence of hydrostatic pressure on high-temperature creep. The bulk of previous studies examining V^* were conducted at low pressure (<300 MPa) and over small pressure ranges in gas-medium deformation machines, limiting precision and raising questions about application to deep geological conditions. We conducted numerous deformation experiments on dry polycrystalline olivine in the D-DIA apparatus at pressures from 1.5 to 9 GPa at 1373 K. Stress and strain were measured in-situ with synchrotron x-rays. Refinement of diffraction techniques has allowed stress resolution of ±0.02 GPa. For the pressure range in this study, we have measured an activation volume of 14 ± 3 cm^3/mol for dry polycrystalline San Carlos olivine. This is a substantial pressure effect, representing a large viscosity increase across the range of pressures from the top to bottom of the upper mantle. The diffraction technique used for stress measurement in these experiments also illuminates the relative strength of differently oriented grains in our polycrystalline sample, providing new experimental evidence for change in dominant dislocation slip systems in olivine with pressure.

2.1 Introduction

As a major component of the Earth's upper mantle, olivine $(Mg,Fe)_2SiO_4$, and its rheological properties are critical to our understanding of tectonic systems and mantle dynamics. Although pressure has only a mild effect on the strength of rocks, conditions in the upper mantle range from 0.3 to 15 GPa, and thus even a very small effect of pressure on olivine strength may profoundly influence mantle evolution. Activation volume (V^*), which measures the response of steady-state deformation of a rock to hydrostatic pressure (P), is given by

$$\dot{\varepsilon} \propto \exp -\left(\frac{E^* + PV^*}{RT}\right)$$

where $\dot{\varepsilon}$ is strain rate, R is the gas constant, T is temperature, and E^* is activation energy, the effect of temperature (Durham et al. 2009). Laboratory measurements of V^* have historically been hampered by the small range of hydrostatic pressures producible by deformation machines. Until recently, pressure in most deformation experiments has been limited to a maximum of ~2 GPa, in the Griggs apparatus, which suffers from poorly resolved stress measurement due to a solid confining medium with finite strength, and the lack of an internal load cell (Ross, Ave Lallemant, and Carter 1980). Gas-medium deformation machines, such as the Paterson apparatus, offer far better stress resolution, but can typically only generate hydrostatic pressure well under 1 GPa (Hirth and Kohlstedt 1996; Hirth and Kohlstedt 2003; Hansen, Zimmerman, and Kohlstedt 2011). Measurements of experimentally

accessible proxies for creep strength in olivine polycrystals, such as dislocation recovery and silicon diffusion, have yielded a wide range of values for V^*, from $V^* \approx 0$ cm^3/mol to $V^* = 30$ cm^3/mol (Kohlstedt, Nichols, and Hornack 1980; Karato, Rubie, and Yan 1993). The recent availability of very bright synchrotron x-rays has helped motivate the development of a new generation of high pressure apparatus, including the deformation-DIA (D-DIA), a solid medium device designed to impart deformation at fixed pressures of up to 15 GPa (Wang et al. 2003). This vastly expanded range of pressures, combined with the ability to precisely measure stress conditions within samples, now provides an ideal tool to better determine V^* for olivine and other mantle minerals.

The physics determining V^* is likely to be complex, due to the various interdependent deformation mechanisms that are active in the deep earth. Water-induced transitions in dominant slip system for dislocation creep of olivine have long been of interest (Hirth and Kohlstedt 1996; Jung and Karato 2001). The new generation of high-pressure equipment has been utilized to show that dominant slip systems may also be influenced by pressure. Raterron et al. (2009) deformed oriented olivine single crystals at high pressure in the D-DIA, demonstrating that while the (010)[100] "a-slip" system is weak at low pressure, it is strongly pressure dependent ($V^* = 12 \pm 4$ cm^3/mol), while the (010)[001] "c-slip" system is not strongly pressure dependent ($V^* = 3 \pm 4$ cm^3/mol), and is weaker than a-slip at high pressure.

Ohuchi et al. (2011) attempted to explain observed lithospheric seismic anisotropy by deforming fine-grained polycrystalline olivine at high pressure (up to 7.3 GPa) and temperature in simple shear geometry, also using D-DIA. In these experiments, they confirmed a fabric transition in their samples consistent with a shift from [100](010) to [001](0*kl*) slip, induced by an increase in pressure and temperature. However, relative strength of these competing slip system has heretofore been not been observed in situ in a deforming polycrystalline sample.

A series of equipment and software developments has been implemented in the last several years, vastly improving D-DIA experimental techniques (Durham et al. 2009; Mei et al. 2010). At the NSLS X17B2 beam line, which uses an energy-dispersive x-ray diffraction system, this includes a new 10-element detector assembly and refined collimating slits for collection of diffracted x-rays (Durham et al. 2009; Weidner et al. 2010). New calibration, peak-fitting and stress-calculation programs have in turn been used to speed up and improve stress measurement, allowing for real-time knowledge of stress conditions in ongoing experiments. An improved sample assembly made of soft-fired pyrophyllite and mullite has also allowed for blowout-free deformation experiments on dry olivine samples at pressures up to 9 GPa.

Improved diffraction systems have also revealed new details of the stress state in polycrystalline samples. Because of the way that our detectors

measure the lattice spacing of specific populations of grains, our diffraction patterns now allow some measurement of plastic anisotropy and stress heterogeneity during throughout deformation.

We report here a series of deformation experiments on dry polycrystalline olivine, conducted at 1373 K, and spanning a pressure range of 1.5 to 9 GPa, with stress measured from synchrotron x-ray diffraction (XRD) with uncertainty of ±20 MPa. The pressure range achieved in these experiments is triple that of similar earlier D-DIA studies (Durham et al. 2009; Mei et al. 2010), while stress measurement has become 5 times more precise (Weidner et al. 2010), due to continuing developments in our sample cell and diffraction technique, respectively.

A better determination of V^* has remained critical to our understanding of the upper mantle. Building upon nascent attempts to solve this problem with the new generation of high pressure machines, we are now able to operate the D-DIA near to the limits of design, allowing us to report more a more robust, more precise value for V^*, and a more detailed understanding of the mechanisms that determine this physical property.

2.2 Methods

2.2.1 D-DIA Setup and x-ray configuration

Experiments were conducted using the D-DIA (Figure 1-1) installed at beamline X17B2 at the National Synchrotron Light Source (Wang et al.

2003). During pressurization, the anvils press into the pyrophyllite and mullite pressure medium surrounding the sample. During deformation, the state of stress in the sample is axisymmetric, with the maximum stress σ_1 applied vertically. An x-ray beam with a cross section of approximately 100 mm x 100 mm passes through the narrow gap between horizontal anvils and through the center of the sample (Figure 1-2, inset). We use a "white" x-ray beam (~20 to ~100 keV). Downstream of the D-DIA, tungsten collimating slits define a cone of fixed Bragg angle $2\theta \approx 6.45°$ to the x-ray beam. A semi-circular array of x-ray detectors beyond the conical collimator thus detects only those x rays diffracted at 2θ. There are ten such detector elements, nine of which are spaced evenly from azimuth $\phi = -90°$ to $+90°$ around the path of the x-ray beam, $\phi = -90°$ and $+90°$ being vertical, while a tenth element sits at $\phi = 180°$. One or both of the horizontal anvils on the conical collimator side of the D-DIA (Figure 1-2) are made of x-ray transparent sintered polycrystalline diamond (SD), allowing diffracted x-rays line-of-sight from the sample to the detectors. When only one transparent anvil is used, the 10^{th} detector element is blocked and inoperable. The 4 or 5 opaque anvils are made of tungsten carbide (WC), which provide better fracture resistance at a lower cost than SD anvils, but partially obscure the sample in the x-radiographs in which deformation is observed.

2.2.2 Sample assembly

To maintain a strictly dry deformation environment we utilize a "hybrid" assembly with mullite interior for dryness and pyrophyllite exterior (Durham et al. 2009). Post-test Fourier transform infrared spectroscopy (FTIR) has confirmed low water contents in sample olivine, 35-40 H/10^6Si (Durham et al. 2009). To improve pressure efficiency, the pyrophyllite is fired at 1140 K for 3 hours prior to final construction of the sample assembly.

A complete sample assembly is a ~6.3 mm cube, filling the volume defined by the D-DIA anvils (Figure 2-1). At the center of the assembly is the cylindrical, polycrystalline olivine sample. Sample material is a mixture of 95% San Carlos olivine and 5% enstatite, hot pressed at 1473 K in a Ni capsule at 300 MPa gas confining pressure. The material has an initial mean grain size of ~3-5 μm and a porosity of <1%. Deformation samples ~1.2 mm in length and ~0.9 mm in diameter are cored from the hot-pressed boule. The olivine sample is wrapped in a cylindrical "can" of nickel foil, which acts both as a Ni-NiO redox buffer and also as a strain marker visible in x-radiographs. Above and below the olivine samples are solid alumina pistons and porous alumina plugs. The cylindrical olivine/alumina column fits within an MgO sleeve, which acts as a soft pressure medium, evenly distributing stress on the sample. The MgO, in turn, fits within a graphite sleeve, the furnace. The entire cylindrical column of sample, pistons, plugs, pressure medium, and

furnace then slides into a central hole connecting two of the faces of a hybrid mullite/pyrophyllite cube to complete the cell.

2.2.3 Stress, pressure, and strain measurement

The state of stress in the sample is determined from energy-dispersive diffraction (ED XRD) of synchrotron x-rays directly within the sample. Bragg's law yields the lattice spacing, d_{hkl}, of the (*hkl*) plane (in Miller indices) responsible for the diffraction. Under load, the lattice spacing will change from an initial value d_0 to a value of d (Figure 2-2), and the elastic strain $1 - d/d_0$ is converted to stress using what is essentially Hooke's Law (Singh 1993) and the known elastic constants for olivine (Kumazawa and Anderson 1969). An axisymmetric state of stress in a polycrystalline sample can be determined in ED XRD using a minimum of two non-redundant detectors of diffracted x rays. Our system uses up to 10 detectors for improved resolution (Figure 1-2).

Stress measurements in this study are based on the Bragg reflections (130), (131), (112), (122), and sometimes (140), as their corresponding diffraction peaks fall over a broad range of energy in the olivine diffraction pattern, and these peaks can usually be fit with consistent accuracy and precision. To calculate pressure, the mean d-spacing for each (*hkl*) is found, using the d-spacings measured in all detectors. This mean spacing is then used to calculate an average unit cell volume for olivine in the sample in-situ.

Pressure is then calculated from this unit cell volume and known elastic moduli using a 3rd order Birch-Murnaghan equation of state. The diffraction system is typically calibrated immediately before or after an experiment using ^{57}Co, which provides a fixed energy point for reference, and with powder diffraction standards of known lattice spacing (Al_2O_3 as well as the olivine sample itself at room P,T).

Diffraction patterns for stress measurement are analyzed using Plot85, an energy-dispersive peak fitting software package developed at the Mineral Physics Institute at Stony Brook University. Diffraction exposure times are usually 600 s, which is roughly the same amount of time required for automated peak fitting in Plot85 and subsequent stress calculation from the previous exposure, allowing us to monitor stress and pressure conditions in quasi-real-time during experiments.

2.2.4 Uncertainty in pressure/stress measurement

Careful calibration of our diffraction system must be carried out to ensure accuracy and precision. Tests of repeatability using standard materials and olivine samples (both at room temperature and pressure, and at high pressure) indicate that we can consistently measure stress with a reproducibility of ±20 MPa, based largely on the scale of the apparent scatter in stress in our creep curves. We have under best circumstances been able to achieve ±10 MPa (Weidner et al. 2010). It's worth noting, however, that

because the diffraction system measures a non-random sampling of grains within our sample, the differential stresses measured from each *hkl* reflection may not be exactly representative of the average stress state of all sample grains. While it's difficult to say what the "average" state of stress is for our sample (as a "bulk" stress measurement similar to that from a load cell in a gas apparatus), our measurement of is representative of the real variations in stress within the material. Because the diffraction system samples different populations of grains with each detector and set of olivine lattice planes, we have a measurement of stress heterogeneity, both as function of grain orientation, and throughout different regions of the sample. Nonetheless, we are able to estimate the stresses measured from several lattice planes to reach reasonably precise values for "bulk" stress, such that they can be used to determine olivine flow law parameters.

Pressure calculation relies on an averaging of d-spacings from three different (*hkl*) planes and many detectors, and the uncertainty due to diffraction technique inaccuracy is very small. However, since temperature must be included in the Birch-Murnaghan equation of state calculation, T uncertainty propagates to the estimation of pressure.

2.2.5 Temperature measurement

To provide a simpler and more stable mechanical environment to the sample, we conduct our deformation experiments without the benefit of a

thermocouple, and rely on calibrated curves of heater power vs. temperature to control temperature. Previous work with hydrostatic devices has shown that if sufficient care is taken to standardize sample assemblies, power vs. temperature curves which are determined by calibration experiments are highly reproducible (Durham and Rubie 1998) (Figure 2-3). To test the possibility that the same is true for non-hydrostatic devices, we have run numerous off-synchrotron calibration exercises, wherein a thermocouple was positioned exactly at the center of the deformation assembly, in place of the sample. Power-time-temperature relationship was monitored over the course of what would be an ordinary deformation experiment that included use of the differential rams.

2.2.6 Uncertainty in Temperature Measurement

The primary obstacle to making precise rheological measurements in the D-DIA is the difficulty of precisely controlling and measuring temperature during experiments. Direct temperature measurement with thermocouples is likely to be ineffectual because of the difficulty of placing thermocouples in a fixed position near the sample. Temperature gradients in D-DIA sample assemblies are very large, as high as 100 K mm^{-1} (Liebermann and Wang 1992; Rubie 1999), and thus even a very small movement of thermocouples within the cell will produce large, unpredictable errors in temperature.

Using our thermocouple-free cell, uncertainty in experimental temperatures in can be estimated from a number of possible sources. For our purposes, uncertainty in temperature should be defined in four ways, which are hereafter designated Types 1-4:

1. *Absolute uncertainty:* the possible error between nominal (target) temperature for a given experiment and the true temperature.
2. *Systematic calibration uncertainty:* The possible error between the temperature estimated from calibration experiments for a given furnace power and the temperature generated in a typical olivine sample assembly for the same power. Type 2 uncertainty is included in the estimation of Type 1, and thus must be less than or equal to Type 1 uncertainty. The source of Type 2 uncertainty is minor differences between the design of the calibration assemblies and the design of the olivine deformation assemblies. The principal difference is the presence of a pair of 125-μm-diameter W/Re thermocouple wires, with an alumina sleeve of 0.8 mm outer diameter running radially across the sample assembly. Our calculations show that these wires and sleeves cause only a small downward perturbation of temperature, at most 20 K.
3. *Relative uncertainty run-to-run:* The possible difference between temperatures in different olivine assemblies (as opposed to calibration assemblies) held at the same furnace power. Type 3 uncertainty is

expected to be very small relative to the repeatability of calibration experiments, because the olivine sample assemblies used in deformation are simpler (without the thermocouple and sheath), require little hand-fabrication, and use parts that are mass-manufactured with very tight tolerances.

4. *Relative uncertainty step-to-step:* The possible difference between temperatures in different deformation steps of the same experiment. Because each step is done with the very same sample assembly, and because the slope of the relationship between heater power and temperature is extremely repeatable between calibrations, Type 4 uncertainty is expected to be very small relative to Types 1 & 2. Because Type 4 uncertainty is relatively small, it allows us determine flow law parameters with greater precision by comparing steps of multiple-step experiments.

Reproducibility of T vs. power curves for calibration experiments gives us a baseline for the absolute (Type 1) uncertainty of temperature. We found calibration runs to be repeatable with a maximum variation of ±50 K. There is also a small amount of absolute uncertainty due to interpolation between calibration points for experiments where an identical calibration experiment has not been conducted. The other significant contributor is Type 2, detailed above, as Types 3 and 4 are accounted for in the ±50 K repeatability estimate

for calibration experiments. We thus conservatively estimate that the absolute temperature uncertainty for our experiments is ±100 K.

Run-to-run and step-to-step (Types 3 and 4) uncertainties are especially difficult to precisely quantify. In the run-to-run case, we can reasonable assume that an upper limit on repeatability is the ±50 K observed in calibration samples, which, as discussed above, are much more difficult to build to precise specifications. For steps of the same experiment, we expect the uncertainty to be much smaller, based mostly on the change in furnace behavior between different pressure steps. A conservative estimate of Type 4 temperature uncertainty is ±25 K.

2.2.7 Experimental procedure

The experiment begins with hydrostatic compression of the sample at room temperature, and once at pressure, the sample is heated to the desired run temperature. In most cases we anneal at (P,T) for at least an hour before proceeding with deformation. The experiments are designed to have a constant strain rate, which we execute by setting a fixed differential ram speed (top and bottom rams move inward at the same rate) and monitoring sample length by x-ray imaging. The ram speed is sometimes slowed later during deformation to maintain the constant strain rate. Upon commencement of deformation, 600-s diffraction patterns are taken nearly back-to-back, sometimes alternating between the top and center of sample to

check for stress gradients. At the beginning of collection for each pattern, an x-radiograph image is taken of the sample, allowing the measurement of sample length and subsequent calculation of accumulated strain. When changing experimental conditions between steps, the sample is quenched to room temperature over ~10 min before pressure is increased or decreased, allowing us to reach higher pressures with better stability and efficiency.

2.3 Results and analysis:

A total of seven samples were deformed for this study in 16 different run "steps" (sets of constant $\dot{\varepsilon}$, σ, P ,T). Figure 2-4 shows stress-strain curves for the seven runs, and the results are summarized in Table 2-1. Experiments were conducted at pressures from 1.8 to 8.7 GPa and strain rates from 0.44 x 10^{-5} s^{-1} to 2.50 x 10^{-5} s^{-1}. All experiments were nominally at 1373 K, except for Step 3 of run San 282, conducted at 1473 K. Each (*hkl*) Bragg reflection produces its own creep curve, for reasons of plastic anisotropy, discussed below, and the results for the most prominent 4 (or 5) reflections are plotted in Figure 2-4. While it is possible to analyze each (*hkl*) curve separately for a V*, given the sparse and occasionally noisy data, we reduce the several curves to a single value of steady-state flow stress, choosing by eye a value near the middle of the spread between curves (the faint horizontal lines in Figure 2-4), and it is these values that are tabulated in Table 2-1. On the basis of elasto-plastic self-consistent (EPSC) modeling, Burnley and Zhang

(2008) warn that the "macroscopic" stress in such circumstances may reach or even exceed the highest stress registered by any of the (*hkl*) reflections, so the value of "stress" in Table 2 may be valid for calculating V* but must be further scrutinized before comparing with macroscopic stress measurements. For purposes of graphical analysis in Figure 2-6, Table 2-1 also includes value for flow stress converted to a common T (1373 K) and $\dot{\varepsilon}$ (10^{-5} s^{-1}).

Five of the experiments included steps at two or more pressures, allowing us to compare the strength of the same sample at different pressures while holding the other experimental conditions nearly constant. It is plain to see from Figure 2-4 that P has a strong and positive effect on the strength of our olivine samples. In order derive a value for V* based on Figure 2-6, we need to consider matter of noise and plastic anisotropy.

The near-zero values of stress measured in the low-P steps in Runs 277 and 280 are inconsistent with other measurements in this paper and with the body of work on polycrystalline olivine at P>300 MPa (Hansen, Zimmerman, and Kohlstedt 2011; Hirth and Kohlstedt 2003). Work hardening, apparent in Runs 275 and 289, for example, may play a role, but does not explain how the low stress can be maintained through $\varepsilon > 0.10$. Explaining in terms of temperature inaccuracy requires an error of 100 K in T, assuming a value for E^* of 500 kJ/mol (Equation 1), and seems to be inconsistent with the reasonable (in terms of run-to-run consistency at least) value of stress in the higher-P steps of those runs.

As mentioned above, the work of Burnley and Zhang (2008) suggests that our estimate of stress for purposes of calculating V*, the faint horizontal lines in Figure 2-4, may be systematically inaccurate. We can now identify another possible systematic error in that estimate resulting from a combination of plastic anisotropy, i.e., the existence of slip systems (lattice planes and directions that offer lower resistance to plastic flow), and stress anisotropy, i.e., the existence of a non-zero deviatoric stress. Where the normal to the diffracting lattice plane (called the diffraction vector **k**) is subparallel to the axis of maximum principal stress σ_1, i.e., vertical, the subpopulation of grains in that particular diffraction condition have a more symmetrical crystallographic relationship with respect to the stress axes than do subpopulations of grains with diffraction vectors off vertical (this geometry is illustrated in Figure 2-7). Put in other words, when the sample is under load, every grain seen by the x-ray detectors 1 and 9 (Figure 1-2) will have identical resolved shear stress (i.e., Schmid factor) on a given slip system. The Schmid factor ranges from 0.5, where the resolved shear stress on a slip system is a maximum, to 0, where the slip plane and/or the slip direction is normal to the direction of s_1 and the resolved shear stress is 0. The remaining detectors, for which **k** is far from the axis of σ_1, will see a subpopulation of grains with a range of Schmid factors on that same slip system. Diffraction peaks from off-vertical detectors will therefore broaden slightly with respect to those from vertical detectors, and if the broadening is

in any way asymmetric, then the calculated state of lattice strain, and therefore stress, will be affected. At this point we simply acknowledge that a systematic miscalculation of the state of stress is plausible; the impact this detector "bias" on flow parameters in general, or V* in particular, is difficult for us to even estimate.

Based on SEM analysis of samples deformed previously at similar conditions (figures in Chapter 3), we expect that grain size and microstructure will remain stable through the course of experiments. The amount of accumulated strain in individual deformation steps is likely insufficient to produce strong lattice preferred orientation (Figure 3-7).

*2.3.1 Estimation of V**

Plotting the data from Table 2-1 on axes of log σ vs P at fixed T and $\dot{\varepsilon}$ allows a visualization of the effect of P on the strength of dry polycrystalline olivine (Figure 2-6). The points in Figure 2-6 are taken from the strain rate- and temperature-adjusted columns of Table 2-1, and the error bars are based on the analysis above. It is clear that the P effect on strength within any given run is strongly positive (Figure 2-4). V* values calculated from individual multi-step runs are shown in Figure 2-5. The agreement in slope, i.e., V* between steps of any single run is generally good, but the vertical positions of such lines in absolute stress are badly scattered. We attribute this to the very large run-to-run T uncertainty (>100 K), discussed above. Of

the five P-stepped runs in Table 2 (only 289 was single-step), two are anomalously weak at low P, although have reasonable strengths at high pressure. Insufficient strain to reach steady-state flow conditions, as revealed by single-step, low-P run San 289, provides a possible explanation. Discounting the two anomalously weak steps, we estimate from the values in Table 2-1 that $V^* = 14 \pm 3$ cm^3/mol.

2.3.2 Effect of pressure on dominant slip system:

Although olivine has a number of known slip systems, one system usually slips more easily than others, producing a large portion of the total deformation. An important effect of slip system dominance is the development of lattice-preferred orientation (LPO), fabric in geologic usage, with manifestations such as elastic anisotropy of the upper mantle (e.g. Margheriti et al. 1996; Ekström and Dziewonski 1998; Plomerova et al. 2006). Another effect is the variation of differential stress with diffraction condition seen in the laboratory (Figure 2-7), which arises from the same detector sampling bias discussed in the previous section. The geometric requirement that a particular **k** lie in the plane defined by the line of the x-ray beam and the point location of the detector limits the range of Schmid factors for grains meeting that requirement. This is perhaps easiest to visualize in the most symmetric geometry of the vertical detector–stress

coordinate system (discussed above and shown in Figure 2-7), where the allowable Schmid factor for any given slip system is single valued.

This information may be used to infer the most likely dominant slip system for deformation. Analysis of the (130) reflection is particularly convenient, because it appears as a strong single peak in diffraction patterns, and because of its orientation in the olivine unit cell (Figure 2-7). Of particular interest are two dislocation slip systems, (010)[100] and (010)[001], which are likely candidates to be the dominant slip systems at a range of mantle conditions (Jung and Karato 2001; Raterron et al. 2009; Ohuchi et al. 2011; Hilairet et al. 2012). When grains are oriented such that (130) will produce diffraction to detectors 1 and 9 (at ϕ=0° and ϕ=180° azimuth respectively), the olivine [001] direction will necessarily will lie near the plane normal to the direction of greatest compressive stress. As a result, little shear stress will be resolved in the [001] direction, and the (010)[001] slip system will be inactive (Schmid factor ≈0). The (010)[100] slip system, however, will be favorably oriented for slip, with Schmid factor ≈0.5. We see a robust trend in the (130) measurement of stress relative to other (*hkl*). For deformation above ~6 GPa, the (130) consistently reports the highest differential stress of any (*hkl*) we are able to use for stress measurement, implying that the ϕ= ±90° orientation is particularly strong, despite the favorable orientation for (010)[100]. This suggests that the (010)[100] slip system is not dominant at these experimental conditions. In lower pressure

experiments (<6 GPa), the (130) plane reports stresses amidst the other (*hkl*), indicating a greater role of (010)[100] in deformation.

2.4 Discussion

A V^* value of 11-17 $cm^3\ mol^{-1}$ for olivine would have a large effect on the mechanical behavior of the upper mantle. At a constant stress, an activation volume of 14 cm^3mol^{-1} would lead to a reduction of strain rate of seven orders of magnitude at the bottom of the upper mantle due to pressure alone. Thus, in order to reconcile the predicted strength of mantle rocks with otherwise equivalent models that do not account for strengthening effect of pressure, the thermal structure of the mantle would have to be hotter. Our estimation of V^* is consistent within uncertainty with earlier D-DIA studies by Durham et al. (2009) and Raterron et al. (2009), polycrystalline and single-crystal deformation respectively, which employed less precise iterations of the same energy-dispersive diffraction technique. Kawazoe et al. (2009) also reported a similar range for V^* (15-20 $cm^3\ mol^{-1}$) from torsion experiments on dry polycrystalline olivine in the rotational drickhamer apparatus (RDA).

Our evidence for a pressure-induced transition in dominant slip system from (010)[100] to (010)[001] slip is consistent with the findings of two recent high-pressure studies on polycrystalline olivine, which rely in post-deformation fabrics and in-situ measurements, respectively. Ohuchi et al. (2011) deformed polycrystalline samples in a simple shear geometry to

produce high shear strains (near 1 in most experiments) and found fabrics consistent with (010)[100] domination in experiments conducted at 1473 K up to 5.2 GPa pressure, and a different fabric, suggesting (010)[001] slip, at 7.6 GPa. The single-crystal experiments by Raterron et al. (2009) also show that the (010)[100] slip system is suppressed at high pressure. Hilairet et al. (2012) produced an early demonstration of the enormous potential for in-situ analysis of texture and deformation mechanisms using synchrotron XRD. They conducted D-DIA tests on polycrystalline olivine in pure shear (as in this study), and used a monochromatic x-ray diffraction system for stress measurement. Evidence for dominant mechanisms was collected with two data analysis techniques. The first uses the software MAUD (e.g. Lutterotti et al. 2007), which is able to construct an inverse pole figure (representing grain orientations in the sample) directly from diffraction patterns (a capability pursued in Chapter 4). Thus, they obtain in-situ estimations of texture in deforming samples, in this case at 3.0 and 5.1 GPa. Secondly, they used elasto-plastic self-consistent modeling (e.g. Turner and Tomé 1994) in comparison with stress measurements from specific *hkl* in deformation experiments. Their results also suggested a large contribution of (010)[100] at pressures below 3-4 GPa, decreasing relative to (010)[001] with increasing pressure. Lutterroti et al. (2007) noted that the transition in dominant slip system might occur over a wide range of pressures. Because of the apparently complex interplay of mechanisms in high-pressure creep, they suggest that

the quest for "the V^*", a single canonical value to describe the behavior of olivine over a wide range of conditions, should cease in favor of a careful analysis of the mechanisms themselves. This point is well justified: certainly more work on individual mechanisms is necessary for a complete understanding of high-pressure creep. Our experiments, indeed, are likely to sample a range of conditions that will produce different deformation regimes. Because we deform samples in pure shear to relatively small strain, determination of mechanisms from post-deformation microstructures is difficult. Our prediction of the role of various mechanisms is estimated from flow law parameters determined by gas-medium deformation experiments, mostly around 300 MPa (Hirth and Kohlstedt 2003; Hansen, Zimmerman, and Kohlstedt 2011), which suggest that the dry grain boundary sliding accommodated by dislocation creep (dry GBS) is the most important. The role of GBS and other mechanisms in D-DIA experiments at similar conditions is extensively discussed in Chapter 3.

Although a mechanism-by-mechanism approach should also be pursued, measuring the direct effect of pressure on olivine aggregates remains important in a practical sense, allowing for drastic improvements in models of large-scale mantle dynamics. As techniques are refined, we will further be able to dissect the complex physics behind the observed pressure effect, and our view of mantle will become still clearer.

2.5 Conclusions

This study was undertaken with the primary goal of producing and analyzing a robust dataset on the effect of pressure on the mechanical behavior of olivine. We conclude that the activation volume of dry olivine, over a wide range of upper mantle conditions is 14 ± 3 cm^3/mol. Our diffraction data also show evidence of a transition in dominant slip system as a result of increasing pressure, to a slip system other than (010)[100].

Acknowledgments:

We are grateful for the support of the Office of Basic Energy Sciences of the Department of Energy (Grant No. DE-FG2-07ER15839), and from the National Science Foundation (Grant No. EAR-0968863). We also benefitted greatly from the help of Kurt Leinenweber, for the supply and co-development of our cell parts. Thanks also to the beam line staff at NSLS X17B2, which in turn is supported by the Consortium on Material Properties Research in the Earth Sciences (COMPRES).

Bibliography

Durham, W. B., S. Mei, D. L. Kohlstedt, L. Wang, and N. A. Dixon. 2009. "New Measurements of Activation Volume in Olivine under Anhydrous Conditions." *Physics of the Earth and Planetary Interiors* 172 (1-2): 67–73.

Durham, W. B., and D. C. Rubie. 1998. "Can the Multianvil Apparatus Really Be Used for High Pressure Deformation Experiments?" *Properties of the Earth and Planetary Materials at High Pressure and Temperature* Geophysical Monograph (101): 63–70.

Ekström, Göran, and Adam M. Dziewonski. 1998. "The Unique Anisotropy of the Pacific Upper Mantle." *Nature* 394 (6689): 168–72.

Hansen, LN, ME Zimmerman, and DL Kohlstedt. 2011. "Grain Boundary Sliding in San Carlos Olivine: Flow Law Parameters and Crystallographic-Preferred Orientation." *Journal of Geophysical Research* 116 (B8): B08201.

Hilairet, Nadège, Yanbin Wang, Takeshi Sanehira, Sébastien Merkel, and Shenghua Mei. 2012. "Deformation of Olivine under Mantle Conditions: An in Situ High-pressure, High-temperature Study Using Monochromatic Synchrotron Radiation." *Journal of Geophysical Research: Solid Earth (1978–2012)* 117 (B1).

Hirth, G., and D. Kohlstedt. 2003. "Rheology of the Upper Mantle and the Mantle Wedge: A View from the Experimentalists." *Geophysical Monograph* 138: 83–105.

Hirth, G., and D. L. Kohlstedt. 1996. "Water in the Oceanic Upper Mantle: Implications for Rheology, Melt Extraction and the Evolution of the Lithosphere." *Earth and Planetary Science Letters* 144 (1-2): 93–108.

Jung, H., and S. Karato. 2001. "Water-Induced Fabric Transitions in Olivine." *Science* 293 (5534): 1460–63.

Karato, S.I., D.C. Rubie, and H. Yan. 1993. "Dislocation Recovery in Olivine under Deep Upper Mantle Conditions: Implications for Creep and Diffusion." *Journal of Geophysical Research* 98 (B6): 9761–68.

Kawazoe, T., S. Karato, K. Otsuka, Z. Jing, and M. Mookherjee. 2009. "Shear Deformation of Dry Polycrystalline Olivine under Deep Upper Mantle Conditions Using a Rotational Drickamer Apparatus (RDA)." *Physics of the Earth and Planetary Interiors* 174 (1): 128–37.

Kohlstedt, DL, HPK Nichols, and P. Hornack. 1980. "The Effect of Pressure on the Rate of Dislocation Recovery in Olivine." *Journal of Geophysical Research* 85 (B6): 3122–30.

Kumazawa, M., and O. L. Anderson. 1969. "Elastic Moduli, Pressure Derivatives, and Temperature Derivatives of Single-Crystal Olivine and Single-Crystal Forsterite." *J. Geophys. Res* 74 (5): 5961–77.

Liebermann, Robert C., and Yanbin Wang. 1992. "Characterization of Sample Environment in a Uniaxial Split-Sphere Apparatus." *Geophysical Monograph Series* 67: 19–31.

Lutterotti, L., M. Bortolotti, G. Ischia, I. Lonardelli, and H.-R. Wenk. 2007. "Rietveld Texture Analysis from Diffraction Images." *Zeitschrift Fur Kristallographie Supplements* 2007: 125–30.

Margheriti, L., C. Nostro, M. Cocco, and A. Amato. 1996. "Seismic Anisotropy beneath the Northern Apennines (Italy) and Its Tectonic Implications." *Geophysical Research Letters* 23 (20): 2721–24.

Mei, S., AM Suzuki, DL Kohlstedt, NA Dixon, and WB Durham. 2010. "Experimental Constraints on the Strength of the Lithospheric Mantle." *J. Geophys. Res* 115: B08204.

Ohuchi, T., T. Kawazoe, Y. Nishihara, N. Nishiyama, and T. Irifune. 2011. "High Pressure and Temperature Fabric Transitions in Olivine and Variations in Upper Mantle Seismic Anisotropy." *Earth and Planetary Science Letters.*

Plomerova, J., L. Margheriti, J. Park, V. Babuška, S. Pondrelli, L. Vecsey, D. Piccinini, V. Levin, P. Baccheschi, and S. Salimbeni. 2006. "Seismic Anisotropy beneath the Northern Apennines (Italy): Mantle Flow or Lithosphere Fabric?" *Earth and Planetary Science Letters* 247 (1): 157–70.

Raterron, P., E. Amiguet, J. Chen, L. Li, and P. Cordier. 2009. "Experimental Deformation of Olivine Single Crystals at Mantle Pressures and Temperatures." *Physics of the Earth and Planetary Interiors* 172 (1-2): 74–83.

Ross, J.V., H.G. Ave Lallemant, and N.L. Carter. 1980. "Stress Dependence of Recrystallized-Grain and Subgrain Size in Olivine." *Tectonophysics* 70 (1): 39–61.

Rubie, D. C. 1999. "Characterising the Sample Environment in Multianvil High-Pressure Experiments." *Phase Transitions: A Multinational Journal* 68 (3): 431–51.

Singh, A. K. 1993. "The Lattice Strains in a Specimen (cubic System) Compressed Nonhydrostatically in an Opposed Anvil Device." *Journal of Applied Physics* 73 (9): 4278.

Turner, P. A., and C. N. Tomé. 1994. "A Study of Residual Stresses in Zircaloy-2 with Rod Texture." *Acta Metallurgica et Materialia* 42 (12): 4143–53.

Wang, Y., W. B. Durham, I. C. Getting, and D. J. Weidner. 2003. "The Deformation-DIA: A New Apparatus for High Temperature Triaxial Deformation to Pressures up to 15 GPa." *Review of Scientific Instruments* 74: 3002.

Weidner, D. J., M. T. Vaughan, L. Wang, H. Long, L. Li, N. A. Dixon, and W. B. Durham. 2010. "Precise Stress Measurements with White Synchrotron Xrays." *Review of Scientific Instruments.*

Run	Press Load (T)	Target T (°C)	Approx. Pressure (GPa)	Avg Diff Stress (MPa)	Strain Rate (10^-5 s^-1)	Strain Rate Adjusted Stress (10^-5), n=3.5	T Adjusted Stress 1373 K
San 250[1]	60	1100	7.1	370	0.65	418.46	418.46
[2]	97	1100	8.7	730	0.92	747.60	747.60
[3]	97	1100	8.7	no measurement			
[4]	50	1100	1.8	50	1.31	46.29	46.29
San 275[1]	30	1100	3.45	25	0.83	26.37	26.37
[2]	100	1100	8	515	0.44	651.15	651.15
San 277[1]	40	1100	4.6	2	1.17	1.91	1.91
[2]	80	1100	7.25	175	0.50	213.33	213.33
San 280[1]	30	1100	3.45	30	1.02	29.83	29.83
San 280[2]	80	1100	7.25	435	0.49	533.34	533.34
San 280[3]	80	1200	6.25	110	0.71	121.31	239.55
San 282[1]	50	1100	5.3	450	2.50	346.35	346.35
San 282[2]	50	1100	4.75	20	1.00	20.00	20.00
San 289	10	1100	2.1	190	0.54	226.58	226.58
San 292[1]	10	1100	1.5	125	0.52	150.51	150.51
San 292[2]	60	1100	6.5	600	0.53	718.95	718.95

Table 2-1. Experimental conditions. Stress values are approximate averages of the stresses calculated from multiple olivine lattice planes. "Strain Rate Adjusted Stress", the second column from left, is the stress from each experiment adjusted to a common strain rate using a stress exponent of (n=3.5, See equation 1). "T Adjusted Stress" is the Strain Rate Adjusted Stress adjusted to a common temperature of 1373 K.

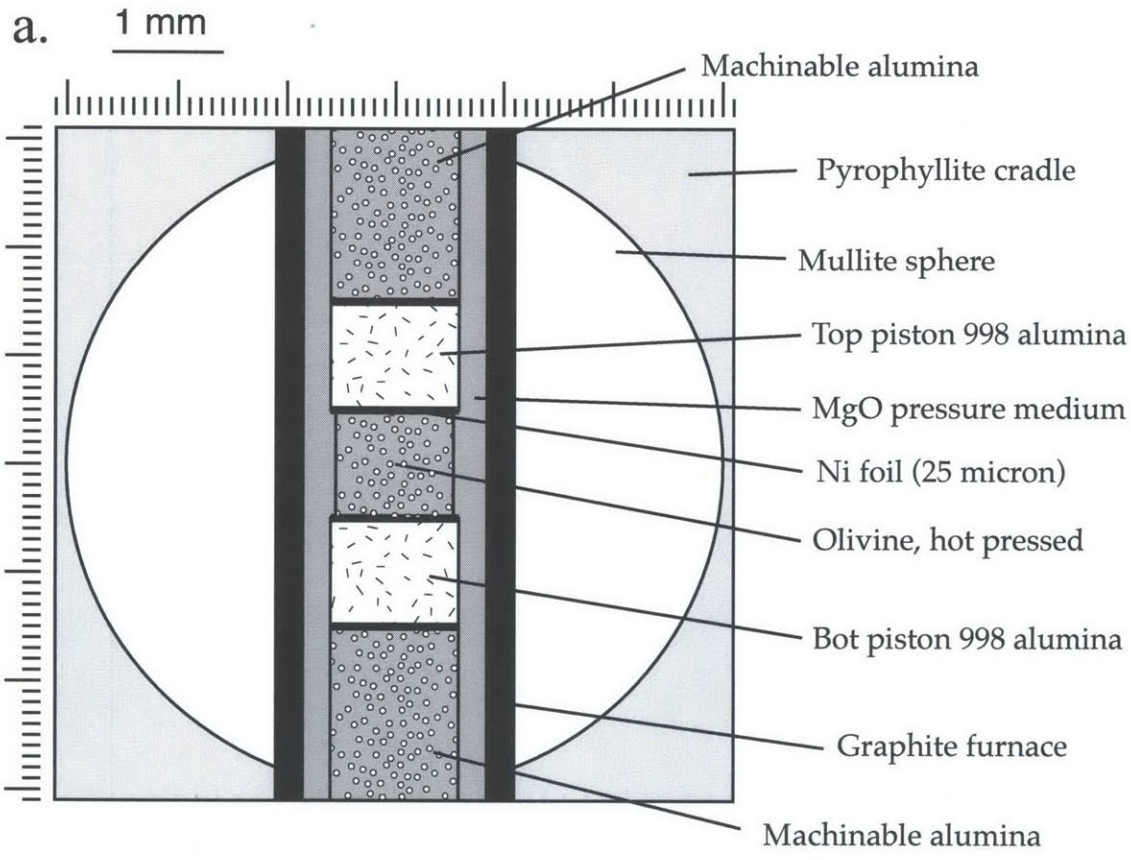

Figure 2-1. Schematic diagram of a typical sample, to scale.

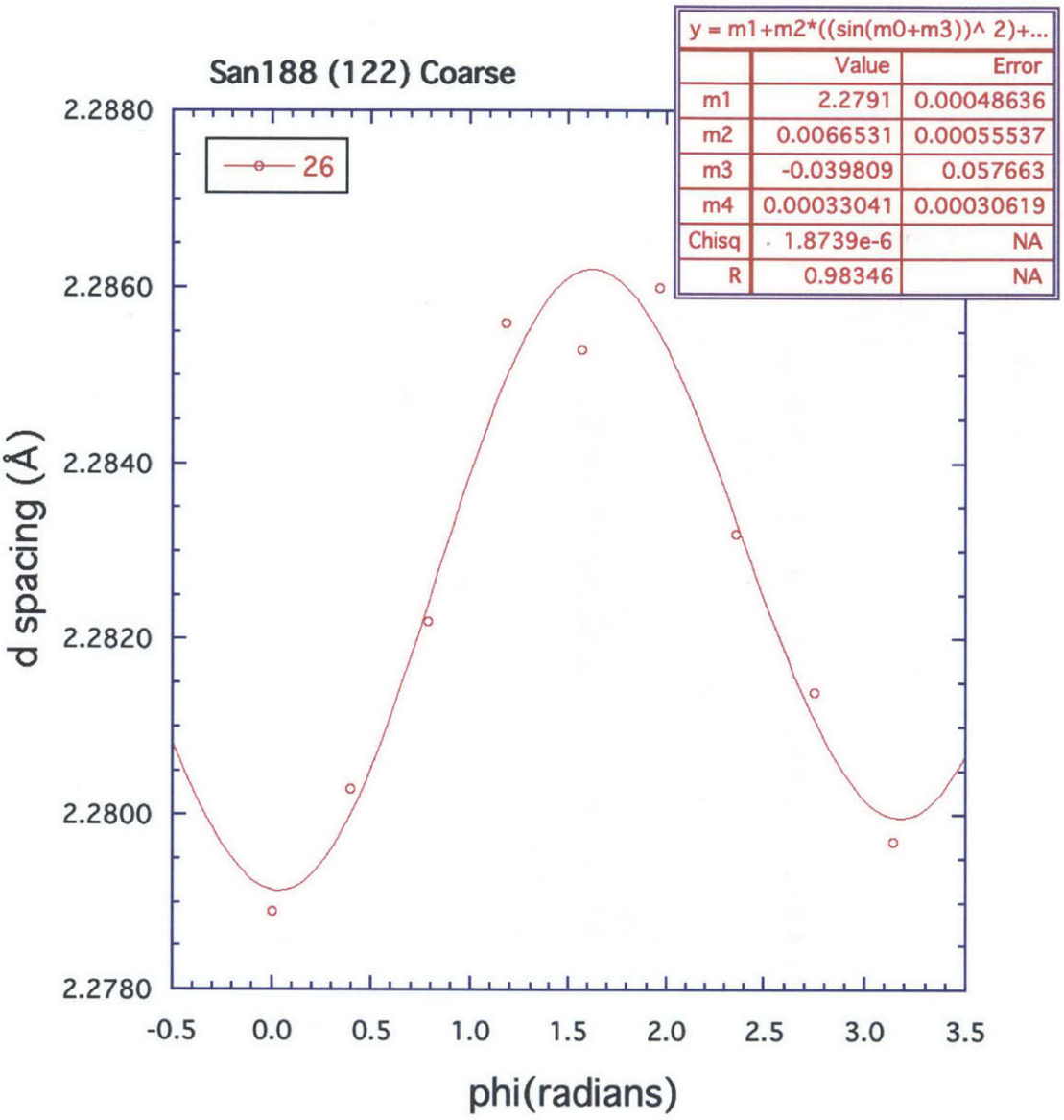

Figure 2-2. Example curve fit to d-spacing vs. detector angle for one peak in a 9-detector diffraction pattern [lattice plane: (122), pattern San188-26]. Each point in the plot represents the d-spacing of (122) planes as measured by a different detector. The d-spacing is smallest at 0 and л, as expected for an axisymmetric stress state with the greatest compressive stress in the vertical direction. Parameters from the curve fit are used to calculate the state of differential stress in the sample.

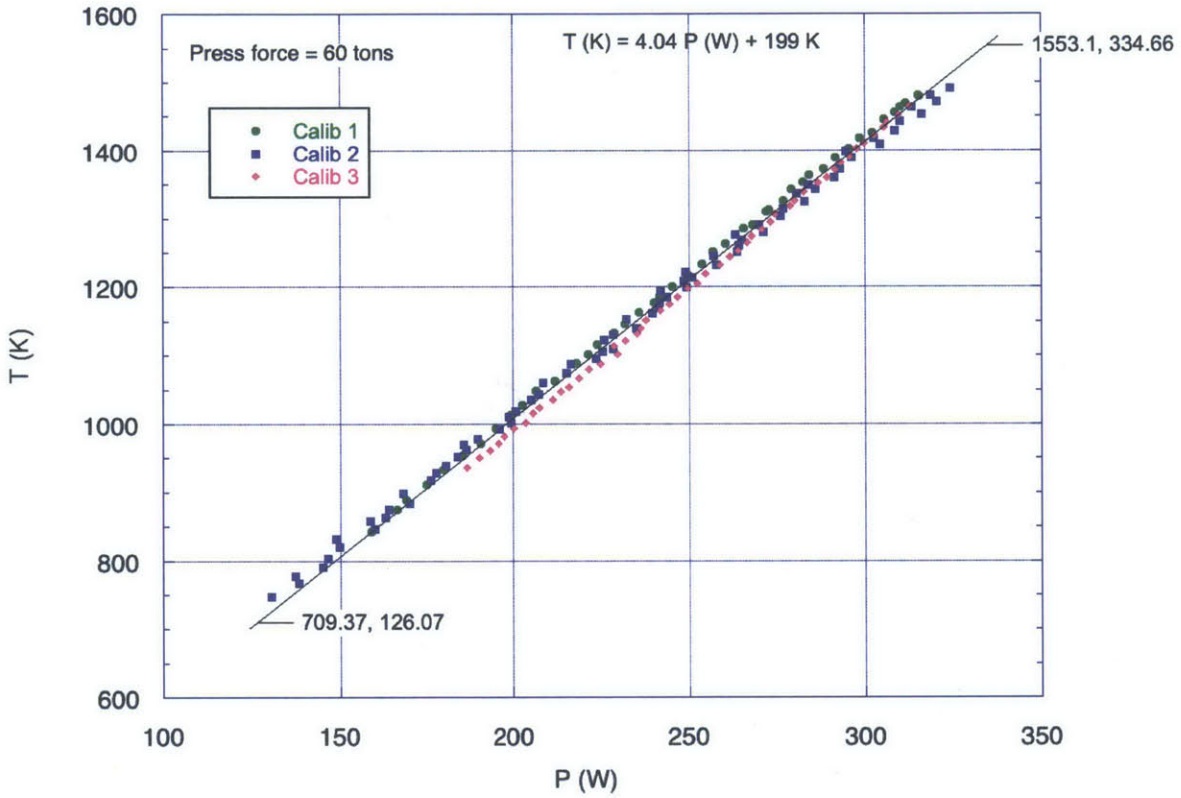

Figure 2-3. Calibration of temperature vs. furnace power at the center of a hybrid sample assembly. Calibrations were done several months apart (courtesy of W. Durham).

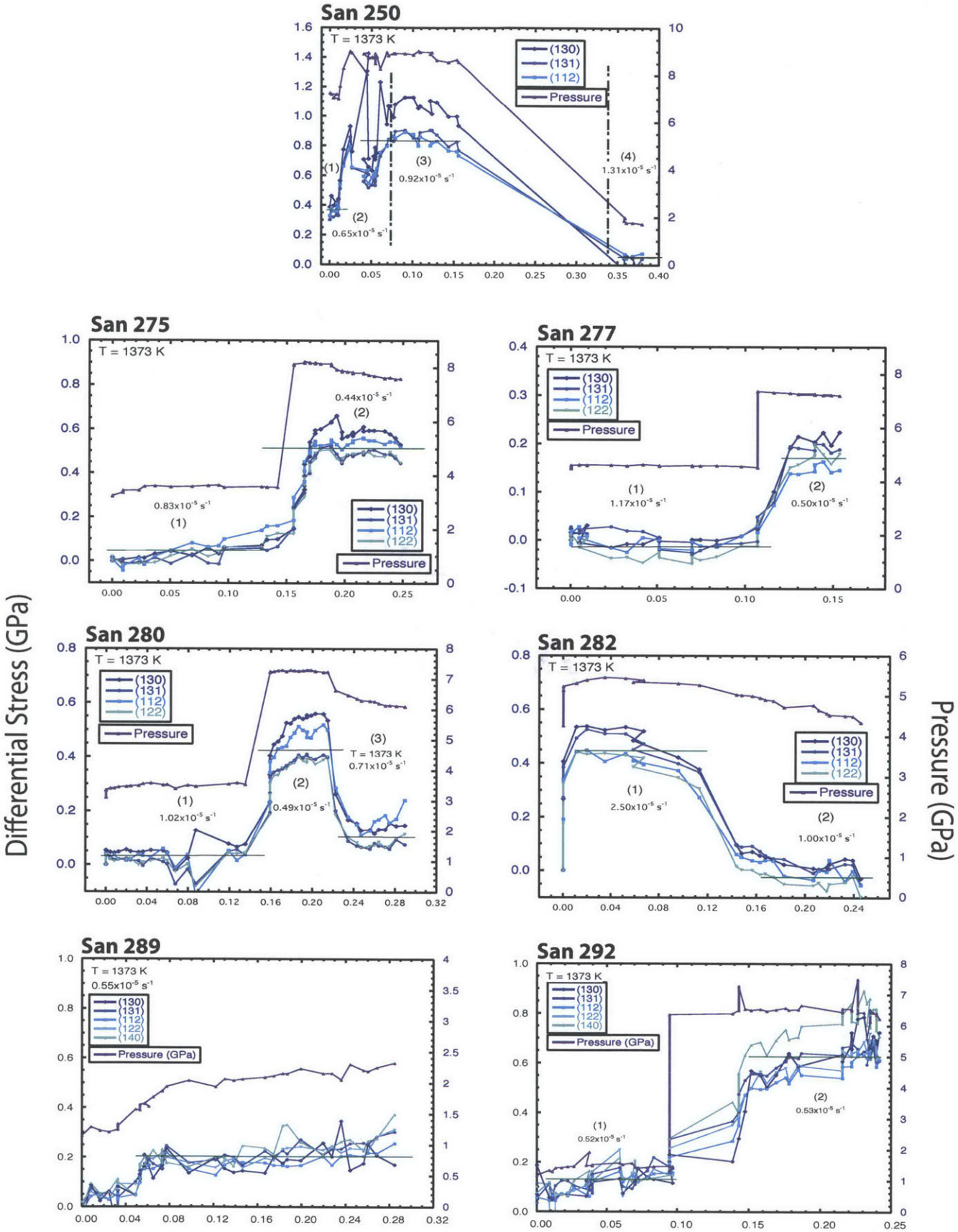

Figure 2-4. Creep curves for all experiments, showing pressure and stress calculated from several olivine *hkl*. All experiments except San 282 and San 289 feature multiple pressure steps, for the measurement of *V**.

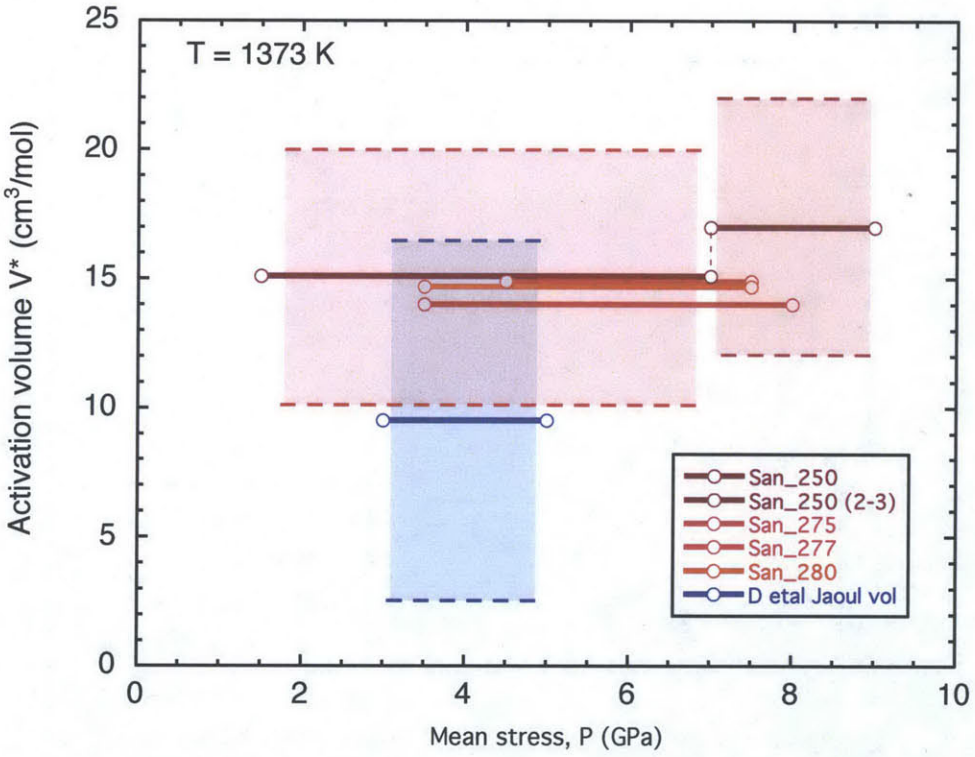

Figure 2-5. Activation volume for individual runs. Each red-colored bar represents the pressure range of an individual multiple-step experiment, indicated on the horizontal axis, while position on the vertical axis represents the V* calculated from that experiment. Shaded regions represent uncertainties.

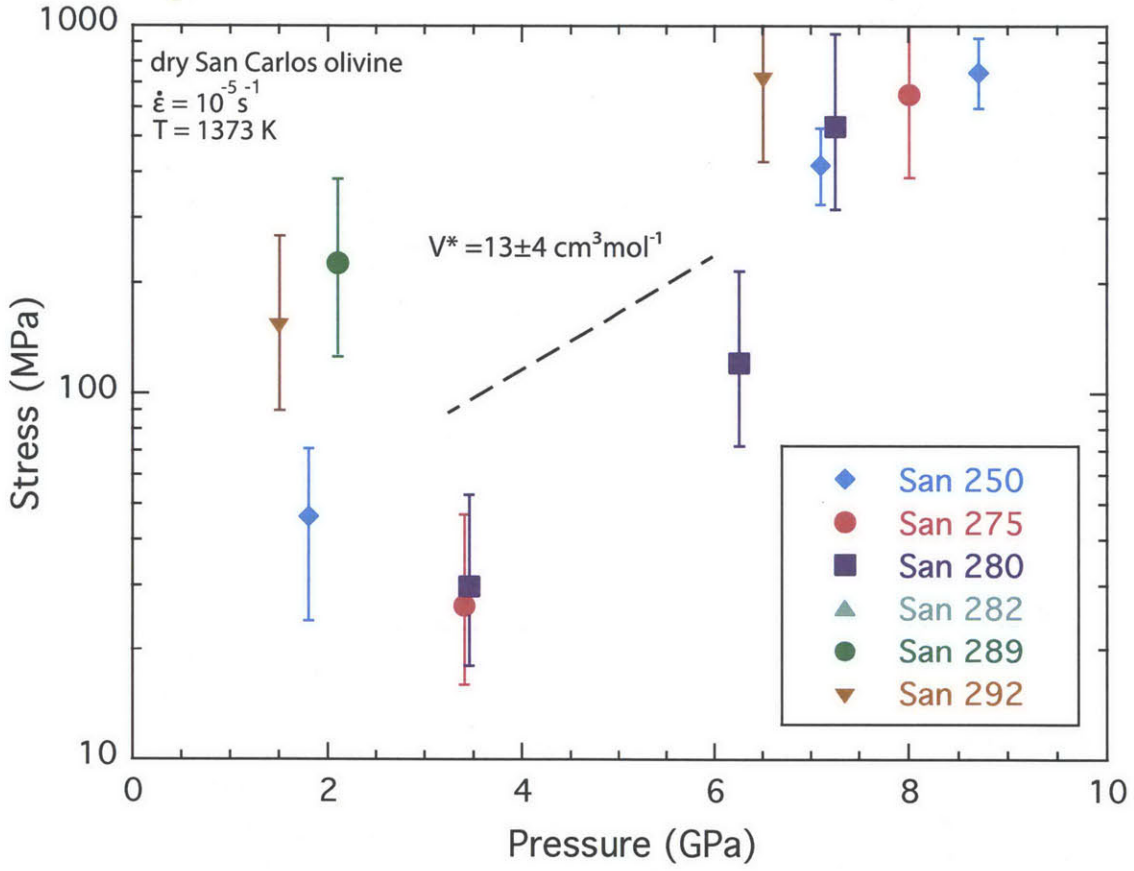

Figure 2-6. Plot showing the relationship between mean differential stress and pressure for each experimental step. There is significant offset in the absolute magnitude of stress between different experiments (likely due to high uncertainty in our absolute measurement of temperature), but a robust trend in the relative stresses at different pressure steps in the same experiments.

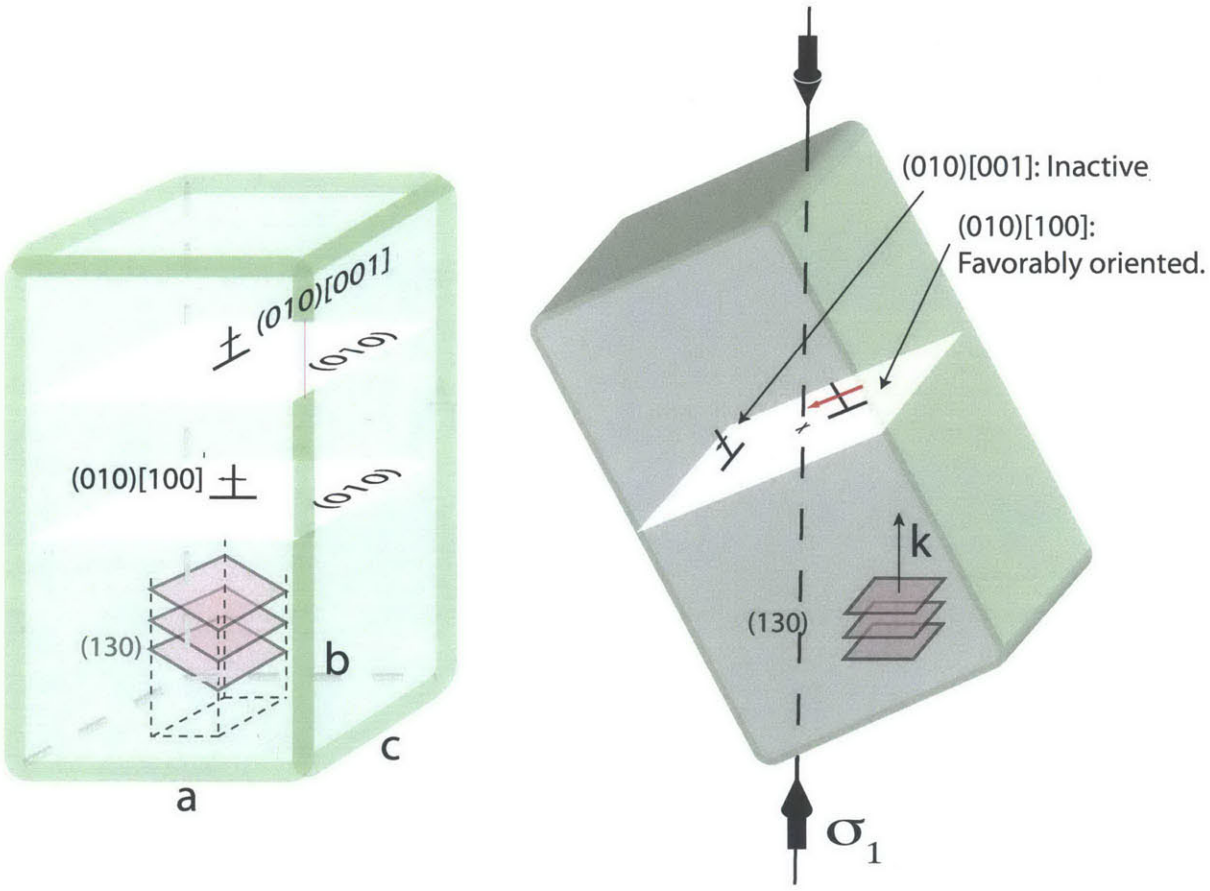

FIgure 2-7. Above left is the unit cell of the olivine crystal structure. The orientation of the (130) lattice planes are identified in red, and the (010) "b" plane is in white. Two important slip systems for olivine are identifed, (010)[001] and (010)[100]. At right is the same unit cell, oriented with respect to the axis of greatest compressive stress, such that (130) will diffract x-rays to detectors 1 and 9 (see Fig . 2). In this orientation, the (010)[100] slip system is oriented favorably for slip, while the (010)[001] slip system is inactive. In experiments with P < 6 GPa, high stresses measured from (130) indicate that this orientation is particularly strong, and thus (010)[100] slip is not likely to be a dominant slip system at those conditions.

Chapter 3

Grain size sensitivity, dynamic recrystallization, and deformation mechanisms in olivine at high pressure

ABSTRACT

A number of the deformation mechanisms in olivine aggregates are affected by grain size. In order to determine role of different mechanisms during deformation at upper mantle conditions, the D-DIA apparatus was used to deform dry polycrystalline olivine in a dual sample cell with samples of two distinct grain sizes. The cell was designed to provide similar stress and temperature conditions for both the coarse-grained (50-70 μm) and fine-grained (3-10 μm) samples. Deformation was observed *in situ* with the use of x-radiographs. Stress was measured in both halves of the sample assembly (fine and coarse), with the use of synchrotron x-ray diffraction equipment. Improvements to the diffraction system allowed comparison of stresses between sample halves at much higher resolution than in previous D-DIA experiments, such that olivine flow law parameters previously determined in other deformation experiments may be tested. Both the coarse and fine grain sizes deformed at similar strain rates, inconsistent with expectations of deformation with a large component of strain by grain-size sensitive mechanisms. Coarse grain samples showed evidence of grain size reduction early in experiments, likely to a ~15 μm mean size observed in the samples post-deformation. The rate of grain size reduction is observable in situ, in diffraction patterns, providing a measurement at the rate of recrystallization. Post-experiment SEM images showed a large variation in grain size, and some apparent shear zones in the initially coarse samples, suggesting a large role of strain localization and recrystallization in deformation. In one case, significantly higher differential stress was observed in the fine-grained sample than the adjacent coarse sample in the same experiment, challenging the current understanding of stress conditions in D-DIA sample assemblies.

3.1 Introduction

Measurements of the mechanical properties of olivine are essential to our understanding of mantle processes, as olivine is the most abundant upper mantle phase and is also the weakest under most of the likely range of mantle conditions (Duffy and Anderson 1989; Gwanmesia et al. 1990; Kirby 1983). As mentioned in previous chapters, studies of polyphase aggregates containing olivine and the other major upper mantle minerals (pyroxenes, pyrope) have confirmed that rheological behavior is typically olivine-dominated (Hitchings, Paterson, and Bitmead 1989; Tullis, Horowitz, and Tullis 1991). Both experimental observations and theoretical treatments have shown that the rheological behavior of many crystalline materials is well described by a power law relationship between strain rate ($\dot{\varepsilon}$) and differential stress (σ). Dry polycrystalline olivine has been shown to obey a law of the form

$$\dot{\varepsilon} = A\sigma^n d^{-p} \exp\left(-\frac{E^* + PV^*}{RT}\right)$$

where A is a constant, n is the stress exponent, E^* is activation energy, and R is the gas constant (Hirth and Kohlstedt 2003). The activation volume (V^*) measures the response of high temperature, steady-state deformation to hydrostatic pressure (Sammis, Smith, and Schubert 1981). T is absolute temperature, P is pressure and d is grain size. Parameters in the olivine flow law have been studied and constrained for a number of deformation

mechanisms (e.g., dislocation creep, diffusion creep), largely by deforming samples in gas apparatus with P≤300 MPa (e.g., Hirth and Kohlstedt 1995).

With the much greater pressure capabilities of the D-DIA apparatus, it is now possible to test the applicability of flow laws determined at low pressures to the conditions of the deeper mantle. Like lower-pressure gas medium deformation machines, the D-DIA is capable of independently controlling pressure (mean stress) and differential stress (σ_1-σ_3, σ_1 is maximum principal stress, compressive is stress positive by geosciences convention). However, technical difficulties have limited the scope and accuracy of early D-DIA measurements. Recently, several equipment updates have led to great improvement in D-DIA performance. The updates include the introduction of a new sample assembly design, and a higher-resolution x-ray detection system. The result is a nearly tenfold reduction in stress uncertainty (~100 MPa to ~10 MPa), and much lower frequency of mechanical failure during experiments. The improved performance of the D-DIA has made it increasingly promising as a tool for high-pressure rheological measurements.

The primary goal of this study was to test widely used flow laws for grain-size sensitive grain-boundary sliding (GBS) and diffusion creep, and size-insensitive dislocation creep. Accurate flow law parameters are particularly important in interpreting recent high-pressure olivine deformation experiments performed on synthetic fine-grained (d < 100 μm)

polycrystals, which are usually conducted at conditions near the boundary of fields dominated by dislocation and diffusion-driven mechanisms (Hirth and Kohlstedt 2003). The large uncertainties in existing measurements of V^* and other material properties make it particularly difficult to determine which mechanism of deformation will be most active at high pressure. By deforming two samples with different grain sizes under the same conditions, grain-size sensitivity of deformation can be observed and checked against previously resolved values for each mechanism.

Because the grain sizes in the coarser-grained samples proved to be unstable at our experimental conditions, we were also able to demonstrate another unique capability of our energy-dispersive diffraction system: in situ monitoring of grain size. Our slit system only collects x-rays diffracted by grains at specific orientations relative to the path of the beam. We refer to such grains, those that are observed by detectors, as meeting the "diffraction condition". Because there are fewer grains per volume in coarse-grained samples, fewer grains meet the diffraction condition. This is apparent in coarse-grain diffraction patterns, where peak intensity varies widely depending on which orientations happen to be in the path of the beam. By watching the peak intensities in diffraction patterns throughout the run, we can clearly see the reduction of grain sizes in samples, in situ, providing insight into recrystallization kinetics.

3.2 Methods

3.2.1 D-DIA setup

Experiments were conducted in a D-DIA (Figure 1-1) at the National Synchrotron Light Source, beamline X17B2. The D-DIA features six opposing anvils, which define a cubic volume. A single main pump operates all rams simultaneously by pressing down on guide blocks (B, Fig. 1-1) in which the horizontal rams and differential rams are set. Individual hydraulic pumps also control the differential rams, allowing them to be advanced faster or slower than the horizontal rams. To increase differential stress while maintaining constant pressure (mean stress), the differential rams are advanced as the main ram is simultaneously reversed. Thus, the state of stress in the sample is axisymmetric, with σ_1 applied vertically (Figure 1-2). When at pressure, the anvils press into material surrounding the sample, until the anvils gap is only 100-200 μm. The x-ray beam passes through the narrow gap between horizontal anvils and through the center of the sample (Fig. 1-2, inset). One of the downstream anvils is made of x-ray transparent sintered polycrystalline diamond (SD) such that photons diffracted in the sample can pass through the anvil. Downstream of the D-DIA, tungsten collimating slits define a fixed angle, 2θ, to the x-ray beam. X-rays diffracted at 2θ, the aforementioned "diffraction condition", will then go through the

tungsten collimating slits and to an assembly of detectors. As in previous chapters, nine detector elements are spaced evenly from -90° to 90 azimuth (ϕ) around the path of the x-ray beam (ϕ = -90°, 90° being vertical). In these experiments, the tenth detector at ϕ = 180° is blocked by an opaque anvil, and thus is not used for diffraction measurements. The five opaque anvils are made from tungsten carbide (WC), which provides better fracture resistance at a lower cost than SD anvils, but also partially obscure the sample in radiographs, with which deformation is observed.

3.2.2 Sample assembly

Early experiments demonstrated the need for a sample assembly that is both mechanically stable (i.e. provides consistent, evenly-distributed stress on the sample) and that maintains the desired water content. A "hybrid" assembly combining a mullite inner sphere for dryness and an unfired pyrophyllite exterior was recently developed (Durham et al. 2009), and has greatly lowered the rate of failed experiments. Post-test Fourier transform infrared spectroscopy (FTIR) has confirmed low water contents in sample olivine, 35-40 H/Si[6]. The experiments in this study use a nearly identical pressure medium to those from the previous chapter on V^*, except that the pyrophyllite in this case in unfired, and as a result, slightly softer.

A complete sample assembly is a ~6.3 mm cube, filling the volume defined by the D-DIA anvils (Figure 3-1). At the center of the assembly is the

olivine. In this study, there are separate fine and coarse-grained samples (FG and CG, henceforth) contained within each cell. Each sample is composed of powdered San Carlos olivine, hot pressed in a Ni capsule at 300 MPa confining pressure and 1473 K for 4 h in a gas apparatus at the University of Minnesota, by S. Mei. The FG sample has an initial mean grain size of ~3-8 μm and a porosity of <1%. The CG sample has an initial mean grain size of ~50-70 μm, and slightly higher porosity, demonstrated by compaction upon hydrostatic compression at the beginning of experiments. The olivine samples are wrapped in a cylindrical "can" of nickel foil, which acts both as a Ni-NiO redox buffer and strain marker visible in x-radiographs. Above and below the olivine samples are solid alumina pistons and porous alumina plugs. The cylindrical olivine/alumina column fits within a boron nitride sleeve (BN), which acts as a pressure medium, evenly distributing stress on the sample. The BN, in turn, fits within a graphite sleeve, the furnace. This entire cylindrical assembly (sample, pistons, plugs, pressure medium, furnace) then slides into a drill hole in the face of a hybrid mullite/pyrophyllite cube to complete the cell.

3.2.3 Stress and strain measurement

Diffraction of synchrotron x-rays is used to determine the state of stress in samples. From diffraction, Bragg's law yields the spacing of sample lattice planes for each detector. Thus, lattice spacing is known as a function

of angle to applied load. Elastic strain is then calculated and then converted to stress using Hooke's law and known elastic constants (Singh 1993).

Stress measurements here are based on spacing of olivine lattice planes associated with Miller indices (*hkl*) = (130), (131), (112), and (122), as the corresponding diffraction peaks can be fit with consistent accuracy. In CG samples, the (130) and (122) peaks tend to be less reliable, often having low intensity. To calculate pressure, the mean spacing for each (*hkl*) is found. The average lattice parameters of the olivine unit cell are then estimated by least squares fitting to the combined lattice spacing measurements from the three most reliable (*hkl*) [usually (131), (112), (122)]. Pressure for each diffraction pattern is then calculated from the unit cell volume and known elastic moduli with a 3rd order Birch-Murnaghan equation of state. The diffraction system is periodically calibrated using fixed energy sources (^{57}Co) and standards of known lattice spacing (Al_2O_3).

The measurement of stress with x-rays is required for the D-DIA to be useful as a precise deformation apparatus, but comes with difficulties. The calculation of stress requires careful fitting of diffraction patterns to find spacing of lattice planes. These patterns may be noisy, and fitting typically has required a trained eye and many hours. In past D-DIA experiments, uncertainties in stress have been large, as stress calculation is very sensitive to error in the fitting of diffraction peaks. To combat the precision issue, new x-ray collimating slits were installed during this study, resulting in sharper,

more distinct peaks that can be fit automatically and with much greater accuracy (Figure 3-2). In addition, the number of x-ray detection elements was increased from 6 to 9. As mentioned above, each detector only samples grains in which lattice planes are oriented such that they meet the diffraction condition. Thus, not all grains in the path of the incident beam are represented in diffraction patterns, and those represented are not randomly oriented. More detectors allows for a larger population of grains to be used for stress calculation, further reducing uncertainty.

Diffraction patterns taken of the samples before and during deformation are analyzed using Plot85, an energy-dispersive peak fitting software package developed at the Mineral Physics Institute at Stony Brook University. Plot85 identifies peak positions in the energy domain and calculates lattice spacing using Bragg's law. As mentioned above, the elastic strain measured by diffraction and the elastic moduli of olivine are used to calculate differential stress, by the method of (Singh 1993).

As discussed in the previous chapter, differential stresses measured from different olivine lattice planes, $\sigma(hkl)$ henceforth, may be different. This is a consequence of plastic anisotropy (Merkel 2006): As in most crystalline materials, dislocations in olivine can slip on several different slip systems (Durham and Goetze 1977; Durham, Goetze, and Blake 1977; Carter and Ave'Lallemant 1970). As a result, grains favorably oriented for slip will yield at lower stresses, while stronger neighboring grains will bear more load.

Because of the fixed 2θ used for diffraction in this study, each σ(*hkl*) is measured from grains with particular orientations relative to the macroscopic state of stress on the sample. The grains sampled in calculating one σ(*hkl*) may be strong or weak relative to another group of orientations.

3.2.4 Temperature Measurement

The inclusion of a thermocouple in a D-DIA sample assembly is problematic, often causing complex tractions and tilting of the sample. To avoid these issues, a thermocouple is not included in the cell design. Instead, the amount of power to the furnace required for a given set of experimental conditions is determined through a separate calibration experiment. As discussed in Chapter 2, each calibration experiment is done with identical methods (e.g., time of pressurization, ram load), but the normal olivine sample is replaced with an alumina "dummy sample" with a thermocouple in the center. Earlier studies in hydrostatic devices have demonstrated that power v. temperature curves determined by calibration experiments are highly reproducible (Durham, Rubie, and Series 1998) (Figure 2-3). It should be noted that large temperature gradients are expected within the sample column, 100 K/mm or more (Liebermann and Wang 1992).

3.2.5 Experimental Procedure

At the beginning of an experiment, the sample cell is first compressed hydrostatically with the use of only the main ram pump. During pressurization, the differential ram pumps may be adjusted slightly to suppress any lengthening or shortening of the sample. Pressurization typically takes 2-3 h, depending on the pressure conditions of the experiment. Upon reaching the desired load, power through the graphite furnace is increased to bring the sample to run temperature.

After completion of pressurization and heating, the differential rams are then set to a constant speed, beginning deformation of the sample. The ram speed is sometimes slowed later during deformation to maintain a constant strain rate. Upon commencement of deformation, 600 s diffraction patterns are taken nearly back-to-back, alternating between the FG and CG samples. At the beginning of collection for each pattern, an x-radiograph image is taken of the sample, allowing the measurement of sample length and subsequent calculation of accumulated strain.

3.3 Results and analysis

Four experiments were conducted for this study, two before the installation of the new collimating slits and detectors, and two after. In the first experiment (San 179), the samples and pistons were too long, causing the samples to buckle during initial pressurization. Although the strain rate

behavior of the two samples in San 179 were similar to other runs, the principal stress axes may have tilted significantly. In subsequent experiments the column pieces were shorter, and differential ram speeds were decreased by a factor of four, in an effort to produce lower differential stresses and higher quality diffraction patterns. The third experiment, San 187, was conducted at 1573 K in an effort to further lower stresses in the sample, but at the risk of causing grain growth, which did indeed occur. Several hours into the run, diffraction patterns from both the CG and FG samples showed "graininess", or inconsistency in the intensity of olivine peaks. Some peaks were completely absent from many diffraction patterns. Highly inconsistent peak intensities are characteristic of poor sampling statistics, where diffracted x-rays from only a small number of grains reach the detectors. The patterns became less grainy towards the end of San 187, but accurate stress calculation was impossible for most of the run. In the remaining two experiments (San 181 and San 188) samples were successfully deformed to strains of ~25%, and are the basis of this study (Figure 3-4). Temperature was 1473 K for both San 181 and San 188 although pressures were ~5 to ~5.5 GPa in San 181, compared to ~2.5 to ~3 GPa for San 188. In all cases, pressure dropped slowly during deformation. At the time which the experiments for this study were conducted, real-time calculation of pressure was not available, making it difficult correct for this trend.

3.3.1 Strain rates

In both San 181 and San 188, strain rates became roughly constant after a transient period to ~5% strain (Figure 3-5). In both experiments, strain rates were about the same for FG and CG samples. In San 181, the CG sample strained slightly faster, while in San 188, the FG sample strained slightly faster.

3.3.2 Stress conditions

Because the fine and coarse samples are pressed back-to-back between alumina pistons and confined on the sides by BN, it was expected that the stress conditions for both samples would be the same during steady state deformation. In the higher-pressure San 181, $\sigma(131)$ and $\sigma(112)$ were roughly the same in both coarse and fine-grained samples (Figure 3-4). In San 188 however, all $\sigma(hkl)$ in the coarse-grained samples were consistently 70-100 MPa higher than in their fine-grained counterparts. While both sample parts in San 188 work hardened throughout most of the experiment, those in San 181 weakened dramatically through the first 5-6% of strain. After the first 6%, San 181 stress rose to 450 MPa, slightly stronger than San 188, which was conducted at lower pressure.

The cause of higher stress in San 188 CG is likely due to the strength of the BN pressure medium, which causes σ_3 to increase as the sample pushes against it. Thus, a faster-deforming sample will feel more resistance

from the medium, resulting in lower differential stress, but slightly higher pressure. Indeed, pressure was between 200-300 MPa higher in San 188 FG than in San 188 CG after ~5% strain.

3.3.3 Estimation of uncertainty in stress, strain, and temperature measurements

One primary source of uncertainty in stress measurements is the limited precision with which lattice spacing can be determined from diffraction patterns. Systematic error may result from miscalibration of the system, which can be checked only at the beginning and end of experiments. Calibration error is expected to be small (<5 MPa), based on the scale of changes in energy and 2θ that is observed between experiments. The main factor in uncertainty of x-ray stress measurements is the precision with which diffraction peaks position can be identified in the energy domain of diffraction patterns (i.e. the accuracy of peak-fitting software). The primary measure of accuracy is scatter of measured stresses around a best-fit curve, which has been reduced with the new collimating slits to ±10 MPa (Weidner et al. 2010). The other expected source of uncertainty in stress results from uncertainty in temperature. Temperature uncertainty makes little difference in calculating differential stress, but has a large effect on pressure. With the current technique, temperature error may be over 75 K, which would lead to pressure uncertainty of ~300 MPa (Durham et al. 2009). Because of the

excellent reproducibility of furnace power vs. T curves, the relative difference between temperature measurements in subsequent experiments is expected to be much less (<25 K). It should also be noted that pressure and differential stress are calculated from patterns taken near the center of the sample, and thus are representative of this region.

Sample length is measured directly from radiographs (Figure 3-3), and thus the only source of uncertainty is in the resolution of the radiographs, and user error in consistently measuring the length of the sample in the same way.

3.3.4 Microstructural observation and interpretation

Samples were deformed to over 20% in order to facilitate post-experiment analysis of dominant slip system and resultant lattice-preferred orientation (LPO). Scanning electron microscope (SEM) and electron backscatter diffraction (EBSD) observations were conducted at the University of Minnesota characterization facility with A. Suzuki. Orientation contrast (OC) images of samples show that the mean grain size of the CG samples was significantly reduced during deformation, to only 10-20 μm. Images of San 181 are especially clear, showing some 60 μm grains still intact, but also large regions of reduced grain size (Figure 3-6). San 188 CG appears to have a mix of grain sizes as well. FG samples were similar to the starting material, with 3-6 μm grains. EBSD observations showed only very weak LPO in all

samples (Figure 3-7), most likely indicative of (010)[100] or (010)[001] slip, which are expected for dislocation glide in olivine. The relatively weak fabric in samples is evidence against dislocation creep as the primary mechanism of deformation, although the strains reached in these experiments may be insufficient to produce a strong texture.

While microstructure in FG samples changed little throughout the experiments in this study, profound changes in the microstructure of CG samples were observed both in-situ (in diffraction patterns) and in post-experiment analysis, suggesting that reworking of CG material likely had a large influence on the behavior of these aggregates during deformation. During both San 188 and San 181, peak intensity in diffraction patterns from CG samples became more consistent at ~5% strain (Figure 3-8). This is interpreted as evidence for relatively quick grain size reduction by dynamic recrystallization. The size of recrystallized grains has been extensively studied (Jung and Karato 2001; Karato, Toriumi, and Fujii 1980; Ross, Ave Lallemant, and Carter 1980), and is primarily dependent on stress, in the absence of water. Thus, as stress stabilized in San 188 and San 181, grain size likely also stabilized for the remainder of the experiment. This assertion is supported by consistency in diffraction patterns beyond ~6% strain in either experiment. Regions of fine grains visible in the San 181 CG sample suggest possible strain localization (Poirier 1980; White et al. 1980). San 188

CG contains some fine grains, but appears to be more homogenous than San 181 (San 188 images are far less clear).

The occurrence of substantial grain size reduction in CG samples presents an opportunity to demonstrate the capability of our diffraction system for observing sample microstructures in situ.

As mentioned above, samples with large grain sizes are likely to have fewer grains that meet the "diffraction condition" for each of our detectors. This shows up in diffraction patterns as irregularity in the size of diffraction peaks. If no grain within the path of the beam meets the diffraction condition for a particular detector, the associated peak will not appear in a the diffraction pattern collected by that detector. On the other hand, if a single grain does meet the diffraction condition, and that grain takes up a large volume within the path of the beam, the associated diffraction peak will be very large. We refer to this irregularity in diffraction patterns as "graininess". Graininess is frequently observed in samples where high experimental temperatures cause grain growth. In this study, the CG samples, known to start with 50-70 μm grain size, also produced grainy diffraction patterns at the start of experiments, but as these samples deformed, their diffraction patterns rapidly became more regular, eventually appearing similar to the diffraction patterns for their FG counterparts. Our suspicion that this change in diffraction patterns was the result of grains

recrystallizing to smaller sizes during deformation were confirmed in post-experiment microscopy.

Although grain size reduction is qualitatively obvious in situ diffraction patterns, quantifying grain size or the rate of grain size reduction is more difficult, as the amount of sample volume containing grains at the diffraction condition can only be estimated probabilistically. We discovered that the goodness of fit (GoF, as represented by R^2) for the curve fit of d-spacing vs. ϕ of detector (e.g., Figure 2-2) corresponds to the graininess of diffraction patterns. For diffraction patterns of coarse-grained materials where few grains are in the diffraction condition, the fitting of diffraction peaks is less precise, and thus the R^2 of the d-spacing vs. ϕ curve fit is typically low. For fine-grained materials where diffraction patterns are of consistent shape and easily fit, The relationship between d-spacing and orientation will be closely fit by the curve, and thus R^2 is typically high.

Plotting the GoF for each set of diffraction patterns through the course of San 188 (Figure 3-8), we see that the GoF rapidly improves during the first several hours of deformation. By 5% strain (after 4 hours of deformation), R^2 of curve fits for the San 188 CG approached .99, close to the value of fits in the corresponding FG sample. The GoF continues to improve very slightly until about 8%, after which it stays near .99 for the remaining duration of the experiment. We interpret this trend as in situ evidence that the CG sample recrystallizes rapidly under these deformation conditions. From our post-

experiment orientation contrast images, we have evidence that the sample stabilizes to an average grain size of ~10-15 μm by the end of each experiment.

3.4 Discussion

Olivine flow law (Eq. 1) parameters compiled in Hirth and Kohlstedt (2003) for A, E^*, n, and p, and a V^* of 14 × cm^3/mol, determined in Chapter 2, predict that the contribution to strain rate from grain-boundary sliding accommodated by dislocation creep (GBS) and that from dislocation creep alone would be nearly the same for 60-μm grain samples at the conditions of San 181 and San 188. The same parameters predict GBS domination for smaller grain sizes. Without assistance from recrystallization or strain localization, both CG samples at an initial grain size of 60 μm would be expected to strain several orders of magnitude more slowly than their FG counterparts. Even if recrystallization produced a uniform grain size of 10-15 μm in CG samples, the difference in strength from FG samples would still be easily resolvable due to the grain size dependence of GBS [$p = 2$ in Eq (1)].

In both experiments, the strain rates of FG and CG samples were nearly identical after the initial period of grain size reduction. During San 188, stress was 70-100 MPa higher in the CG sample than in the FG sample, with ~15 MPa uncertainty (Weidner et al. 2010). Thus, grain size sensitivity

is observed, but is far milder than predicted by the flow law for uniform grain sizes. The distinct regions of fine grains observed in the San 181 CG sample are likely sources of the discrepancy between observed strain rates and those predicted by Hirth and Kohlstedt (2003). Similar localized regions of high strain have been observed at many scales, and are known to accommodate large amounts of strain through processes such as shear heating and continual recrystallization (Rogers 1979; White et al. 1980). Shear zones within San 188 are less obvious than in San 181 (possibly due to the lower quality of OC images from San 188), which may explain the slightly higher grain size sensitivity observed in San 188. Because San 188 was performed at lower pressure, the difference in microstructure from San 181 raises the question of pressure influence on strain localization. San 188 FG was deformed at pressures 7-10% higher than San 188 CG, meaning that the affect of pressure may have countered the weakness of the FG sample. Samples deformed in San 181 were stronger than San 188, suggesting a positive value of V^* for olivine. Further measurements are needed to confirm this result, on samples with better-constrained microstructures.

As discussed above, grain size sensitivity in both experiments was much less than expected from flow law parameters. The simplest explanation, backed by the shear zones observed in San 181 CG, is that fast strain took place in small grains that formed during compaction and recrystallization of CG samples. In this case, flow law parameters for

materials with homogeneous grain size would not be applicable. San 188 may also have experienced some strain localization, but shear zones are less obvious in OC images. The small amount of grain-size sensitivity observed in San 188 CG was far less than expected from published parameters for GBS, even accounting for grain size reduction during deformation. It is difficult to deduce how much of a role strain localization had in this experiment. The obvious alternative to strain localization is that the grain size exponent p in Eq. 1 for GBS ($p = 2$) is too high under the conditions in this study, and that the constitutive law needs to be reevaluated.

3.5 D-DIA advancement and future work

The continuing refinement of D-DIA stress measurement and reduction technique will soon allow constant stress experiments and real-time pressure correction. This study also demonstrated that a BN pressure medium is strong enough to allow different stress states in adjacent samples. With the help of stronger anvil materials, the D-DIA will soon provide high-precision measurements of flow law parameters at a large range of pressures.

Acknowledgments

This project was made possible by funding from the U.S. Department of Energy Basic Energy Sciences division, the National Science Foundation and the Consortium on Material Properties Research in the Earth Sciences

(COMPRES). Thanks is also due to members the Kohlstedt Laboratory at the University of Minnesota, Twin Cities, for help in sample preparation and imaging.

Bibliography

Carter, Neville L., and Hans G. Ave'Lallemant. 1970. "High Temperature Flow of Dunite and Peridotite." *Geological Society of America Bulletin* 81 (8): 2181–2202.

Duffy, T. S., and D. L. Anderson. 1989. "Seismic Velocities in Mantle Minerals and the Mineralogy of the Upper Mantle." *J. Geophys. Res* 94 (1989): 1895–1912.

Durham, W. B., and C. Goetze. 1977. "Plastic Flow of Oriented Single Crystals of Olivine: 1. Mechanical Data." *Journal of Geophysical Research* 82 (36): 5737–53.

Durham, W. B., C. Goetze, and B. Blake. 1977. "Plastic Flow of Oriented Single Crystals of Olivine: 2. Observations and Interpretations of the Dislocation Structures." *Journal of Geophysical Research* 82 (36): 5755–70.

Durham, W. B., S. Mei, D. L. Kohlstedt, L. Wang, and N. A. Dixon. 2009. "New Measurements of Activation Volume in Olivine under Anhydrous Conditions." *Physics of the Earth and Planetary Interiors* 172 (1-2): 67–73.

Durham, W. B., and D. C. Rubie. 1998. "Can the Multianvil Apparatus Really Be Used for High Pressure Deformation Experiments?" *Properties of the Earth and Planetary Materials at High Pressure and Temperature* Geophysical Monograph (101): 63–70.

Gwanmesia, G. D., S. Rigden, I. Jackson, and R. C. Liebermann. 1990. "Pressure-Dependence of Elastic Wave Velocity for Beta-Mg2sio4 and the Composition of the Earths Mantle." *Science* 250 (4982): 794–97. WOS:A1990EG88300031.

Hirth, G., and D. Kohlstedt. 2003. "Rheology of the Upper Mantle and the Mantle Wedge: A View from the Experimentalists." *Geophysical Monograph* 138: 83–105.

Hirth, G., and D. L. Kohlstedt. 1995. "Experimental Constraints on the Dynamics of the Partially Molten Upper-Mantle .2. Deformation in the Dislocation Creep Regime." *Journal of Geophysical Research-Solid Earth* 100 (B8): 15441–49. WOS:A1995RN99200034.

Hitchings, R. S., M. S. Paterson, and J. Bitmead. 1989. "Effects of Iron and Magnetite Additions in Olivine-Pyroxene Rheology." *Physics of the Earth and Planetary Interiors* 55 (3): 277–91.

Jung, H., and S.I. Karato. 2001. "Effects of Water on Dynamically Recrystallized Grain-Size of Olivine." *Journal of Structural Geology* 23 (9): 1337–44.

Karato, Shun-ichiro, Mitsuhiro Toriumi, and Toshitsugu Fujii. 1980. "Dynamic Recrystallization of Olivine Single Crystals during High-Temperature Creep." *Geophysical Research Letters* 7 (9): 649–52.

Kirby, S. H. 1983. "Rheology of the Lithosphere." *Rev. Geophys* 21 (6): 1458–87.

Liebermann, Robert C., and Yanbin Wang. 1992. "Characterization of Sample Environment in a Uniaxial Split-Sphere Apparatus." *Geophysical Monograph Series* 67: 19–31.

Merkel, S. 2006. "X-Ray Diffraction Evaluation of Stress in High Pressure Deformation Experiments." *Journal of Physics-Condensed Matter* 18 (25): 949.

Poirier, J. P. 1980. "Shear Localization and Shear Instability in Materials in the Ductile Field." *Journal of Structural Geology* 2 (1): 135–42.

Rogers, Harry C. 1979. "Adiabatic Plastic Deformation." *Annual Review of Materials Science* 9 (1): 283–311.

Ross, J.V., H.G. Ave Lallemant, and N.L. Carter. 1980. "Stress Dependence of Recrystallized-Grain and Subgrain Size in Olivine." *Tectonophysics* 70 (1): 39–61.

Sammis, Charles G., John C. Smith, and Gerald Schubert. 1981. "A Critical Assessment of Estimation Methods for Activation Volume." *Journal of Geophysical Research: Solid Earth (1978–2012)* 86 (B11): 10707–18.

Singh, A. K. 1993. "The Lattice Strains in a Specimen (cubic System) Compressed Nonhydrostatically in an Opposed Anvil Device." *Journal of Applied Physics* 73 (9): 4278.

Tullis, Terry E., Franklin G. Horowitz, and Jan Tullis. 1991. "Flow Laws of Polyphase Aggregates from End-Member Flow Laws." *Journal of Geophysical Research: Solid Earth (1978–2012)* 96 (B5): 8081–96.

Weidner, D.J., M.T. Vaughan, L. Wang, H. Long, L. Li, N.A. Dixon, and W.B. Durham. 2010. "Precise Stress Measurements with White Synchrotron X Rays." *Review of Scientific Instruments* 81 (1): 013903–013903–5.

White, S. H., S. E. Burrows, J. Carreras, N. D. Shaw, and F. J. Humphreys. 1980. "On Mylonites in Ductile Shear Zones." *Journal of Structural Geology* 2 (1): 175–87.

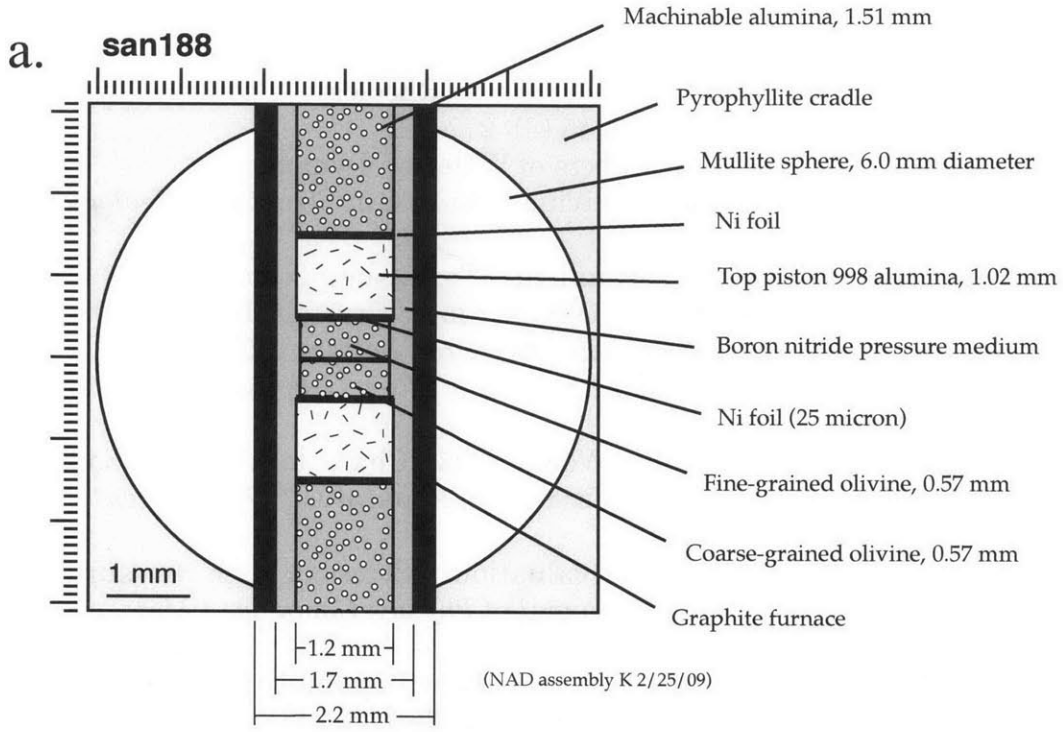

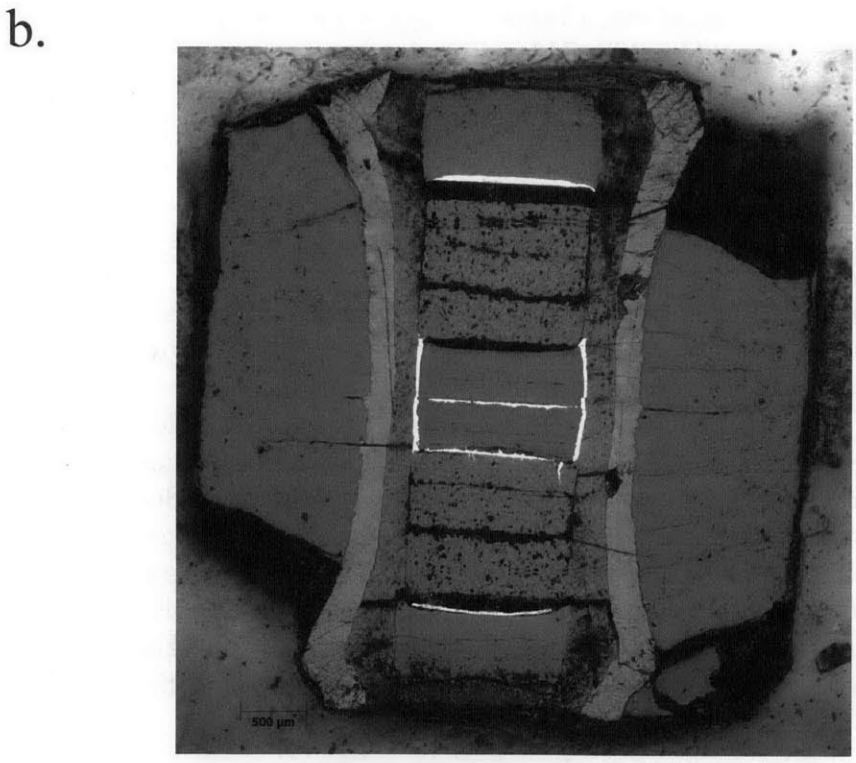

Figure 3-1. Sample assembly San188. a) schematic diagram of the sample assembly before deformation, to scale. b) Polished section after deformation. Some of the pressure medium has been chipped away during preparation.

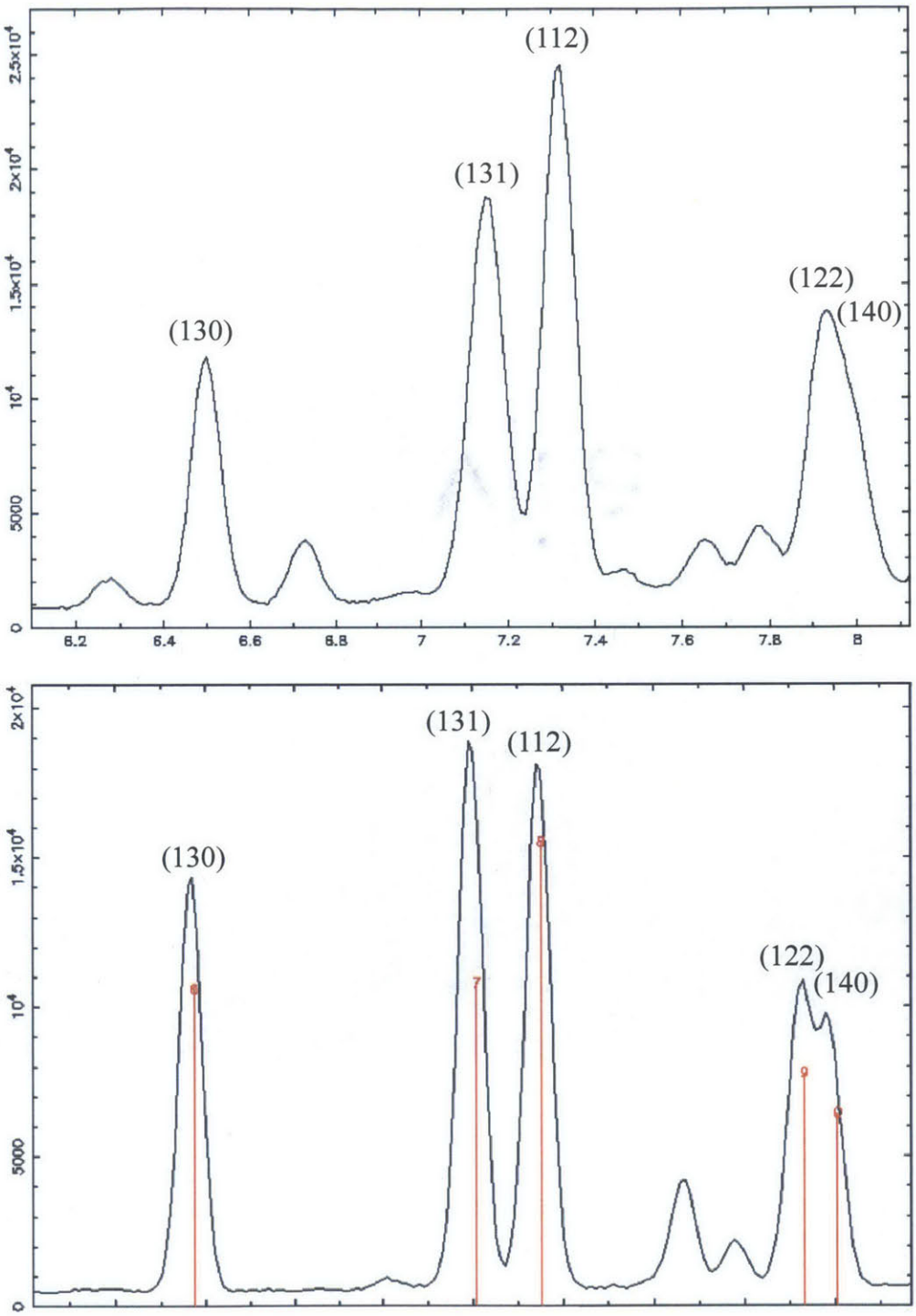

Figure 3-2. Energy-dispersive x-ray diffraction patterns of olivine at room temperature and pressure for a) earlier collimating slits, and b) new collimating slits. Note sharper peaks in b). The improvement in diffraction patterns has allowed much higher precision stress measurement, streamlined data reduction, and promises realtime stress calculation during future experiments. Previously, stress has been calculated after the completion of experiments.

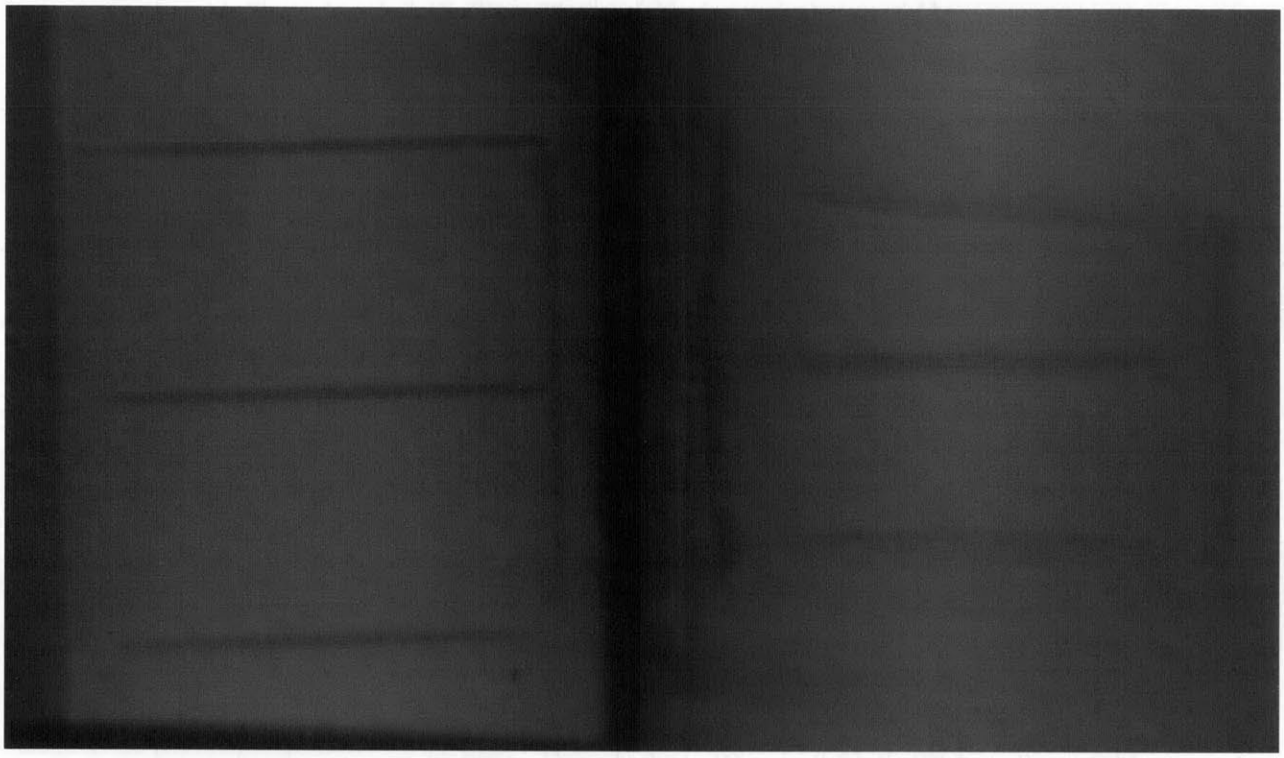

Figure 3-3. X-radiograph images of dual sample San 188 before and after deformation (left and right, respectively). The dark lines are Ni foils jacketing the sample. In the left image, a tungsten carbide anvil can be seen to the right, and a sintered diamond "transparent" anvil appears to the left, partially obscuring the foil.

a.

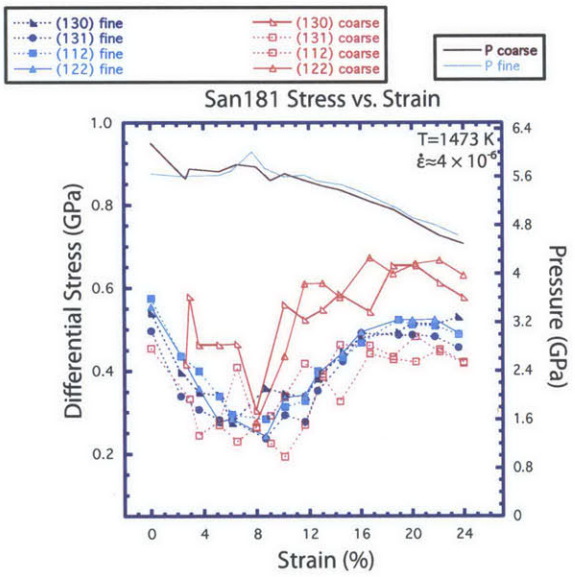

b.

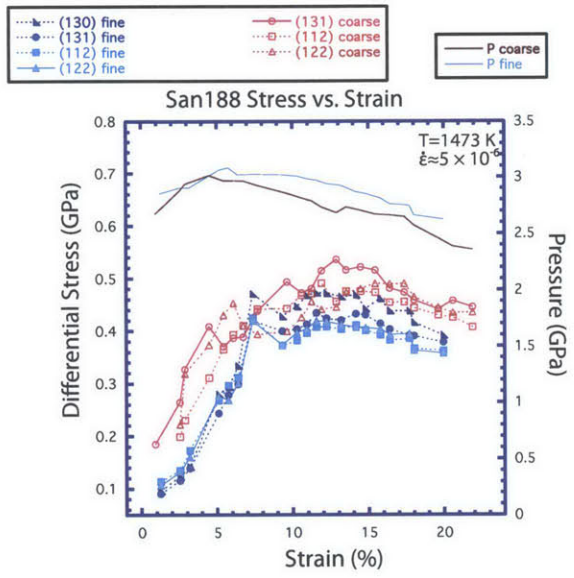

Figure 3-4. Stress vs. strain for (a) San181 and (b) San188. Stress was measured by x-ray diffraction in both fine and coarse samples. Stress appears to be higher in the coarse-grained sample in San188, and possibly in San181.

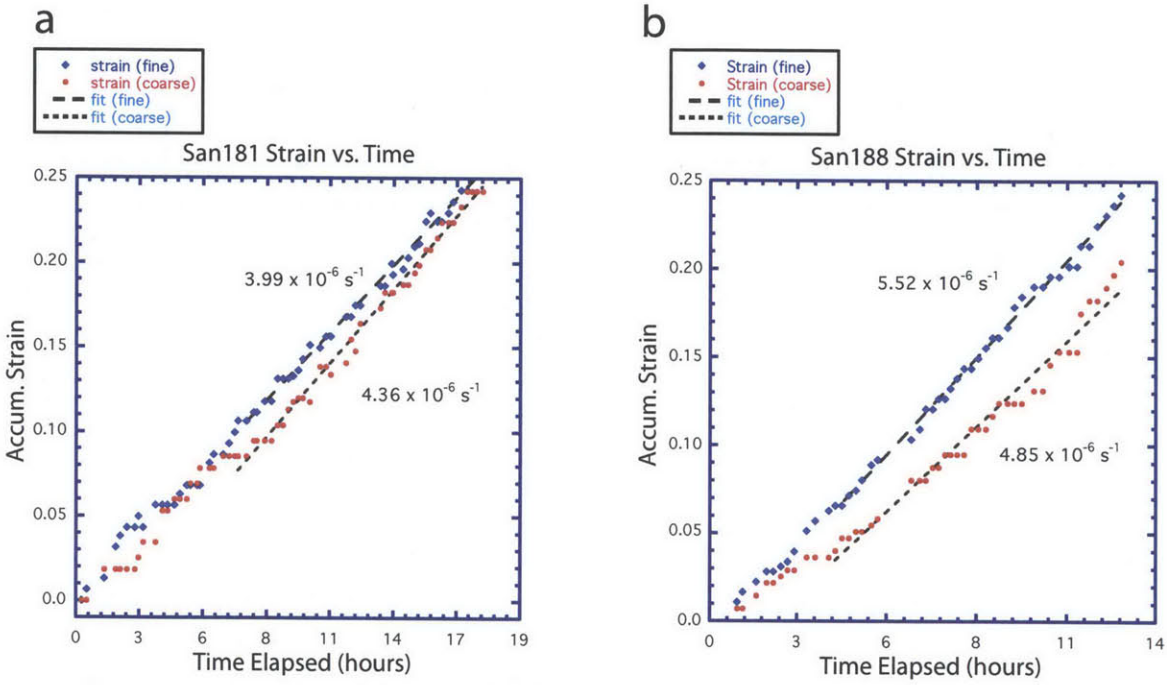

Figure 3-5. Strain vs. time for coarse and fine samples in (a) San181 and (b) San188. Strain was measured from x-radiographs taken of the sample during deformation. In both cases, coarse and fine samples deformed at similar rates.

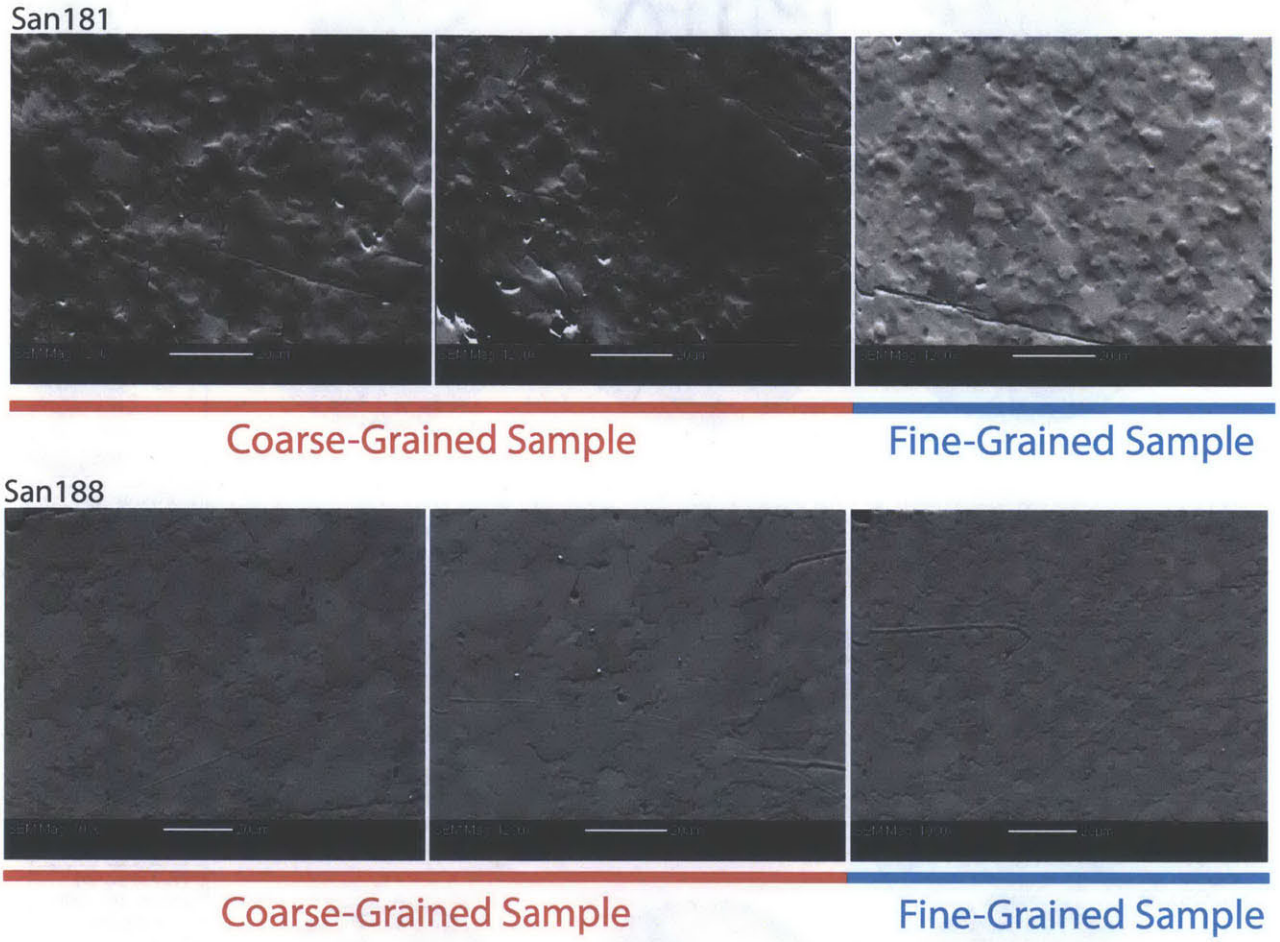

Figure 3-6. Orientation contrast images of coarse and fine-grained samples from experiments San181 and San188 after deformation. Images revealed much smaller grains in the coarse-grained samples than in the starting material. Some ~60 μm grains remained, but were surrounded by finer material.

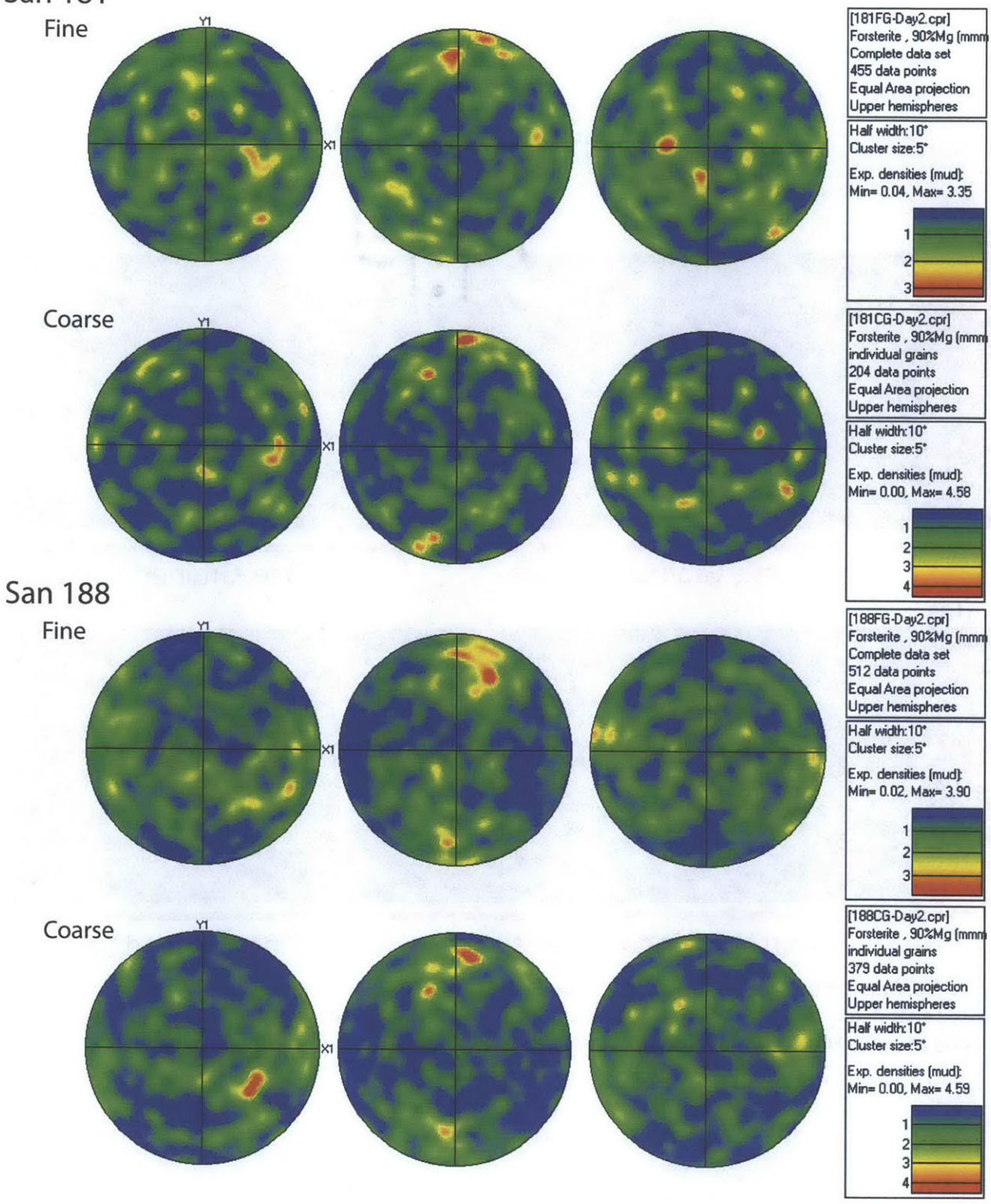

Figure 3-7. Pole figures for fine and coarse parts of San181 and 188 after deformation. Very little LPO developed in either run, although there appears to be a faint A-type fabric {associated with the (010)[100] slip system} in each sample.

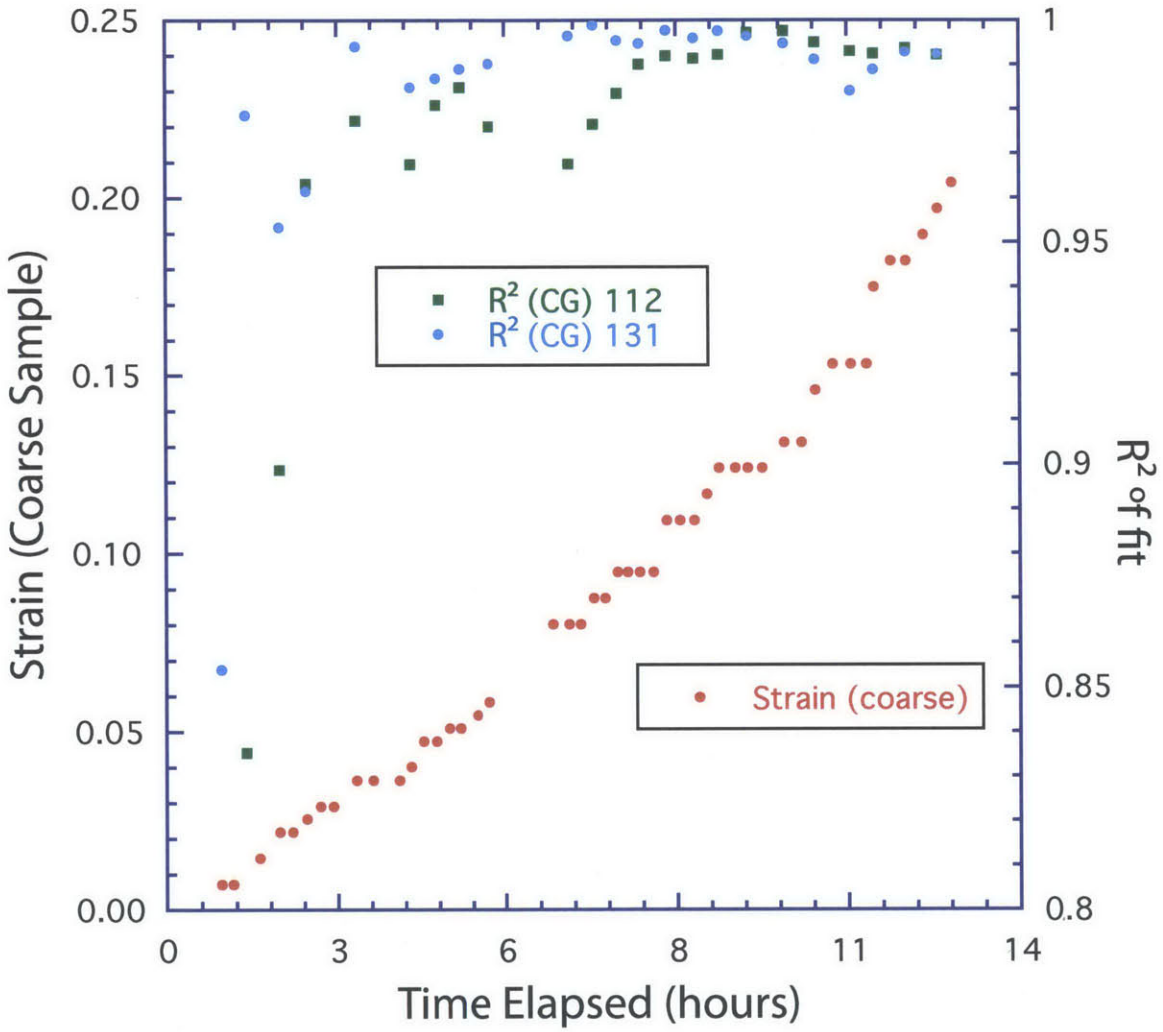

Figure 3-8. R^2 of multi-detector curve fitting of CG diffraction patterns taken during experiment San188. Strain is given for reference. The improvement in goodness of fit early in the experiment is interpreted as evidence for reduction of grain size in the CG sample. Reduced grain size allows more grains to be sampled in diffraction patterns, resulting in d-spacings averaged from a larger number of grains for each orientation.

Chapter 4

In situ measurement of texture in olivine samples with synchrotron x-ray diffraction

ABSTRACT

Unresolved issues in geodynamics demand a better understanding of the bulk mechanical properties of mantle minerals, and also careful analysis of the complex lattice-scale physics behind these properties. The continuing improvement of synchrotron x-ray diffraction techniques, used in conjunction with the D-DIA apparatus, now offers unprecedented richness of data for each experiment. In order to better constrain the mechanisms that are active during the creep of olivine at upper mantle conditions, we attempted to monitor, in situ, the development of lattice-preferred grain orientations (LPO) during deformation experiments. Here, we present results obtained with the use of the *MTEX* toolbox for Matlab and energy-dispersive x-ray diffraction, showing the in situ development of LPO in deforming dry San Carlos olivine samples, at pressures from 2-7 GPa. In at least one experiment, a strong signal of gradually increasing texture is observed, indicating the dominance of the (010)[100] or the (010)[001] slip systems, consistent with predictions from earlier studies on post-deformation microstructures and plastic anisotropy. In other experiments, textures appear and disappear throughout the course of deformation. These in situ observations provide new evidence of the complexity and dynamic nature of mechanisms that may be active within our samples, and in the mantle as well.

4.1 Introduction

For decades, geoscientists have observed that the upper mantle is seismically anisotropic, and that the strength and type of anisotropy varies profoundly both laterally and with depth. Seismic anisotropy in the upper 200 km of the oceanic lithosphere is particularly strong (Ohuchi et al. 2011;

Gung, Panning, and Romanowicz 2003; Montagner and Kennett 1996), decreasing rapidly in the deep upper mantle. Anisotropy also corresponds to other regional features of geodynamic interest, such the strong shear-wave anisotropy below Hawaii (Ekström and Dziewonski 1998) and in subduction zones (Margheriti et al. 1996; Plomerova et al. 2006; Smith et al. 2001). As the olivine crystal structure is elastically anisotropic, these seismic observations can be explained by a lattice-preferred orientation (LPO or fabric, used interchangeably) of olivine grains in the upper mantle. LPO is the product of deformation by dislocation glide (e.g Cordier 2002) and thus, the presence of seismic anisotropy is evidence that dislocation mechanisms are active in these regions of the mantle, and responsible for a great deal of deformation. However, dislocation glide in olivine can happen by several different slip systems, and the dominant slip system depends on the conditions of deformation (Durham and Goetze 1977; Durham, Goetze, and Blake 1977; Carter and Ave'Lallemant 1970). Thus, a comprehensive understanding of the slip systems in mantle minerals, and olivine in particular, would allow seismic observations to be far better understood, and reveal a great deal about the large-scale dynamics of the upper mantle.

A number of studies at lower pressure have shown that the preferred slip system in olivine changes in response to both the water content of a sample, and also the differential stress applied during deformation. Jung and Karato (2001) used a Griggs-type apparatus and post-experiment microscopy

to map three distinct types of olivine fabric, and their associated olivine slip systems, varying with water content and stress: Type-A, (010)[100]; Type-B, (010)[001]; and Type-C, (100)[001]. A Type-D, (110)[001], has also been demonstrated for low water, high stress conditions (Bystricky et al. 2000), and a Type-E (001)[100] is found for moderate stress and water conditions (Jung and Karato 2001). The addition of deeper mantle pressures further complicates the behavior of olivine slip systems. Raterron et al. (2009) examined the influence of pressure on the activity of competing slip systems by deforming oriented single crystals in the D-DIA. The experiments were designed such that adjacent single crystals, each promoting a different slip system, were deformed under the same conditions. They showed that (010)[100] slip (associated with Type-A fabric) dominates at lower pressure in their experiment, but is inhibited by increasing pressure. The (010)[001] system (Type-B), is less affected by pressure, and thus becomes weaker than (010)[100] rates at high-pressure conditions, the transition occurring somewhere between 6 and 10 GPa in relatively anhydrous samples. This transition has also been observed in post-experiment microscopy of polycrystalline samples deformed in the D-DIA (Hilairet et al. 2012; Ohuchi et al. 2011). However, because the sample textures are observed only after the conclusion of experiments, there is little information of the rate of accumulation of LPO. There is also the possibility that the structure of the

sample may be significantly altered during cooling and depressurization, where some additional deformation is often unavoidable.

Synchrotron radiation has been an essential tool for the study of Earth materials at high pressure, as it allows experimentalists to observe and measure the properties of samples that would otherwise be inaccessible during experiments. For rheologists, synchrotron x-ray diffraction (XRD) has primarily been a means to measure stress and strain during multi-anvil experiments. Beyond their value for evaluating the "bulk" stress state in a sample, diffraction patterns taken during deformation contain a wealth of information on the structure and properties of a sample, including LPO. In this chapter, we explore a method of using synchrotron XRD to measure in situ the rate of accumulation and type of LPO in olivine samples. This method, still in development, has the potential to offer rheologists a new window into the physical mechanisms that control deforming samples.

4.2 Methods

4.2.1: Experimental configuration and procedure

We conducted deformation experiments at the D-DIA installation at NSLS beam line X17B2, as in the previous two chapters. Each olivine sample was deformed in pure shear geometry in a hybrid mullite-pyrophyllite dry sample assembly, identical to the single-sample assemblies featured in experiments for Chapter 2. The procedure for experiments was also similar.

For each step, the sample is brought to pressure hydrostatically, brought to temperature, and then deformed at a constant strain rate. In several of the experiments, deformation steps were conducted at two different pressure conditions.

Because the goal of these experiments was to analyze fabric development in samples, special care was taken to deform the samples at stable conditions that would produce clear, easily processed diffraction patterns. For this purpose, we chose low strain rates (~0.5×10^{-5} s^{-1}) to keep differential stress relatively low. Each sample was deformed to a strain of 20% or more for each step, to allow detectable amounts of LPO to form. Thus, each experimental step required >8 hours of continuous deformation. Some samples were deformed beyond 40% total strain in multiple steps, roughly the maximum amount of strain that our sample assemblies will typically accommodate in pure sure geometry before failure.

4.2.2 Diffraction system and stress measurement

As in previous chapters, each experiment utilized synchrotron x-ray diffraction as a means to measure stress conditions within the sample assembly, and also to monitor the accumulation of strain as the olivine sample shortens. The configuration of the diffraction system remains approximately the same as in Chapter 2, with ten detector elements measuring d-spacing of olivine planes at different orientations with respect to

the stress field. The detector system requires a minimum of one of the six D-DIA anvils to be made of an x-ray-transparent material (sintered diamond, in our case), such that diffracted x-rays may pass through the apparatus to the collimating slits and detectors. Whenever possible, we used four transparent anvils, allowing us to use all 10 detector elements and to observe nearly the entire sample assembly in x-radiographs.

The data reduction technique for stress measurement remains identical to Chapter 2, with the (130), (131), (112), (122), and (140) Bragg reflections in olivine used for stress calculation. The Plot85 software package was again used to fit peaks in each diffraction pattern. We again measure strain rate by monitoring the position of strain markers at the sample ends, which are visible in x-radiograph images.

4.2.3 Texture measurement and the MTEX package

From our earliest D-DIA experiments at NSLS X17B2, we noticed that the relative height and width of diffraction peaks sometimes varied between different experiments, or even changed within a single experiment. Peak centroid is a function of d-spacing (as defined by Bragg's Law), whereas peak area for a given (*hkl*) is a function of the volume of diffracting material at a particular orientation in sample. Therefore, peak areas indicate LPO. Because the sample can be moved in the path of the beam, the system can

also be used to measure conditions and structure locally, anywhere in the sample.

The potential for measuring sample fabric and structure has also been demonstrated in angle-dispersive (AD) x-ray diffraction experiments (Hilairet et al. 2012). In AD XRD, the incident beam of x-rays is monochromatic, containing only a single frequency of photons. Instead of collimating slits and discrete detector elements, there is a single detector plate, which records the Bragg angle and azimuth around the beam of every diffracted photon. LPO is indicated by a variation in density of photons around the azimuth. Unlike in the ED XRD case, a continuous range of grain orientations within the path of the beam is sampled, and thus diffraction patterns contain more information on sample textures (Figure 4-2). Nonetheless, the relative simplicity ED XRD patterns lends itself to simpler quantification, and the broad range of x-ray frequencies allows a sufficient number of grains to be sampled.

In each ED diffraction pattern, the (130), (131), (112), (122) and (140) diffraction peaks are fit, as in previous chapters. These peaks are selected for their prominence in the olivine diffraction pattern, allowing them to be consistently identified and fit with good accuracy. As in experiments from previous chapters, the peak positions are used to calculate the state of pressure and differential stress throughout each run. The intensity of each peak (effectively, the area under the peak, minus the background), is then used to calculate the distribution of grain orientations. Intensity data is fed

into the *MTEX* software package via a MATLAB script developed in conjunction with Andrew Walker and Simon Hunt of University College, London (Hunt et al., in prep), which includes information on the structure of the material, the geometry of slit system and detector assembly, and the sensitivity of each detector. From these inputs, *MTEX* is used to calculate an orientation distribution function (ODF), an inverse pole figure, and an estimate of the fabric strength. In preliminary results for $CaIrO_3$ perovskite deformed in simple shear, comparisons between *MTEX* estimates of fabric and those observed in samples with EBSD microscopy match closely in fabric type, but MTEX tends to underestimate the strength of sample fabrics. This is most likely due to the limited fraction of sample grains that are observable with the detector system (Hunt et al., in prep).

Because diffracted photons must travel different lengths through transparent anvil material on the way to each respective detector (except detectors 1 and 9, which are not blocked by anvils), a correction must be made to account for biases in the intensity of diffraction patterns. A reference pattern is chosen from the beginning of the experiment, typically from before the start of pressurization (the "open press" pattern), or from after pressurization and before the start of deformation ("hydrostatic pattern at pressure", or HPP). This pattern for each detector is subtracted from all subsequent patterns, and thus defined as the "zero texture" pattern. The choice of open press versus HPP is a matter for debate. The former offers the

advantage of a pattern before the material has been through pressurization, which may produce some differential stress and thus some fabric. The HPP pattern, on the other hand, features a compressed anvil configuration that is much more similar to the configuration during the subsequent deformation, and thus the path length through the transparent anvils to each detector is roughly the same as during the experiment. For this reason, we chose the HPP as our reference pattern each run that was analyzed for this study. The sensitivity of our texture analysis routine is demonstrated by the apparent change in texture estimates in multi-step experiments. When a sample is hydrostatically squeezed to a much higher pressure condition, the gap between anvils closes significantly as the anvils press further into the soft pressure medium. As a result, the path length of x-rays traveling through the "transparent" anvil(s) is changed, and the relative intensity of peaks in different detectors changes also. This effect can be seen clearly in plots of texture intensity in both dual-step experiments for this study, San 308 and San 325 (Figures 4-8 and 4-9).

4.3 Results and analysis

Four experiments were conducted for this study (Table 4-1), at a range of conditions, with the primary goal of demonstrating the ability to observe fabric in situ, and to attempt to identify the active mechanisms in previous experiments. Of the four experiments, two (San 311 and San 316) were single

step, higher-pressure experiments (6-7 GPa), while the other two (San 308 and San 325) experiments featured two steps, one at the low end of the D-DIA's pressure capability (2-3 GPa), and another substantially higher (~6 GPa).

As in previous chapters, uncertainty in temperature measurements is a primary obstacle to comparing the results of different experiments. Our estimate of temperature uncertainty is discussed in detail in Chapter 2.2.6. We expect that for the experiments in this chapter, which use the same temperature calibration and estimation technique, the uncertainty in temperature is similar. Our estimate is that the absolute uncertainty of T (defined as Type 1 in chapter 2), is ±100 K, while it is much lower between different steps in the same experiment, conservatively estimated at ±25 K. The better precision between steps in the same experiment is due to the fact that the steps utilize the same sample cell, and thus will not suffer from variation in the structure of the furnace or pressure medium.

The measurements of stress, pressure, and strain rate are otherwise better constrained than temperature, and the grain size and structure of these samples is expected to remain stable over the course of these experiments (Discussed in detail in Chapter 3). Thus differences in behavior between experiments, at conditions that otherwise appear to be similar, are most likely due to variations in temperature.

San 308, the first experiment conducted in this series, was the only one to have a full 180° arc of 9 detectors operable (Figure 1-2), and as a result, features the highest quality measurements of stress. This can be seen in plots of stress throughout the course of the experiments (Figures 4-4 to 4-7), where the scatter in stress measurements from each of the five lattice planes is indicative of the precision of peak fitting and stress calculation (Weidner et al. 2010). San 311 and San 316 utilized 8 available detectors (detector 4 was offline), while San 325 featured 7 available detectors (detectors 3 and 4 offline).

4.3.1 Stress and strain rates

All experiments for this study were conducted at constant strain rates, which can be controlled with very good precision in the D-DIA. Strain rates for all experiments were between 8×10^{-6} s^{-1} and 6×10^{-6} s^{-1}. These strain rates are close to the slowest we can practically achieve at the X17B2 D-DIA installation, as each involves several days to complete, including up to 20 hours of continuous deformation in order to accumulate 40% strain. In the dual-step experiments, we again observed strengthening of the samples at higher pressures, consistent with the pressure dependence found in Chapter 2. In the high-pressure, single-step experiments (San 311 and 316), stresses began at 200-250 MPa, and decreased rapidly before remaining low for the remainder of the experiments (mostly >150 MPa in both cases). Because of

the noisy stress measurements in the latter three experiments, it is difficult to see the difference in stress measurements between different (*hkl*), (a consequence of plastic anisotropy, as discussed in Chapters 2 and 3). However, in Step 2 of San 325, plastic anisotropy is particularly apparent, with the stresses measured from the (130) and (140) planes far higher than stresses measured from the other three lattice planes. This observation is consistent with the ordering of stress measured by different lattice planes in many of the experiments featured in Chapter 2, and thought to be evidence of a situation where (010)[100] slip is not dominant (Figure 2-6). In San 308, Step 2 features similar conditions to San 325 (Step 2), and ordering of (*hkl*) in San 308(2) and San 325(2) is largely similar.

4.3.2 Rate of LPO accumulation and fabric type

Of the four experiments, San 308 features the strongest signal of LPO development, as measured in situ with the use of the *MTEX* package (Figure 4-9). Henceforth, we refer to the low index planes in olivine, the (100), (010), and (001) as the a, b, and c planes, respectively, and the corresponding low-index directions as the a, b, and c directions. In San 308, texture begins to develop early in the experiment, with the poles of the olivine b plane going towards vertical in the laboratory/sample reference frame (Figures 4-3 and 4-4). Simultaneously, the a and c directions begin to move towards horizontal. This signal in the diffraction data is consistent with both Type-A fabric,

produced by the (010)[100] slip system, and also with Type-B fabric, associated with (010)[001]. However, because of the axisymmetric pure shear deformation geometry, it is impossible to distinguish which of these two slip systems is dominant, because they both slip on the olivine b plane (hence why the b directions concentrate towards vertical in both cases). As olivine has an orthorhombic crystal structure, the a and c directions are mutually orthogonal to the b-plane, and thus will simultaneously go towards horizontal in the sample frame for either the A-type or B-type textures.

In San 308, this "b-plane-slip" signal continues to strengthen gradually throughout the first step (conducted at ~2.5 GPa). In the second step, the b-plane-slip texture rapidly becomes stronger after pressurization, before decreasing somewhat (Figure 4-4 and 4-8). The apparent spike in texture after pressurization is likely not entirely real, but instead a product of the anvil configuration effect described above. As visible in the radiographs at right in Figure 4-3, the anvils push further into the sample assembly during pressurization, which means that x-rays have a longer path through the transparent anvils to most of the detectors, which changes the relative intensity of peaks in the pattern, affecting texture measurements slightly. The same effect is visible in the apparent texture intensity of San 325 (Figure 4-9).

San 325 was designed to repeat the conditions of San 308, and we were successful recreating similar strain rates, stresses and pressures. Unlike San

308, a "b-plane-slip" texture did not develop in the first step of San 325. Briefly, at the end of San 325(1), a weak texture suggesting slip on the (001) plane was observed. Late in the second step, however, a fabric similar the to the "b-plane-slip" texture of 308 did show up in our in situ data. The plot of texture index throughout San 325 (Figure 4-9) shows that texture appears to strengthen and weaken significantly several times throughout the course of the experiment, although the apparent increase in texture strength around pattern 40 may be an artifact of pressurization, as discussed above.

In the two high-pressure, single-step experiments (311 and 316), only a small amount of texture is detected during the course of either experiment (Figures 4-5, 4-6, 4-9), and in the weak textures that are detected for these experiments, the poles of the (001) and (100) planes appears to move towards vertical. Thus, there is no evidence from the in-situ texture data that the "b-plane slip" mechanism active in San 308 (and possibly in the second step of San 325) is dominant in these experiments.

4.4 Discussion

Of the four experiments in this study, San 308 gives the clearest indication of a distinctive texture forming in situ, consistent with the Type-A and Type-B fabrics that are predicted for experiments at these conditions (Raterron et al. 2009; Jung and Karato 2001). San 325, intended to reproduce the conditions of San 308, instead appeared to develop cyclical textures

(Figure 4-9), only showing similar behavior to 308 at the very end of the experiment (Figure 4-7). These apparent transient textures raise several points about our experimental technique: (i) Because the uncertainty in temperature is high, and because the active deformation mechanisms are difficult to predict with certainty, samples that show relatively similar macroscopic behavior may be hiding subtle but substantial differences in deformation physics. (ii) While mechanisms may be analyzed with post-experiment microscopy, the complexity and dynamic nature of deformation physics may confound this approach (i.e. the sample microstructure which remains at the end of an experiment may not tell the whole story). Both of these points underscore the value of comprehensive in situ analysis of micro-scale sample microstructures and behavior.

4.5 Conclusions and Future Work

At the outset, this project was undertaken to attempt to develop a new body of in situ evidence for previously suggested mechanism transitions in olivine. Our very first experiment, San 308, shows what appears to be a robust signal of texture development, specifically a Type-A or Type-B texture, as predicted for these experimental conditions by a number of previous studies (e.g. Ohuchi et al. 2011; Jung and Karato 2001). In subsequent experiments, this signal is not so clear, with a similar pattern of texture accumulation appearing only at the end of one other run. While all

experiments demonstrated what appears to be steady-state macroscopic deformation, our in situ texture analysis provides evidence of possible transient textures, suggesting that the mechanisms active in these samples may be evolving.

One substantial shortcoming of our experimental approach is the pure shear geometry in which we deform our samples. This geometry places two critical restrictions on our analysis of texture. The first is that we are limited to strains of <~40%. From the results of our initial experiment, San 308, it appeared that this amount of strain was sufficient to produce textures that could be easily detected with our in situ technique, but some subsequent experiments produced only very weak signals. The second issue is that two of the most prominent fabrics in olivine, Type-A and Type-B, are indistinguishable in pure shear. In the future, both of these issues can be confronted by conducting experiments in simple shear, which allows much higher strains, and also a clear identification of slip directions.

Acknowledgements

This work was made possible by contributions and support from Simon Hunt and Andrew Walker, at University College London, who helped produce and continually improve our fabric analysis code. Financial support was provided by the Office of Basic Energy Sciences of the Department of Energy, and by the National Science Foundation. Thanks are also due to the beam

line staff at NSLS X17B2, which in turn is supported by the Consortium on Material Properties Research in the Earth Sciences (COMPRES).

Bibliography

Bystricky, M., K. Kunze, L. Burlini, and J.-P. Burg. 2000. "High Shear Strain of Olivine Aggregates: Rheological and Seismic Consequences." *Science* 290 (5496): 1564–67.

Carter, Neville L., and Hans G. Ave'Lallemant. 1970. "High Temperature Flow of Dunite and Peridotite." *Geological Society of America Bulletin* 81 (8): 2181–2202.

Cordier, Patrick. 2002. "Dislocations and Slip Systems of Mantle Minerals." *Reviews in Mineralogy and Geochemistry* 51 (1): 137–79.

Durham, W. B., and C. Goetze. 1977. "Plastic Flow of Oriented Single Crystals of Olivine: 1. Mechanical Data." *Journal of Geophysical Research* 82 (36): 5737–53.

Durham, W. B., C. Goetze, and B. Blake. 1977. "Plastic Flow of Oriented Single Crystals of Olivine: 2. Observations and Interpretations of the Dislocation Structures." *Journal of Geophysical Research* 82 (36): 5755–70.

Ekström, Göran, and Adam M. Dziewonski. 1998. "The Unique Anisotropy of the Pacific Upper Mantle." *Nature* 394 (6689): 168–72.

Gung, Yuancheng, Mark Panning, and Barbara Romanowicz. 2003. "Global Anisotropy and the Thickness of Continents." *Nature* 422 (6933): 707–11.

Hilairet, Nadège, Yanbin Wang, Takeshi Sanehira, Sébastien Merkel, and Shenghua Mei. 2012. "Deformation of Olivine under Mantle Conditions: An in Situ High-pressure, High-temperature Study Using Monochromatic Synchrotron Radiation." *Journal of Geophysical Research: Solid Earth (1978–2012)* 117 (B1).

Jung, H., and S. Karato. 2001. "Water-Induced Fabric Transitions in Olivine." *Science* 293 (5534): 1460–63.

Margheriti, L., C. Nostro, M. Cocco, and A. Amato. 1996. "Seismic Anisotropy beneath the Northern Apennines (Italy) and Its Tectonic Implications." *Geophysical Research Letters* 23 (20): 2721–24.

Montagner, J.-P., and B. L. N. Kennett. 1996. "How to Reconcile Body-Wave and Normal-Mode Reference Earth Models." *Geophysical Journal International* 125 (1): 229–48.

Ohuchi, T., T. Kawazoe, Y. Nishihara, N. Nishiyama, and T. Irifune. 2011. "High Pressure and Temperature Fabric Transitions in Olivine and Variations in Upper Mantle Seismic Anisotropy." *Earth and Planetary Science Letters.*

Plomerova, J., L. Margheriti, J. Park, V. Babuška, S. Pondrelli, L. Vecsey, D. Piccinini, V. Levin, P. Baccheschi, and S. Salimbeni. 2006. "Seismic Anisotropy beneath the Northern Apennines (Italy): Mantle Flow or Lithosphere Fabric?" *Earth and Planetary Science Letters* 247 (1): 157–70.

Raterron, P., E. Amiguet, J. Chen, L. Li, and P. Cordier. 2009. "Experimental Deformation of Olivine Single Crystals at Mantle Pressures and Temperatures." *Physics of the Earth and Planetary Interiors* 172 (1-2): 74–83.

Smith, Gideon P., Douglas A. Wiens, Karen M. Fischer, Leroy M. Dorman, Spahr C. Webb, and John A. Hildebrand. 2001. "A Complex Pattern of Mantle Flow in the Lau Backarc." *Science* 292 (5517): 713–16.

Weidner, D.J., M.T. Vaughan, L. Wang, H. Long, L. Li, N.A. Dixon, and W.B. Durham. 2010. "Precise Stress Measurements with White Synchrotron X Rays." *Review of Scientific Instruments* 81 (1): 013903–013903–5.

Run	Press Load (T)	Target T (°C)	Approx. Pressure (GPa)	Avg Diff Stress (MPa)	Strain Rate (10^-6 s^-1)
San 308[1]	20	1100	2.2	100	6.5
[2]	70	1100	6.0	730	7.4
San 311	70	1100	6.1	120	7.8
San 316	80	1100	6.2	50	6.8
San 325[1]	30	1100	2.7	100	6.1
[2]	70	1100	5.5	300	6.6

Table 4-1. Approximate conditions for experiments.

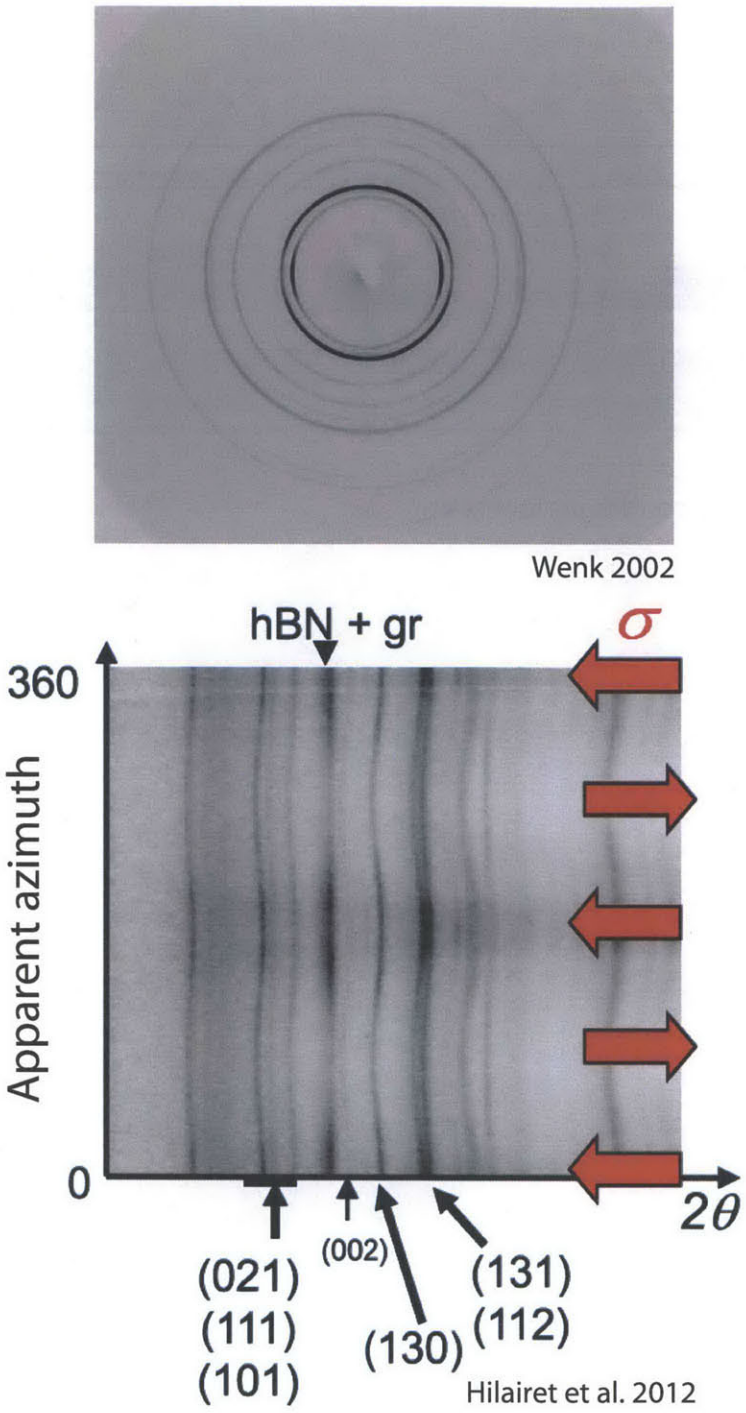

Figure 4-1. Top: Angle-dispersive x-ray diffraction pattern from Wenk 2002. This pattern was taken of a sheet of rolled polycrystalline copper. The radius of each Debye ring indicates the d-spacing of a single *hkl*, while variations in the thickness and darkness of lines are indicative of texture. Bottom: an angle-dispersive pattern of polycrystalline olivine from Hilairet et al. (2012), is rearranged to show variations in radius and thickness of olivine lattice planes (labeled) as a function of azimuth. Sinusoidal variations in Debye ring radius indicate differential stress (stress directions noted with arrows) . Texture is particularly obvious in this figure as well, with darkening of rings at 0° and 180°.

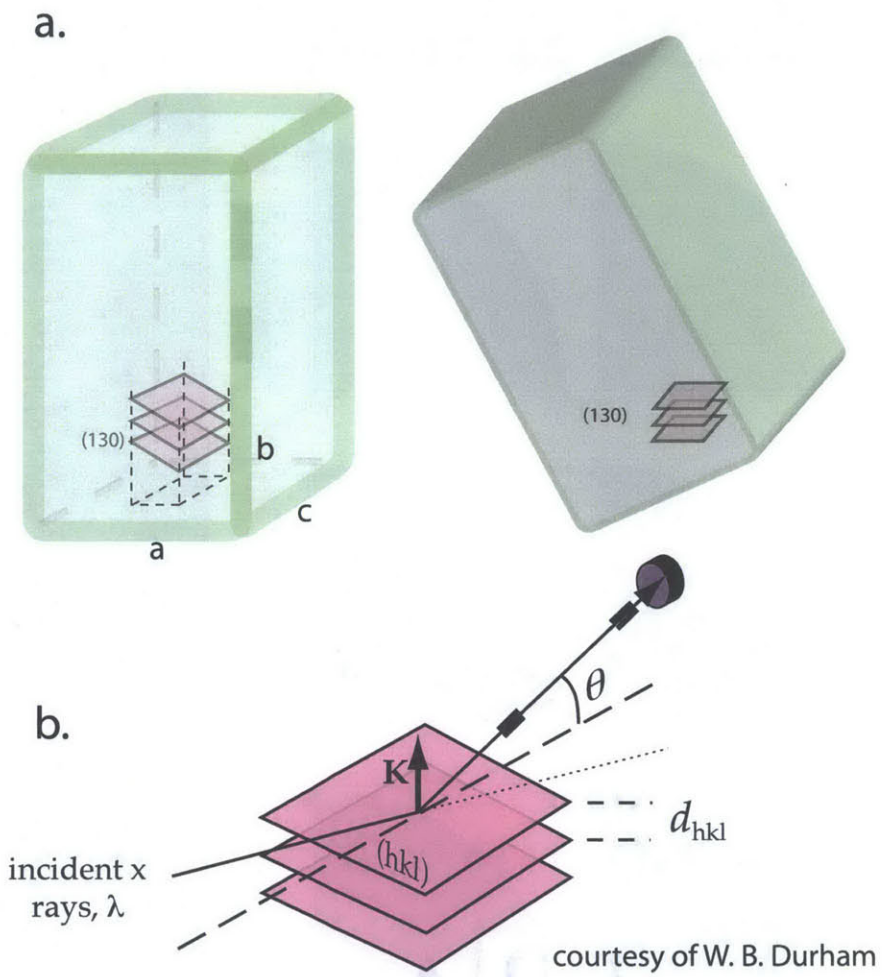

Figure 4-2. Definition of the diffraction condition. a) cartoon of the unit cell for the olivine crystal structure. In the left image, the orientation of the (130) lattice planes are defined. In the right image, the unit cell is oriented such that the diffraction condition is met for detectors 1 and 9 and the (130) plane. b) the path of the incident beam photons diffracted to detector 1 are shown.

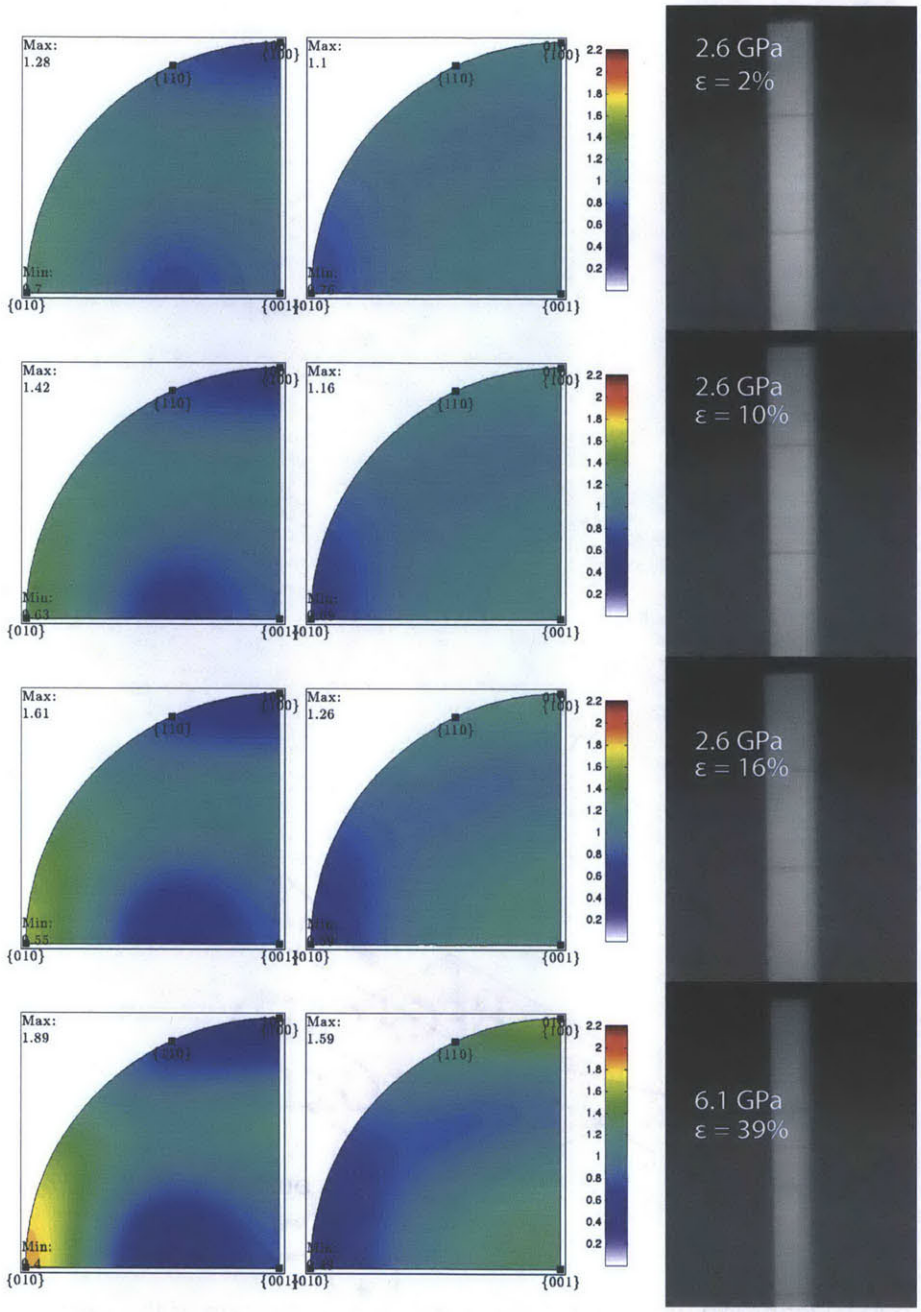

Figure 4-3. Development of texture in experiment San 308. From top to bottom, each pair of pole figures corresponds with a x-radiograph of the sample to right, progressing in deformation from the very beginning of the sample to almost 40% strain. Pressure conditions and strain are indicated on the x-radiographs. Each pole figure at left shows the vertical direction in the sample frame plotted with respect to the olivine crystallographic directions. The right pole figures show the horizontal direction in the sample. Throughout both steps of San 308, a the poles of the olivine (010) plane concentrate near vertical, while the (100) and (001) go towards the horizontal plane. This observation is consistent with either the (010)[100] or the (010)[001] mechanisms.

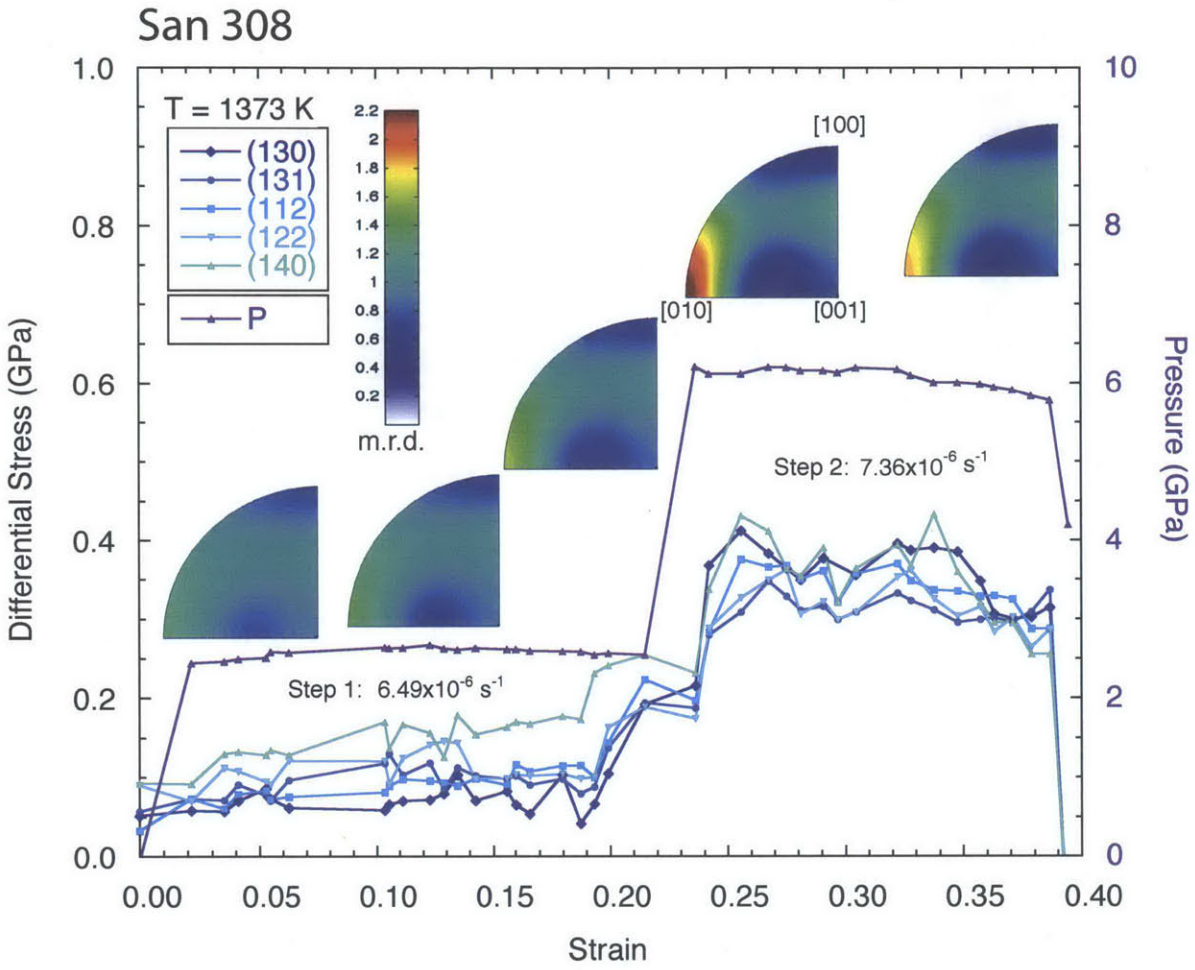

Figure 4-4. Deformation experiment San 308. The traces show stress measurements from five olivine lattice planes, as well as estimated pressure, and inverse pole figures showing the development of fabric throughout the experiment, as calculated using a custom routine for the *MTEX* package for *MATLAB*. Each inverse pole figure shows the orientation of the vertical direction in the sample with respect to the olivine crystallographic reference frame. In this experiment, apparent fabric steadily developed throughout the run, indicating either a Type-A or Type-B fabric, associated with the (010)[100] and (010)[001] slip systems.

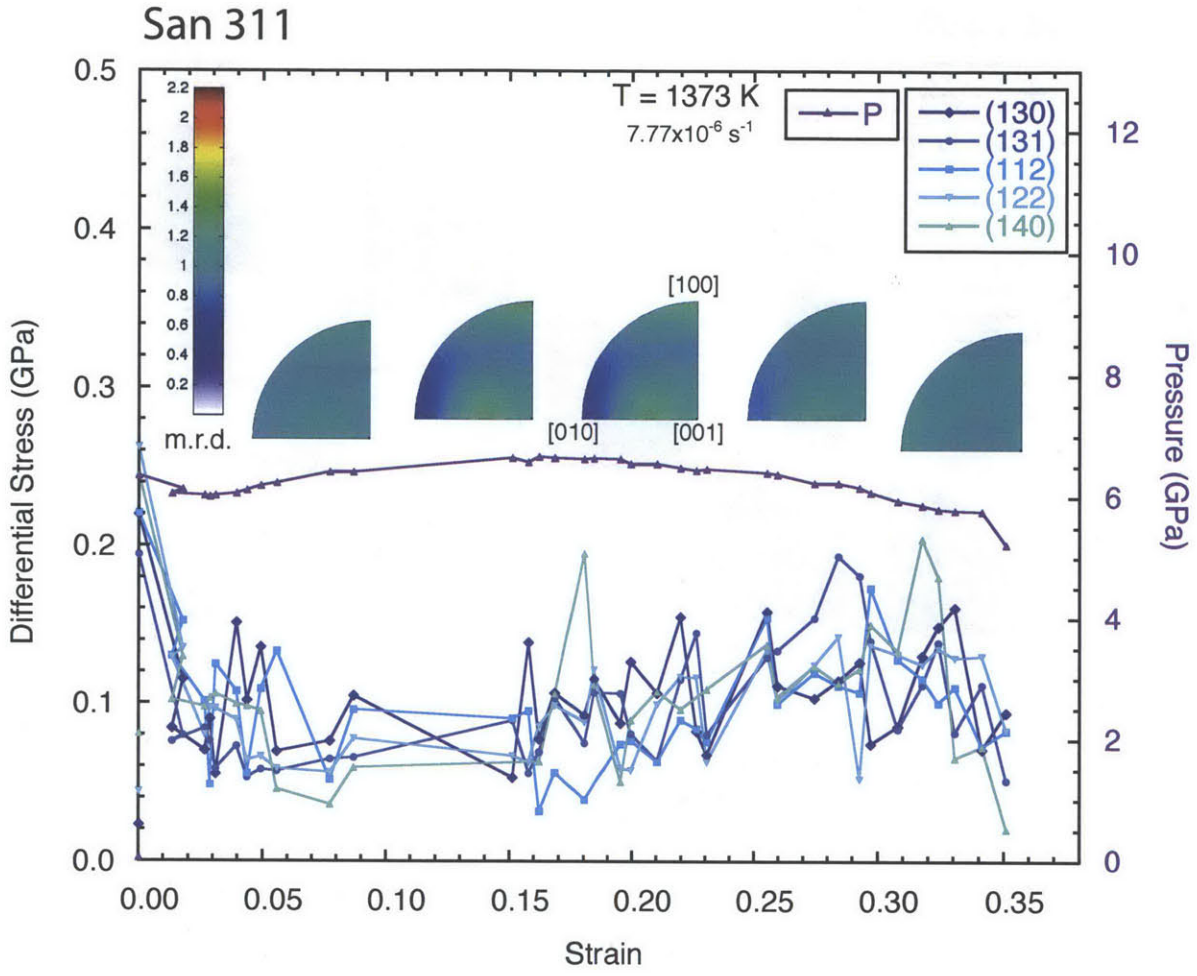

Figure 4-5. Experiment San 311. This experiment features a single step at constant P, T and strain rate, with the sample deformed to over 35% strain in pure shear in order to generate fabric that is observable in situ from diffraction data. Unlike San 308 which began developing a distinctive Type-A or Type-B fabric immediately, San 311 showed only a very week fabric during deformation, with the [001] and [001] directions concentrating near the vertical direction in the sample, as shown here in inverse pole figures.

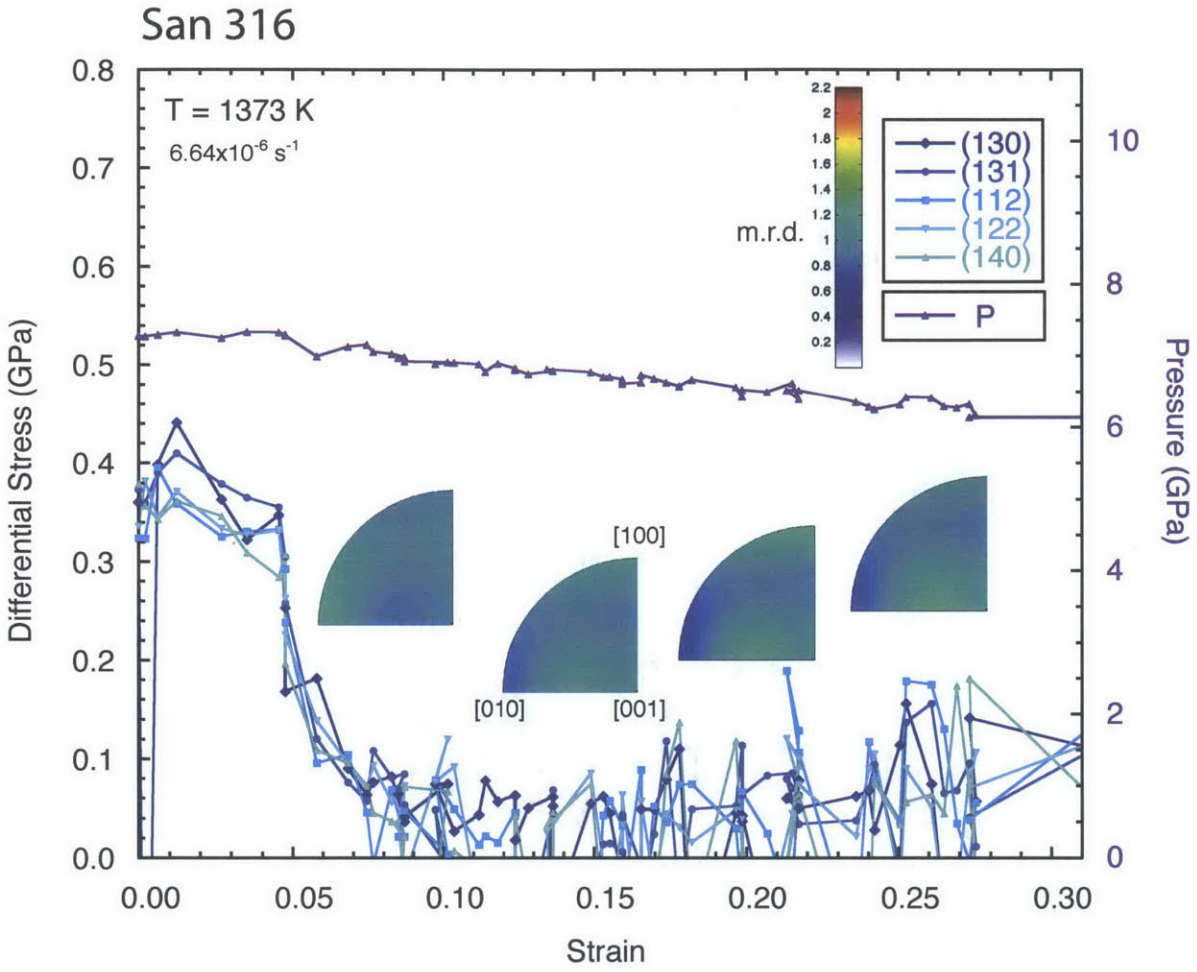

Figure 4-6. Experiment San 316. This sample was deformed in a single step, at similar conditions to San 311. Much like in San 311, only light fabric development was detected throughout the course of the run, with low differential stresses measured from x-ray diffraction.

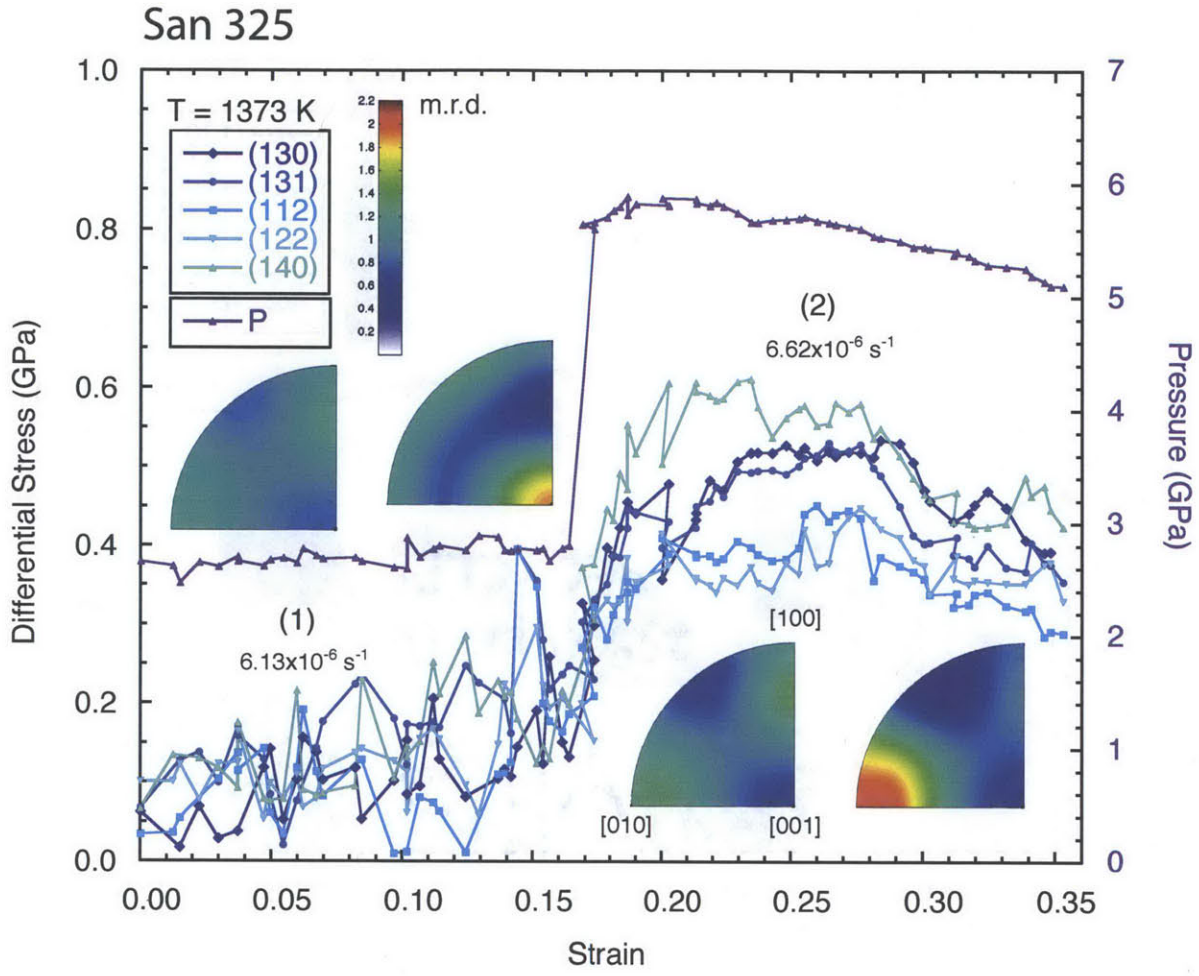

Figure 4-7. Experiment San 325. This sample was deformed in two steps, one at lower pressure (~3 GPa) and one at high pressure (5-6 GPa), similar to San 308. Unlike 308, a Type-A or Type-B fabric was not detected in the first step of the run, although some fabric of this type was measured towards the end of the second (high pressure) deformation step.

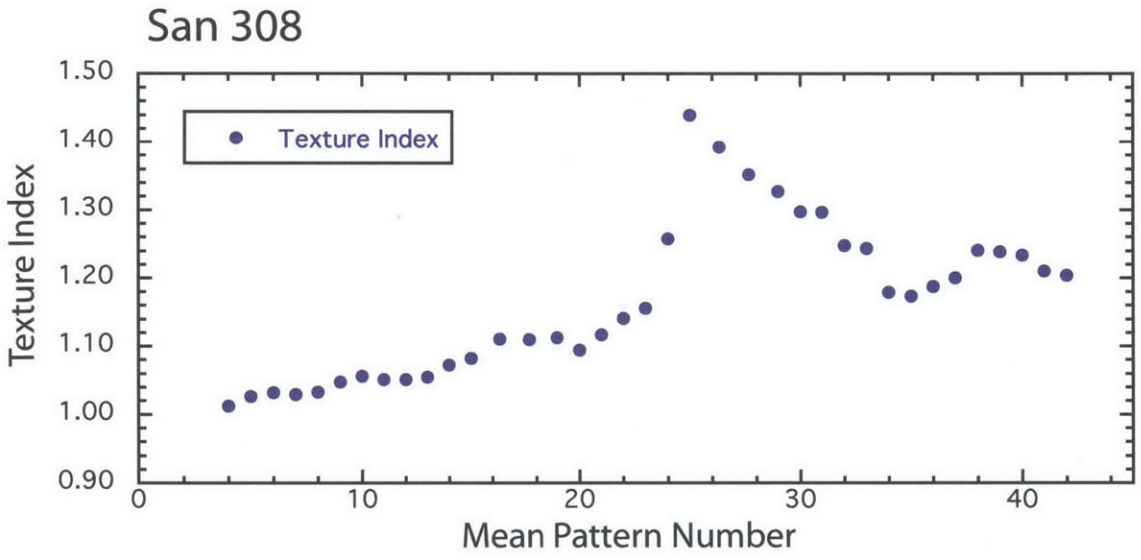

Figure 4-8. Development of fabric in experiment San 308. This plot shows the texture index (a measure of LPO strength, 1 for a random orientation, going to ∞ for a single crystal) throughout the course of experiment San 308. Each point represents the texture index averaged from three consecutive patterns. Fabric increases monotonically except for a spike after the sample is pressurized to ~6 GPa for the second experimental step. This spike may be an artifact due to the changed position of the D-DIA anvils during pressurization, which would change the path length of x-rays throught the transparent anvils.

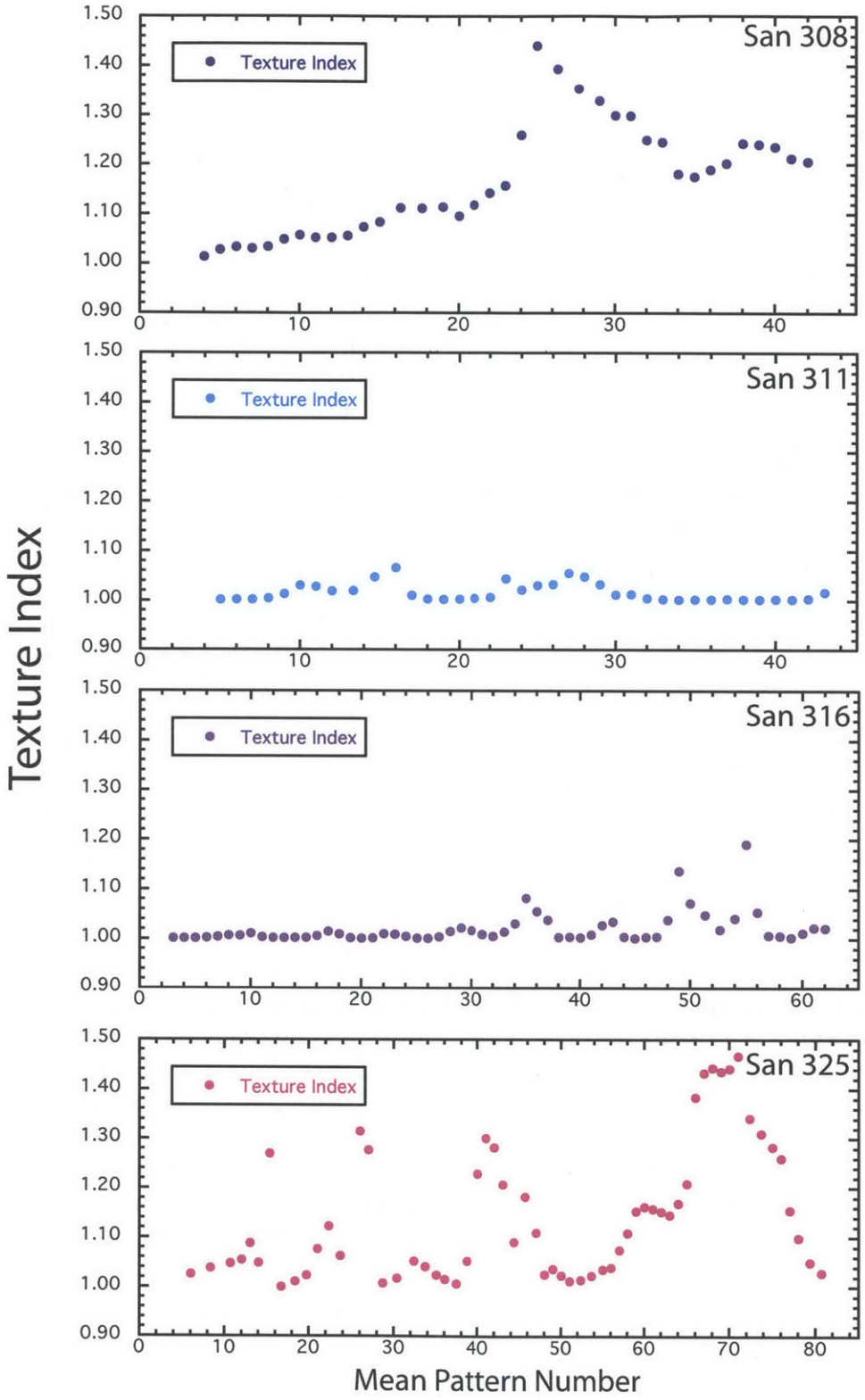

Figure 4-9. Comparison of texture index between experiments, on a common vertical scale. San 308 and San 325 develop stronger fabric than the two higher-pressure, single step experiments. San 308 shows a monotonic increase in fabric strength (with an artifact from pressurization, discussed in Figure 4-8), while fabric development in San 325 appears to be cyclical.

Chapter 5

Concluding Remarks

This project was undertaken with a simple purpose: to use new technology to solve an old and stubborn problem in geophysics. The challenge was to test the mechanical properties of Earth materials at conditions of the deep earth, for decades confounded by our inability to precisely generate, control, and measure non-hydrostatic stress states at high pressure. In the development of the D-DIA and other new multi-anvil machines for deformation, the goal was primarily to expand the range of conditions over which traditional creep tests could be conducted. Synchrotron x-ray diffraction was first and foremost a sophisticated replacement for the simpler stress gauges of earlier devices. The strategy for our experimental study was thus the same as in many earlier projects based on creep experiments: explore parameter space experiment-by-experiment, varying conditions one at a time and measuring the behavior of the sample on a macroscopic scale.

With this approach, we achieved a primary objective: a robust measurement of activation volume (V^*) over a broad range of upper mantle pressures. Unlike our samples, the mantle is not dry, simple in composition, or uniform in structure. Nonetheless, our measurement represents a firm

foundation, and experiments exploring more complex structures and chemistry can be built upon this work in the future.

A serious critique by Lutterotti et al (2007), noted in Chapter 2, has been made of this approach to determining V*. They point out that because of the complex interplay of mechanisms in high-pressure creep, the quest for "the V^*", a single canonical value to describe the behavior of olivine over a wide range of conditions, should cease in favor of a careful analysis of the mechanisms themselves. We believe that determining V* in the manner of our experiments remains important in a practical sense, as it provides a sense of the potential effect of pressure on the bulk behavior of the dynamic mantle, and can be incorporated straightforwardly into models.

Nonetheless, much of the remainder of this thesis is devoted to elucidating the subtleties of deformation physics present in our experiments. Although we are still in the nascent stages of deciphering all the information in our diffraction data, the synchrotron technique allows us to observe, in situ, the active deformation physics in fantastic detail. This includes in situ monitoring of plastic anisotropy and local stress heterogeneity, grain size, the development of lattice-preferred orientation (LPO), and even the partitioning of stress between multiple phases in the same polycrystalline sample. These capabilities have the potential to drastically change our approach to rheological research, since each experiment, in isolation, tells a comprehensive story about not just the macroscopic behavior of the material, but about the mechanisms, structure, and heterogeneity down to the lattice scale.